ABSTRACT

JOLLY, MICHAEL WARD. Development and Characterization of a Novel Textile-based Hemoperfusion System for the Treatment of Hyperphosphatemia. (Under the direction of Dr. Marian McCord).

The overall goal of this research is to develop, optimize and characterize a novel textile-based hemoperfusion system for use as an adsorption vehicle for the selective adsorption of phosphate from blood. This goal is addressed by combining an adsorbent system, composed of trimesic-acid surface-treated alumina powders (TMA-Alumina), with a hemocompatible textile substrate. Previous works have characterized the phosphate-selective adsorption exhibited by TMA-Alumina for use in the treatment of wastewater systems. When combined through a chemical surface treatment, this phosphate-selective complex consists of a basic, activated alumina and an overlaid aromatic benzenecarboxylic acid (Trimesic Acid or 1,3,5-benzenetricarboxylic acid) that are combined through strong hydrogen bonding. This research first focuses on the evaluation of various alumina powders for their phosphate adsorption capabilities, following the application of the TMA-surface treatment. The application of the TMA surface treatment to the alumina powders is first confirmed by X-ray photoelectron spectroscopy. Phosphate adsorption characteristics of each TMA-treated alumina powder are then evaluated in a bench-top assay with exposure to a simple phosphate solution. Following determination of phosphate adsorption characteristics, the TMA-alumina powder type exhibiting the highest phosphate adsorption is chosen for subsequent grafting experiments using a multitude of grafting methods. These grafting methods include melt-pressing using a Carver® Press, thermal spraying using a low-

velocity flame-spraying technique and chemical deposition using atomic layer deposition and sequential vapor infiltration techniques. Grafting yields were calculated for each grafting method and characterization using Scanning Electron Microscopy was performed to select the most viable method for use in the creation of the textile-based hemoperfusion system. The most viable grafting method was utilized to produce samples for assessing adsorption characteristics in bench-top phosphate adsorption and phosphate-selectivity studies. A simulated hemoperfusion circuit was developed and utilized for evaluating the hemoperfusion system in a scenario relevant to the end-use application of the hemoperfusion system. Phosphate adsorption profiles of the TMA-alumina-loaded textile hemoperfusion system were investigated in the hemoperfusion system using circulating phosphate solution and bovine whole blood, separately. Finally, the TMA-alumina loaded textile substrates were exposed in a bench-top setting to heparinized human whole blood and bovine whole blood to determine the extent of alumina particulate deposition or aluminum ion dissociation observed. When TMA-alumina is combined with a hemocompatible textile substrate, the resulting hemoperfusion system is shown to be effective in the selective reduction of phosphate from phosphate solution, complex ionic solution (lactated Ringer's solution) and bovine whole blood in bench-top and hemoperfusion-based flow systems.

Development and Characterization of a Novel Textile-Based Hemoperfusion System for the Treatment of Hyperphosphatemia

by
Michael Ward Jolly Jr.

A thesis submitted to the Graduate Faculty of
North Carolina State University
in partial fulfillment of the
requirements for the Degree of
Master of Science

Textile Engineering

Raleigh, North Carolina

2013

APPROVED BY:

_____	_____
Dr. Marian McCord Chair of Advisory Committee	Dr. Xiangwu Zhang
_____	_____
Dr. Julie Willoughby	Dr. Andrew Dimeo

BIOGRAPHY

Michael Ward Jolly Jr. was born to Lora Pritchard Davis and Michael Ward Jolly, Sr. in Lenoir, North Carolina on June 7, 1987. After moving from Lenoir with his family in 1991, Michael took up residence in Lexington, North Carolina where he spent the majority of his childhood. In 2001, Michael moved to Fleetwood, NC where he attended Ashe County High School and excelled in math and science. Following high school graduation, Michael was accepted to North Carolina State University, where he earned a Bachelor of Science degree in Biomedical Engineering. During his undergraduate studies, Michael became fascinated with the rapidly evolving biomedical field and was continually inspired both by the ability of newly emerging biomedical innovations to greatly improve the lives and outcomes of patients and the potential of such innovations to revolutionize the field of medicine. Intrigued by the marriage of medical device design and advanced material engineering that was taking place in the research lab of Dr. Marian McCord, Michael began doing experimental work with the group in the summer of 2010. Greatly inspired by his time in Dr. McCord's lab and excited by the prospect of developing and studying functional biomaterials, Michael applied to the Textile Engineering Master's program in the fall of 2010 and was accepted. Michael will complete his Master's degree in Textile Engineering in May of 2013 and aims to use the insights and skills that he has gained to make meaningful and lasting contributions to the improvement of societal healthcare.

ACKNOWLEDGEMENTS

I would like to extend my immense gratitude to Dr. Marian McCord, who has been a tremendous source of inspiration for me. Dr. McCord, my advisor and thesis committee chair, worked hard to provide funding for this research endeavor and delivered invaluable guidance throughout the entirety of the project. Dr. McCord's brilliance and scientific acumen are surpassed only by her warmth and empathy and I am truly blessed to have had her as a mentor and to be able to call her a friend. Without Dr. McCord, my goal of obtaining a Master's degree could not have been obtained.

I would also like to thank Dr. Melanie Joy for her advisement and persistent thoughtfulness throughout this journey. As a friend and mentor, Dr. Joy provided sound advice and immense financial assistance throughout the duration of this project. Her vital direction during the experimental process, ceaseless generosities, and help and understanding when things got messy encouraged me stay the course when times were trying and helped make my dream of a Master's degree come true.

I also owe Dr. Quan Shi a great deal of gratitude for his training and guidance throughout much of the experimental work discussed herein, for his support, and for his loyal friendship.

Finally, I wish to thank my wonderful family and many close friends, whose enthusiasm and support provided the motivational fuel to make this achievement a reality.

A great deal of gratitude goes out to the following organizations, whose generous financial support provided the resources that made this research possible: The Wallace H. Coulter Foundation, the North Carolina Translational and Clinical Sciences Institute (NC TraCS), and The Golden LEAF Biotechnology Training and Education Center at North Carolina State University.

TABLE OF CONTENTS

LIST OF TABLES

LIST OF FIGURES

1. Background

Hyperphosphatemia is generally defined as a systemic mineral disturbance that results in an abnormally high content of inorganic phosphate in the blood. While hyperphosphatemia can result from a number of causes, it is most commonly triggered by insufficiencies in the renal handling of ingested phosphate which results in excessive accumulation. Although the threshold phosphate concentration that defines hyperphosphatemia varies throughout the literature, a serum phosphate level that exceeds 4.5 mg/dL currently reflects a value that is clinically diagnostic.[1–4] Despite significant technological developments in the treatment modalities for hyperphosphatemia, the existing regimen is unsuccessful in the long-term maintenance of safe phosphate concentrations.[5] As a result, elevated serum phosphorus levels occur in 90% of patients with kidney disease[6] and contribute to significantly increased risks of cardiovascular disease and mortality.[6,7]

1.1 Phosphate in the Body

Inorganic phosphate exists within the body as freely circulating ions or in complexes with non-carbon atoms and has central roles in cellular metabolism, the construction and maintenance of the skeletal system, enzymatic activity and calcium homeostasis.[1,8] Found in various anatomical regions of the body, phosphate is temporarily stored in reservoirs that are vital to the regulation of the overall phosphate homeostasis of an individual. Roughly 85% of all phosphate found in the body exists as an inorganic component of crystalline tricalcium phosphate ($Ca_{10}(PO_4)_6(OH)_2$ or hydroxyapatite), which is the primary constituent of skeletal bone and teeth.[1,8–12] Fourteen percent of phosphate is present as an intracellular

anion and serves vital roles in both the aerobic and anaerobic energy processes of red blood cells.[1,8,9,12] The final 1% of bodily phosphate is found in the extracellular fluid and comprises the fraction that is detectable as serum phosphorus.[1] Here, phosphate circulates at physiological pH (7.4) in a 4:1 ratio of HPO_4^{2-} and $H_2PO_4^-$ and serves vital buffering roles for the preservation of mineral, electrical and acid-base homeostasis.[12] Almost 90% of the phosphate in this extracellular compartment exists as a free ion and is actively filtered by the kidney, while the other 10% is protein-bound and is therefore not susceptible to renal filtration.[1,9,12]

Phosphate is a ubiquitous component of foods and beverages that are consumed worldwide and manifests in both organic and inorganic forms. Organic phosphates are bound in large quantities to both plant and animal proteins and are also a frequent component of non-protein plant and animal tissues.[4] Inorganic phosphates are a common component of food additives and preservatives for processed foods and beverages.[4] The quantities of ingested phosphate that end up in the blood stream are governed by the complex set of absorption, reabsorption and excretion processes that occur primarily in the intestines and kidneys and are regulated by feed-back loops that are mediated by calcium, vitamin D, parathyroid hormone and phosphatonins.

1.2 Phosphate Homeostasis

In the absence of underlying health complications, adequate phosphate balance is quite easily maintained by renal filtration, hormone and phosphatonin secretion, and the dynamic processes of bone resorption and regrowth. In such scenarios, the incoming

quantities of phosphate that are acquired through dietary consumption and the natural breakdown of cellular components remains balanced with the quantities of phosphate that are lost to urinary excretion and catabolic cellular processes. The result is the successful bodily maintenance of phosphate equilibrium. However, malfunctions in any of the aforementioned regulators of phosphate homeostasis directly results in disturbances in the net phosphate balance. When dietary phosphate intake consistently exceeds phosphate excretion, hyperphosphatemia ensues.

1.3 Chronic Kidney Disease and End-Stage Renal Disease

Renal failure is the leading cause of hyperphosphatemia.[1,9] Excluding cases of acute injury, renal failure is not an instantaneous process, but rather the culmination of a progressive deterioration of organ structure and function.[8,9,13] This deterioration is most often identified in patients prior to the occurrence of complete kidney failure and is diagnosed as Chronic Kidney Disease (CKD). While CKD is a broad classification, and is indiscriminate of cause, it is further subdivided into five stages based on the severity of kidney damage that is present. Early declines in kidney function are compensated for by the hyper-functioning of the viable nephrons that remain, but such overwork eventually atrophies this viable fraction. The continual degeneration is paralleled by persistent reductions in the fluid filtration rates of the nephrons, known as glomerular filtration rates (GFR).[14] The subdivisions of Chronic Kidney Disease therefore mirror clinically relevant ranges of GFR and include all stages of kidney deterioration, from the onset of CKD at stage one to the complete failure of the kidneys at stage five (Table 1).[13]

Table 1. The stages of chronic kidney disease and the associated glomerular filtration rates (GFR), symptoms and disorders. Adapted from[7,13,14].

CKD Disease Stage	Classification	Glomerular Filtration Rate (GFR) (mL/min/1.73m^2)	Associated Symptoms/Disorders
Stage 1	Early-Stage Chronic Kidney Disease	> 90	High blood pressure
Stage 2		60-89	High blood pressure, proteinuria possible anemia
Stage 3		30-59	Onset of uremia
Stage 4	Late-Stage Chronic Kidney Disease	15-29	Onset of hyperphosphatemia and secondary hyperparathyroidism; vascular deposition of calcium-phosphate
Stage 5	End-Stage Renal Disease	< 15	Complete kidney failure, increased cardiovascular mortality

Despite the presence of nephron dysfunction, compensatory mechanisms are sufficient to maintain acceptable serum phosphate levels in patients with early-stage CKD.[4,13,14] Nevertheless, phosphate excretion continues to decline at a level that is concomitant with further kidney degeneration, ultimately resulting in a positive mass-balance of phosphate within the blood at stage-3 of CKD.[8,13] Although clinical methods of intervention are well-established, the deterioration to stage-4 of Chronic Kidney Disease has been shown to occur in over 51% of patients, with over 34% of patients inevitably progressing to End-Stage Renal Disease.[15] Once complete kidney failure ensues, the further advancement of hyperphosphatemia can only be mitigated by immediate therapeutic interventions.

Several negative outcomes are associated with the presence of hyperphosphatemia in End-Stage Renal Disease, with the most deleterious of these being extraskeletal calcification,[7,14,16,17] hemodynamic instabilities,[18] and death.[6,7] The calcification of blood

vessels is commonly seen in patients with elevated serum phosphate concentrations due to the tendency of calcium and phosphate to ionically bind together and form crystalline deposits when present in high concentrations.[14,16] Similar in composition to the hydroxyapatite found in bone, these calcium-phosphate deposits can occur throughout the circulatory system and have been linked to the hardening and successive failure of heart valves.[16] Moreover, vascular calcifications induce hemodynamic disturbances by decreasing the compliance of blood vessels, which leads to increased blood pressures and escalations in cardiac output.[18] Accordingly, the end-result of hyperphosphatemia in End-Stage Renal Disease is the increased predisposition to cardiac disease and heightened mortality.[7,18] In a study of all-cause mortality in ESRD hemodialysis patients, Kimata et al. found that elevated phosphate concentrations were directly correlated to increased death, with hyperphosphatemic patients at an 18% greater risk of cardiovascular death when serum phosphate levels were 5.5-6.5 mg/dL and a 24% greater risk when serum phosphate levels exceeded 6.5 mg/dL.[7] Though Tentori et al. used different phosphate concentration intervals, their global study displayed even greater increases in all-cause and cardiovascular mortality for hyperphosphatemic patients.[6] The group found associated all-cause mortality rates were 1.02, 1.18 and 1.43 times higher and cardiovascular mortality rates were 1.25, 1.61 and 1.81 times higher when phosphate concentrations were 5.1-6.0 mg/dL, 6.1-7.0 mg/dL, and > 7.0 mg/dL, respectively.[6]

1.4 Current Treatment Methods

1.4.1 Hemodialysis

Hemodialysis is the primary treatment method for the reduction of serum phosphorus levels associated with hyperphosphatemia. Although hemodialysis provides efficient phosphate clearance, the use of conventional hemodialysis techniques alone remains incapable of maintaining satisfactory serum phosphate levels that remain, over the long-term, below the clinically defined threshold of hyperphopshatemia.[5,19] For this reason, recent studies have considered the use of augmented hemodialysis strategies to improve long term phosphate maintenance.

Musci et al. calculated the net phosphate balance that ultimately results after subtracting the phosphate removal by thrice-weekly dialysis from the overall phosphate intake from dietary sources.[19] The data displayed in the table below (Table 2), follows these calculations and utilizes the average of ranges proposed by the authors for the dietary intake of phosphate and the dialytic removal of phosphate via thrice-weekly hemodialysis. The net phosphate balance using conventional thrice-weekly hemodialysis procedures, the most frequently prescribed treatment regimen for hyperphosphatemic patients, was shown to be positive, ultimately resulting in the deposition of excess phosphate within the body.[19]

Realizing the inadequacies of conventional hemodialysis in maintaining satisfactory serum phosphate levels, alterations to the currently prescribed hemodialysis regimen were explored by various authors throughout the literature.[11,19–22] Pohlmeier reviewed the landscape of dialytic treatments explored in the literature and suggested that the utilization

of dialyzers with enhanced phosphate clearance does not lead to substantial overall differences in phosphate removal.[20] The authors suggested that the rate limiting step involved in dialytic procedures is not the clearance by the dialyzer, but rather the slow paced phosphate exchange within the body from the intracellular reservoir to the extracellular pool. This led the authors to assert that improved patient outcomes would result from increasing the frequencies of dialysis treatments to combat the phosphate rebounding typically observed on days in-between dialysis sessions, as intracellular phosphate slowly migrated into the extracellular pool.[20] Musci et al. found that changing the hemodialysis type from conventional thrice-weekly hemodialysis to nocturnal hemodialysis was capable of bolstering long-term phosphate reductions in hyperphosphatemic patients, echoing findings by Pohlmeier et al. that increasing the duration of individual dialysis sessions provides improved long-term phosphate maintanence.[19] Statistical analyses by Kjellestand et al. on reported clinical data assessed the effects of varying treatment frequencies, durations and dialytic phosphate clearances and added evidence to support the observations by Musci et al. and Pohlmeier et al. that longer durations of hemodialysis procedures should be performed in order to provide maximum enhancements to phosphate management.[21] Tonelli et al. demonstrated that long-term improvements in pre-dialysis phosphate levels could also be provided without increasing hemodialysis frequency or duration.[22] Instead, Tonelli et al. found that the long-term use of two dialyzers in parallel during the hemodialysis procedure led to substantially

lower serum phosphate concentrations over the long-run, than those accompanying conventional hemodialysis prodcedures.[22]

Although these findings suggest that varying hemodialysis frequencies, durations and modalities can provide improved long-term phosphate maintenance, the degrees of phosphate maintenance provided by all hemodialysis treatment schemes have been shown throughout the literature to be variable and are often dependent on the characteristics of the individual patient. Moreover, such benefits have not yet proved significant enough to supplant the use of thrice-weekly, 4-hour hemodialysis sessions as the current gold-standard for hemodialysis procedures. In reference to factors separate from long-term health benefits, significant financial burdens associated with hemodialysis on both patients and healthcare providers continue to persist, despite the mass-production of dialysis equipment and associated technological advances.[23] Furthermore, the nature of all existing hemodialysis treatment regimens requires that significant proportions of a patient's time are spent in dialysis clinics, thereby reducing quality of life and, in the worst case, lowering patient compliance for hemodialysis. The recommendations made by various authors for increasing dialysis durations or frequencies will only exacerbate this problem. For these reasons, the provision of alternatives to hemodialysis or augmentations to bolster the effectiveness of hemodialysis treatments may provide improvements in patient health and quality of life, while lowering the costs associated with current hemodialysis-based treatment routines.

Table 2. Daily and weekly phosphate dietary intake and removal by dialysis along with calculated phosphate balances, as derived from averaging of reported ranges from measurements on patients receiving daily hemodialysis.[19]

	Phosphate Intake (mg)	**Removal of Phosphate by Dialysis** (mg)	**Net Phosphate Balance** (mg)
Daily	61.95	39.82	+ 22.13
Weekly	433.64	278.77	+ 154.83

1.4.2 Dietary Phosphate Restriction

Due to the pervasive nature of phosphates in protein foodstuffs; dairy, eggs and meat account for approximately 60% of an average individual's daily dietary intake of phosphorus.[24] Organic phosphates are also present in cereals, legumes, fruits, vegetables, alcoholic beverages and soft drinks.[4,24] Depending on the individual's eating habits, inorganic phosphates may encompass up to 50% of the daily dietary phosphorous intake.[4] As the level of dietary phosphate intake is a key determinant of serum phosphorus concentrations, the dietary restriction of phosphate is commonly prescribed for hyperphosphatemic patients. However, poor patient compliance restricts the effectiveness of this therapy and there are indications that low-protein diets can cause significant malnutrition and increase the mortality risk of ESRD patients.[5]

1.4.3 Oral Phosphate Binders:

Over 90% of the population that is living with kidney failure are prescribed oral phosphate binders to provide more adequate control of serum phosphorus levels.[10] Oral phosphate binders are pelletized adsorption vehicles for dietary phosphates that are designed to be ingested. Consisting of chemical species that form insoluble complexes with phosphate,

these compounds are prescribed to hyperphosphatemic patients in an effort to mitigate the proportion of ingested phosphate that is absorbed in the gastrointestinal tract. By providing a method to minimize the amount of phosphate available for gastrointestinal absorption, this strategy has proven to be an effective method for correcting the net positive phosphate balance that inevitably accompanies the reductions in renal phosphate clearance associated with end-stage renal disease. Though various formulations of oral phosphate binders have been developed to address phosphate management insufficiencies, significant side-effects have always plagued their use.[9,10] Owing to their pervasive nature in the patient population suffering from kidney disease, various phosphate binder formulations are currently manufactured and prescribed. The major categories include phosphate binders composed of calcium-based compounds, lanthanum, magnesium hydroxide, and sevelamer carbonate.[10] While each of these formulations is effective at reducing the quantities of phosphate that are absorbed in the GI tract, they all suffer from a host of accompanying side-effects and poor patient compliance.[9,10,20,25] Moreover, the more sophisticated, and less side-effect producing oral phosphate binders suffer from high-costs.[10] Associated side-effects of phosphate binders include hypercalcemia, gastrointestinal abnormalities (vomiting, nausea, constipation and abdominal pain), metabolic acidosis, peripheral edema, and the tendency of constituent compounds to accumulate in bone.[9,10]

Although significant technological advancements have enhanced the versatility and effectiveness of hemodialysis therapies, the long-term management of serum phosphorus levels in patients with end-stage renal disease is seldom realized by this treatment modality

alone.[5,19] Furthermore, despite proven success in reducing serum phosphorus concentrations, the use of dietary phosphate restriction and oral phosphate binders suffer from poor patient compliance and are associated with significant side-effects.[4,10] Improvements in patient outcomes and the elimination of the need for oral phosphate binders could be achieved by augmenting existing hemodialysis procedures with the addition of a safe, effective and phosphate-selective therapy. The research and results contained within this body of work are aimed at addressing this unmet clinical need. To this end, the objective of this research is the development of a textile-based device that exhibits efficient and selective phosphate removal from whole blood, while displaying a requisite degree of biocompatibility.

2. Hemoperfusion

2.1 Hemoperfusion Devices

Despite the high phosphate clearance of modern dialysis therapies, various studies and practice recommendations have emphasized the need for serum phosphate levels of patients with kidney dysfunction to be more effectively regulated.[9,11,22,24,26–28] Hemoperfusion is an adsorption-based modality of extracorporeal therapy with proven viability in the removal of a variety of target substances from whole blood and plasma and may be an effective tool to augment current dialysis regimens. The technique involves the direct contact of flowing blood or plasma with a biocompatible adsorbent system (hemoadsorbent), to which targeted solute molecules exhibit a favorable binding affinity. Hemoperfusion circuits are more simple to construct and to operate than those used for

dialysis and primarily consist of a hemoperfusion device, a blood pump, gauges to detect pressure drops across the hemoperfusion device and the administration of heparin to prevent extracorporeal thrombosis.[29,30]

Depending on the medium in which they function, hemoperfusion devices can be classified as whole-blood-based or plasma-based adsorption methods.[31] Whole blood techniques involve direct passage of heparinized blood over an adsorbent system and have been shown to be effective in the extraction of various toxins, drugs, electrolytes, proteins, antibodies, and cells. Plasma-based adsorption, aided by plasmapheresis, has been utilized for the efficient removal of toxins, drugs, electrolytes and proteins. In the latter technique, plasma is first separated from whole blood by filtration or centrifugation and the resulting plasma is exposed to an adsorbent before being returned to the circulating blood. The requirement of expensive plasmapheresis equipment renders plasma-adsorption techniques much more difficult to execute and less cost-efficient than whole-blood hemoperfusion. Furthermore, because whole-blood hemoperfusion systems do not require plasmapheresis, they are more compatible with existing dialysis configurations and are much better suited for wide-scale adoption by clinicians and physicians. It is therefore most pertinent to consider the application of whole-blood hemoperfusion techniques.

2.1.1 Combined Hemoperfusion and Hemodialysis

The adsorptive mechanism of action employed by whole-blood hemoperfusion methods confers potential benefits that are absent from hemodialysis procedures. These benefits include high adsorption efficiency, discriminatory solute clearance and the ability to

efficiently remove protein-bound and middle and high molecular weight molecules.[23] Nevertheless, the selective adsorption exhibited by hemoadsorbents would necessitate a complex combination of dozens of hemoperfusion systems to adequately replace the function of modern hemodialysis systems. Moreover, the predominance of hemodialysis and its longstanding acceptance as the gold standard of renal replacement therapy demands that hemoperfusion be incorporated into existing dialysis procedures to be a clinically viable option.[32]

Hootkins et al. found that the concurrent use of high-flux hemodialysis with charcoal hemoperfusion in patients, using relatively low blood flow rates (250 mL/min), was more effective in the removal of theophylline compared to both the consecutive use of high-flux hemodialysis and hemoperfusion and the stand-alone application of each procedure.[33] Hemodialysis alone, even with typical blood-flow rates (300-400 mL/min), was shown to display poor clearance of theophylline and the individual use of hemoperfusion resulted in rapid saturation of the hemoadsorbent.[33] However, when applied in series, Hootkins et al. observed that the combination of the hemodialysis and hemoperfusion was successful at removing 94% of circulating theophylline, while also correcting acid-base and electrolyte imbalances.[33] Sasamura et al. echoed the last finding by Hootkins et al., observing that while the chemotherapy drug methotrexate was efficiently extracted from patients by the application of charcoal hemoperfusion alone, the application of hemodialysis permitted superior maintenance of fluid and electrolyte balance and corrected uremia.[34] The group also attributed the much greater methotrexate removal rates afforded by hemoperfusion

vs. hemodialysis to the propensity of methotrexate to bind to larger proteins that cannot easily traverse the dialysis membrane,[34] a pertinent consideration for phosphate removal, as 10% of blood-phosphate is protein bound.[1,9,12] Lee et al. evaluated the optimal configuration of combined hemodialysis and coated charcoal hemoperfusion systems (blood flow rate of 200 mL/min) for removing paraquat from simulated blood solutions. The experimental results indicated that, in the context of molecules displaying high affinity for the hemoadsorbent, the combined system provided the most optimal extraction when arranged with the patient positioned upstream from a dialyzer that is upstream from the hemoperfusion cartridge (deemed the HDHP system, Figure 1).[29] Inserting the experimental results into their mathematical model revealed a good-fit of the data to the generated one-pool model and confirmed that the total removal of paraquat by hemoperfusion and hemodialysis follows the sequence of hemodialysis-hemoperfusion > hemoperfusion alone > hemodialysis alone.[29] While the clearance of molecules by hemoperfusion and hemodialysis is specific to the target-molecule's molecular weight and chemistry, recent studies by Tonelli et al. have provided evidence suggesting that the addition of a sorbent device to existing hemodialysis treatments can also enhance the clearance of phosphate.[22] However, the single-pool model generated by Lee et al. is not applicable to the extraction of phosphate, which shows kinetics that several authors have described as being based on multiple pools.[4,5,11,28,35]

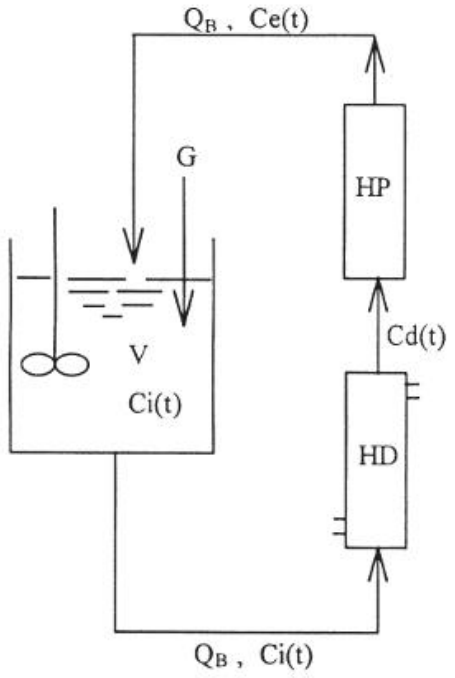

Figure 1. Schematic of optimal hemodialysis-hemoperfusion configuration, as described by Lee et al. Figure reprinted from.[29]

2.1.2 Early History of Hemoperfusion

The first reported conceptualization of hemoperfusion techniques for the removal of substances from blood was made in 1948 by Muirhead and Reid in a set of experiments that assessed the urea reduction potential of a column containing anion (decidite) and cation (amberlite) exchange resins.[36] Although the authors found that the in-vitro exposure of whole blood to this column only minimally reduced urea concentrations, the publication of their results shed light on an unexplored avenue for blood detoxification.[36] Still, over 15 years elapsed before the clinical utility of hemoperfusion systems was finally confirmed, with Yatzidis showing that many uremic toxins were more effectively removed from uremic dogs through the use of an activated charcoal hemoperfusion system than by the

application of hemodialysis.[37] While the results published by Yatzidis showed promising adsorption efficiency, the device had biocompatibility issues, and triggered the onset of hypotension, hypocalcaemia, hypokalemia and hypoglycemia in test subjects.[23,37,38] As each of these disorders are characterized by insufficiencies in associated blood solutes, the author concluded that the removal of other off-target blood constituents was a particularly significant problem in hemoperfusion.[37] Although Yatzidis discounted reductions in circulating platelets and clotting factors, other authors later elucidated that thrombocytopenia, a blood abnormality characterized by reductions in circulating platelets, is a risk factor associated with the shedding of fine granules from hemoadsorbent columns.[23,39] To address the issue of thrombocytopenia, Chang et al. explored the possibility of minimizing the adhesion of platelets on activated charcoal hemoadsorbents by microencapsulation of the adsorbent. By utilizing a technique that the group had originally developed for the encapsulation of enzymes,[40] the authors were able to successfully coat the charcoal hemoadsorbents in an inert and semi-permeable polymer matrix that showed inherent porosity.[41,42] Deemed "artificial cells," subsequent clinical trials showed that activated charcoal encapsulated in such polymer membranes could be safely employed (often in conjunction with hemodialysis) to remove a wide-range of drugs and toxins.[41–43] While microencapsulation reduces the adsorption efficiency of the charcoal, due to the need for solutes to diffuse through both the porous polymer network and into the pores of the underlying adsorbent,[30,44] the technique is successful at mitigating the detachment of charcoal micro-particles and effectively reducing protein and platelet adhesion to levels

comparable to that seen in dialysis.[41–44] A thorough review of the use of other microencapsulation agents in hemoadsorbents, focusing on agarose but also describing albumin-collodion, hydrogels, cellulose acetate and albumin, has been published by Sideman et al.[45]

Despite the persistent exploration of hemoperfusion systems and the in-vivo use of charcoal hemoadsorbents in the 1960's and 1970's, the technique has largely disappeared from clinical practice since. Statistical analysis performed by Holubek et al. on data compiled by the American Association of Poison Control Centers' Toxic Exposure Surveillance System (TESS) found that from 1985-2005, the number of toxic exposure cases where dialysis was administered rose sharply, while treatment by hemoperfusion significantly diminished.[46] In explaining the 300% increase in dialytic procedures and the 182% decrease in hemoperfusion procedures prescribed for correcting acute toxicity over the period,[46] various authors cited rapid technological advances in hemodialysis, the decreased availability of hemoperfusion cartridges, the unfamiliarity of nephrologists with hemoperfusion, shifting paradigms in the prescription of potentially toxic drugs and evidence of rapid hemoadsorbent saturation.[31,38,46]

2.1.3 Hemoadsorbents

While hemodialysis has almost completely supplanted hemoperfusion as a renal replacement therapy in clinical practice, innate limitations in the dialytic clearance of certain molecules and the need for the selective removal of specific substances have recently brought hemoperfusion back into the limelight. Ideal hemoperfusion adsorbents

are engineered to exhibit selective adsorption of only certain molecules; therefore, the target-molecule's properties and the requirements of post-treatment blood composition dictate the necessary adsorbent formulation.[31] The adsorbents used in hemoperfusion systems should display high binding capacity, selective adsorption and excellent biocompatibility, while remaining cost-effective.[23,29,31,38,47] Countless hemoadsorbent formulations have been conceptualized, but the vast majority of those evaluated in either in-vitro or in-vivo settings can be subdivided into three categories based on their matrix composition – activated charcoals, polymers and inorganic materials.

2.1.3.1 Activated Charcoal-based Hemoadsorbents

Activated charcoals, which can be produced from the reconstitution of any simple carbonaceous material, get their name from the activation step of the manufacturing cycle that is used to impart structural porosity to the material. The introduction of this porosity yields a carbonic material with very high surface area (500-1000 m^2/g), whose properties are governed by the choice of the precursor material and the type of activation step employed.[30] Since adsorption is a surface-mediated phenomenon, optimizing the charcoal's surface area provides maximal adsorption capacity and minimizes the necessary adsorbent volume. This is crucial for producing viable charcoal hemoadsorbents, as the minimization of extracorporeal blood volume is a prime concern in all extracorporeal therapies.[39] Activated charcoal is best suited for the removal of water soluble toxins from blood[23,48] and, depending on the properties of the adsorbate, binds these molecules through a

combination of van Der Waals, ion exchange, hydrogen bonding and hydrophobic interactions.[23]

Activated charcoal has been the most widely studied of all hemoadsorbent materials and is still the only hemoperfusion product available for patient use in America.[38] Though other modern clinical procedures involving charcoal hemoadsorbent systems are virtually nonexistent, such systems are currently still in use for treating acute poisonings and drug overdose. Pilapil and Peterson compared charcoal hemoperfusion with low flux hemodialysis and similarly observed that charcoal hemoperfusion was the more clinically proficient technique at eliminating blood-circulating carbamazepine in drug overdose patients.[49] Further testifying to the utility of hemoperfusion techniques in scenarios of drug overdose, the authors found that the charcoal hemoadsorbent displayed very rapid initial drug clearance that eventually declined to levels commonly seen in hemodialysis.[49] Holubek echoed the value of hemoperfusion in reducing circulating drug concentrations in his review on the use of hemodialysis and hemoperfusion in poisonings.[46] Capitalizing on this advantage offered by hemoperfusion techniques, Gambro developed a hemoperfusion device, known as the Adsorba C, which contains 300g of a cellulose-coated activated charcoal hemoadsorbent. While this particular device is not approved for use in the United States, it was introduced in other markets in the 1980's and has since been employed for the removal of many lipophilic and hydrophilic drugs.[50]

Since their inception, charcoal hemoadsorbents have also been studied for their ability to remove circulating uremic toxins from blood. As previously mentioned, Yatzidis unveiled the

clinical use of hemoperfusion with his report that uncoated charcoal removed significant quantities of urea, creatinine, uric acid, phosphate, guanidine, indoles and organic acids from the blood of both dogs and patients with chronic renal failure.[37] However, numerous biocompatibility issues associated with the uncoated charcoal hemoadsorbent system were reported.[37] The aforementioned studies by Chang et al. confirmed the utility of the microencapsulation of hemoperfusion and provided enhanced biocompatibility to charcoal adsorbents.[40–42] Andrade et al. fabricated PHEMA-coated activated charcoal hemoadsorbents and tested their ability to adsorb uric acid and creatinine from sheep. The group observed uric acid clearance rates of ~40 mL/min, with marginally lower creatinine clearance rates.[51] Siemsen et al. evaluated the once-weekly use of a hemoperfusion device containing an uncoated charcoal adsorbent in augmenting the hemodialysis regimens of a small group of ESRD patients. Much like Andrade et al. observed in sheep, Siemsen et al. found that the charcoal hemoperfusion device was successful at removing significant amounts of creatinine and uric acid.[52] Despite the use of uncoated charcoal as the sorbent system, the group reported that only transient hypotension was a recurring complication.[52] Denti et al. studied the safety and efficacy of activated charcoal, both uncoated and coated with cellulose-triacetate, in the removal of molecules of varying sizes from artificial blood. The group observed that uncoated charcoal had much higher adsorption efficiencies which slowly diminished as the molecular weight of the adsorbate increased.[44] Cellulose tri-acetate coated charcoal was shown to exhibit significant adsorption of low molecular weight molecules but was completely unsuccessful at removing molecules of high molecular

weight (less than 5% of 40kD peroxidase adsorbed).[44] The latter effect confirms the inability of high molecular weight substances to traverse the porous cellulose-triacetate matrix. Comparisons made by the same group of the clearance of vitamin-B12 (1,355 Daltons) by both standard hemodialysis and hemoperfusion with cellulose-triacetate charcoal showed the hemoperfusion system to be more effective at the removal of middle molecular weight substances.[44] A more comprehensive review by Winchester and Ronco, regarding the use of charcoal hemoadsorbents for removing uremic toxins in end-stage renal disease, is available.[30]

As illustrated by the numerous quantities and varying types of adsorbates studied in the literature, activated charcoal has the ability to adsorb a wide range of substances. In contrast to other purification systems, where broad-spectrum solute removal could be seen as advantageous, it is most often a disadvantage in hemoperfusion. Blood necessarily preforms numerous complex roles, such as pH balance, mineral homeostasis, cellular nourishment, waste removal and the transmission of endocrine signals. The extraction of off-target molecules can therefore induce deleterious systemic effects on a patient through the significant alteration of blood composition. In spite of its long-standing place as one of the only clinically utilized hemoperfusion systems, activated charcoal's inability to exhibit binding specificity places severe limitations on its use as a hemoadsorbent going forward.[23,53,54]

2.1.3.2 Polymer-based Hemoadsorbents

Typical polymer-based sorbents for hemoperfusion are either ion-exchange resins or non-ionic macroporous resins,[30] although fibers[47,55,56] have been occasionally used. Ion-exchange resins are capable of removing dissolved ions from whole blood by exchanging one loosely-bound surface ion for another. These exchange-resins are better suited for the removal of protein-bound and lipid-soluble substances than activated charcoals.[48] Assemblages of highly cross-linked microspheres constitute the non-ionic resins and impart an extraordinary degree of porosity to the overall macrosphere structure.[30] These macroporous resins are best suited for the adsorption of organic solutes and, despite their extremely high surface area, do so through only weak van Der Waal's forces.[30] As a result, solute binding by non-ionic resins is frequently unstable and quite easily reversed. Resin-based hemoadsorbents are particularly conducive to the customization of their surface properties and can be outfitted with a vast array of surface-bound ligands, namely amino acids, proteins, enzymes, antibodies and antibiotics. By imparting ligands on the surface that show favorable binding characteristics with target-molecules, highly potent and extremely selective adsorption vehicles can be constructed.[57] Such strategies have been the basis behind the recent wave of research involving resin-based hemoadsorbents for the treatment of Sepsis. In Sepsis, endotoxins that are chiefly produced by gram-negative bacteria trigger destructive inflammatory responses that can eventually lead to multiple organ failure.[31,48,55] By covalently linking L-lysine amino acids to the surface of cellulose beads, Fang et al. were able to produce a hemoperfusion system that demonstrated rapid

reduction of endotoxin levels in Septic rabbits, with overall endotoxin reductions reaching almost 93%.[47,58] In a testament to the natural biocompatibility of both cellulose and lysine, the authors observed that endotoxin reductions were accompanied by limited side-effects.[58] Perhaps the most clinically successful polymer-based hemoperfusion system, developed by Toray Industries Inc., consists of a cartridge containing the antibiotic polymyxin-B immobilized on polystyrene fibers.[55] The fiber-bound polymyxin-B has both a high affinity for endotoxin and is capable of disrupting the cell-membrane of gram-negative bacteria.[31,55] Clinical hemoperfusion data indicated that circulating endotoxin was efficiently removed by the styrene-polymyxin-B system and that hemodynamic dysfunction associated with septic shock was subsequently alleviated, leading to marked improvements in liver function.[31,55] As of 2011, Toraymyxin was utilized in the hemoperfusion of over 80,000 patients and contributed to significant reductions in mortality rates versus conventional therapies.[59] Many other polymers and polymer resins have been studied for their potential utility in hemoperfusion systems and have been reviewed by Wang and Yu.[47]

2.1.3.3 Inorganic Hemoadsorbents:

Evidence of the exploration of inorganic adsorbents for use in hemoperfusion is scarce in the literature and the few available reports involving inorganic hemoadsorbents are generally limited to metal oxides[32,45] and silica-based materials.[60,61]

Due to their amphoteric nature and customizable surface properties, metal oxides are particularly intriguing matrix materials for the fabrication of hemoadsorbents. However, biocompatibility is a persistent concern associated with certain metal oxides.[62] Spengler et

al. combined cross-linked dextran with iron(III) oxide-hydroxide to create a novel adsorbent system for the removal of phosphate. The group observed significant calcium and phosphate reductions in preliminary in-vitro tests with sheep whole blood (2.04g of phosphate per liter of adsorbent) and similar results, accompanied by minimal reduction of cellular components and the absence of hemolytic occurrences, in in-vitro sheep models.[32] While the dissociation of the Fe^{3+} ion was a chief concern, heat sterilization of the adsorbent was shown to effectively halt dissociation of the iron-oxide and reduce observed Fe^{3+} concentrations in the test solutions.[32] Subsequent experiments with combined hemoperfusion-hemodialysis in sheep showed that the system safely facilitated the removal of 96.9% of phosphate, with tailored dialysate compositions correcting the calcium reductions seen in-vitro.[32] Sideman et al. observed that zirconium oxide coated in cross-linked agarose also displayed a phosphate removal efficiency of 64% when applied as a hemoperfusion system for the treatment of hyperphosphatemic dogs.[45] While the authors observed low incidence of protein adsorption, high degrees of calcium removal that occasionally outpaced phosphate reduction was noted.[45]

Aluminum Oxide has been shown to be an effective adsorbent for phosphate from simulants,[32] plasma[32] and whole blood[32,63] and is susceptible to surface modification through a large number of chemical reactions.[64] However, the attribution of aluminum ion accumulation to the development of neurological disorders observed in dialysis patients has stymied research involving the use of aluminum oxide as a hemoadsorbent. Perhaps owing to anxiety surrounding this issue, an exhaustive search of the literature identified only one

study where aluminum oxide was utilized for a direct blood-contacting application. Denti et al. created a combined hemodialysis-hemoperfusion system by impregnating cuprophan hollow-fibers with a granular aluminum oxide core.[63] Bench-top results using solutions of phosphate-buffered saline showed the efficient removal of phosphate from a solution of phosphate-buffered saline.[63]

3. TMA-Alumina

Recent advances in wastewater treatment have identified a phosphate selective adsorbent, known as TMA-Alumina, that can provide efficient phosphate reduction from solutions that span a wide range of pH values.[65] By applying trimesic acid (1,3,5 – benzenetricarboxylic acid) to basic alumina in a methanol solvent, the adsorbent complex can be manufactured in large-scale using cost-efficient raw materials that are commercially mass-produced. This chapter provides an incomprehensive background of the industrial synthesis, crystal structures, surface properties and adsorption behaviors exhibited by alumina, as well as an overview of the current state of knowledge surrounding TMA-Alumina.

3.1 Alumina

Alumina is a metal oxide that exists in its equilibrium form (α-alumina), and in the absence of contaminants or doping agents, as a crystalline solid with the chemical formula Al_2O_3. Commonly referred to as aluminum oxide, alumina is primarily produced through the dehydration of various aluminum hydroxides (gibbsite, bayerite and nordstrandite) and aluminum oxy-hydroxides (boehmite, diaspore and pseudoboehmite). These aluminum hydroxides and oxyhydroxides are pervasive in nature and are found in common minerals in

chemically complexed forms. Of the numerous aluminum-containing minerals, bauxite is the most important, as it is the aluminum ore from which most production of the synthetic aluminum oxides originates.[66,67] Bauxite is also the most omnipresent of all aluminum ores and is predominantly composed of three aluminum hydroxide minerals – gibbsite, which is a trihydroxide with the chemical formula $Al(OH)_3$; and boehmite and diaspore, which are oxide-hydroxides with the chemical formula AlO(OH).[66–69]

3.2 The Bayer Process

To extract these aluminum hydroxides from bauxite ores, a process invented in 1888, by the Austrian chemist Carl Joseph Bayer, is used. The Bayer Process, as it has come to be named, begins with the digestion of crushed bauxite ore in highly alkaline sodium hydroxide (pH > 14) at high temperature. After a sufficient duration, this digestion results in the dissolution of gibbsite, boehmite and diaspore from the bauxite ore and effectively separates these aluminum containing minerals from the insoluble "red mud" that is also present in natural bauxite. Once the solid red mud is removed, the resulting aluminate ($NaAlO_2$) solution is cooled, inducing recrystallization of the supersaturated solution to the aluminum hydroxide. The specific type of hydroxide formed during recrystallization is heavily dependent upon the reaction environment.[68,70–73] Indeed, Li et al. showed that dilute aluminate solutions, originating from lower initial concentrations of sodium hydroxide, preferentially recrystallize to form bayerite, while concentrated aluminate solutions result in the formation of gibbsite.[70] This observation was made in the absence of seed crystals, whose addition to the supersaturated aluminate solution can direct the precipitation pathway

towards a particular hydroxide type.[68,70–73] Panias et al. found that the application of gibbsite seeds always dictates the precipitation of the gibbsite tri-hydroxide, in a manner independent of solution temperature and composition.[71] The precipitate type formed in the presence of boehmite seeds depends on both temperature and solution composition.[71] While modifications to the Bayer Process can also enable the production of other hydroxides; gibbsite's ease of synthesis and ability to subsequently form all commercially relevant aluminas make it the most significant of the alumina precursors.[74] For these reasons, the remainder of the discussion involving alumina will assume origination from a common gibbsite starting material. Following the complete recrystallization of the aluminate solution to gibbsite, the solid particulates are filtered from the solution and washed with water to remove any residual caustic soda. Though the calcination of all aluminum hydroxides above 1050°C yields only the most thermodynamically stable α-alumina, various transition phases of alumina can be attained by varying the starting material and the temperature used in the dehydration process.[67,69,74–77] Employing gibbsite as the tri-hydroxide staring material, the application of increasing calcination temperatures first yields the aluminum oxide-hydroxide boehmite, followed by the γ, δ, and θ transition phases of alumina and finally the thermodynamically stable α-alumina (Figure 2).[68,74,75,77,78]

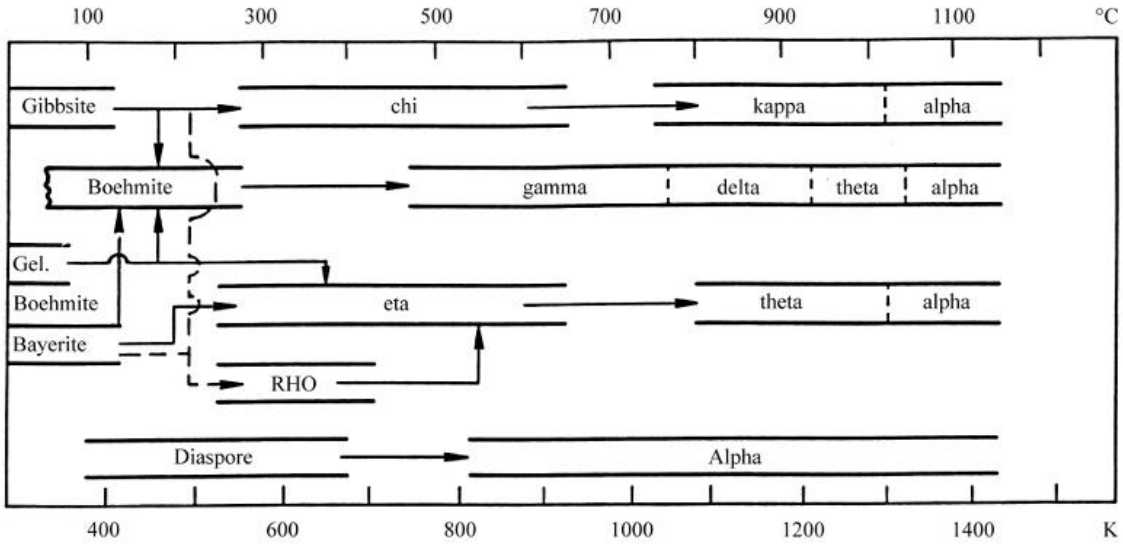

Figure 2. Representation of the transition aluminas and stable alpha-alumina formed by the calcination of various aluminum hydroxides over a range of temperatures.

3.3 Alumina Crystal Structure and Surface Properties

The thermal heating of gibbsite above 300°C results in the dehydroxylation of the material, which introduces spinel structures and creates a system of lamellar pores between the individually stacked platelets.[79] The porous alumina product, known as gamma-alumina (γ-alumina) is characterized by a cubic crystal structure with defect spinel structures,[78] where 70-75% of the aluminum cations present are located in octahedral sites.[80] Like all of the transition aluminas, the oxygen sublattice forms a face-centered cubic structure.[78] Gamma alumina is commercially produced in large quantities and is most widely used in catalyst and adsorbent applications. Further increasing the calcination temperature to a temperature above 750°C promotes further growths in porosity between the stacked platelets, a trait that is characteristic of delta-alumina (δ-alumina).[79] At a calcination temperature of 950°C, thermodynamic energy requirements dictate a re-organization of the aluminum cations in a

manner that causes the reorganization of the cation lattice to a monoclinic structure.[78] Accompanying this re-organization is a relocation of the aluminum cations to octahedral and tetrahedral positions of the sub-lattice in equal numbers.[81] The final phase of alumina, achieved by the high temperature calcination of all other aluminas, is α-alumina, which is stable and is therefore not deemed a transition alumina. The transformation to alpha-alumina involves the realignment of the aluminum crystal sublattice to a rhombohedral structure, as well as reorganization of the oxygen sublattice to a hexagonal close packed structure.[81] In alpha-alumina, two-thirds of the aluminum cations are found in the octahedral interstitial sites.[78]

The presence of aluminum cations in tetrahedral or octahedral vacancies and the relative interaction of each vacancy to the atoms on the material's surface dictate the chemical surface properties of each alumina phase.[77] Variations in the coordination numbers observed for surface atoms on the different types of alumina cause deviations from local charge neutrality and can render an alumina surface basic, neutral or acidic. Aluminum cations with unsatisfied bonds, due to the presence of nearby vacancy sites, serve as electron pair acceptors (lewis acid), whereas negatively charged oxygen surface groups serve as electron pair donors (lewis base).[77] Moreover, the -OH groups bound to tetrahedral aluminum atoms act as Bronsted bases, while Bronsted acids are formed from the bridging of a hydroxyl group between one tetrahedral and octahedral aluminum atom.[75] Basic alumina typically has a pH of 9-10 when combined with water, in a 10% slurry, and is generally used to separate basic and neutral compounds from solution. Acidic alumina has a

pH of 4-5 (in slurry) and is most often used in chromatography applications which involve strong acids that would otherwise chemically bind to the surface of basic alumina.

The overall charge of the alumina surface is another important surface characteristic of the material that strongly dictates the behavior of the material in a variety of applications. Similar to the isoelectric point of a material, the point of zero charge (PZC) describes the pH value at which a material surface carries a net electrical charge of zero. As the surface charge of a material can provide repulsive or attractive electrostatic effects between the surface and surrounding molecules, the PZC is an important parameter to consider when designing or analyzing an adsorption process. Depending on the pH of the surrounding environment, alumina is able to play the role of either a base or an acid and is therefore said to be amphoteric. When the pH of a surrounding solution is greater than the point of zero charge of the alumina (pH > PZC), the surface of the alumina becomes negatively charged. In contrast, when the pH of the surrounding solution is less than the point of zero charge of the alumina (pH < PZC), the surface of the alumina is positively charged. The point of zero charge is routinely assessed and has been studied extensively for alpha-alumina and gamma-alumina, with few studies published on the PZC of other alumina phases. Electrophoretic methods, streaming potential measurements, titrations and potentiometric titration methods have been described throughout the literature as successful methods for the elucidation of the PZC of a material. The point of zero charge for alumina reported in the literature often varies, based on the phase of the alumina analyzed and the presence of any adsorbed ions or molecules. Kasprzyk-Hordern et al. found that the point of zero charge

of alumina varied between 7.0-10.0, depending on the type of alumina and measurement technique used.[77] Kosmulsky et al. analyzed the reported PZC results of 155 different studies that dealt with alpha-alumina or gamma-alumina and found little significant difference between the averages reported for alpha-alumina and gamma-alumina, despite known structural differences for these two alumina types.[82] The analysis made by these authors showed that the average PZC value reported in the 155 studies was 8.55 for alpha-alumina, with a standard deviation of 1.10 and 8.40 for gamma-alumina, with a standard deviation of 1.15.[82]

3.4 Adsorption of Polycarboxylic Acids on Alumina

Various factors influence the adsorption of organic acids onto alumina, including the pH of the medium, the surface area of the alumina, the surface-charge of the alumina (PZC) and the chemical structure and pKa of the organic acid.[83–85] Research on the adsorption of various polycarboxylic acids by alumina surfaces have elucidated the mechanisms and adsorption characteristics involved in these processes. Borah et al. studied the adsorption of hemimellitic, trimellitic and trimesic acids on alpha-alumina and found that the magnitude of adsorption was highest for hemimellitic acid and followed the sequence of hemimellitic acid > trimellitic acid > trimesic acid.[83,84] The authors observed that the adsorption efficiencies of hemimellitic acid and trimellitic acids were 1.1 times and 1.7 times greater than that observed for trimesic acid.[83,84] Moreover, the kinetics of adsorption analyzed by Borah et al. demonstrated that the time to adsorbent saturation was the fastest for hemimellitic acid (60 minutes), was slightly slower for trimellitic acid (100 minutes), and

was the slowest for trimesic acid (120 minutes).[83,84] Mao et al. studied the adsorption of maleic acid and acrylic acid by an acidic version of activated alumina and found that the kinetics of adsorption were heavily dependent on the pH of the tested solutions. The adsorption rates and magnitudes of adsorption of both organic acids were the greatest when the pH of the solution was maintained at a value that was close to, but slightly lower than the pKa of the acids.[85]

Though the overall adsorption kinetics and magnitudes of adsorption on alumina differ for the range of carboxylic acids studied in the literature, the mechanisms proposed by the authors are largely consistent. Borah et al. noted that the adsorption exhibited by hemimellitic acid, trimellitic acid and trimesic acid resulted in the formation of outer-sphere complexes of these acids with the alpha-alumina surface.[83,84] This type of binding was also observed by Mao et al. for acrylic acid and maleic acid on acidic alumina,[85] suggesting that the adsorption of carboxylic acids on alumina proceeds by the same mechanism, regardless of whether the carboxylic acid is aliphatic or aromatic. Mao et al. also found that the kinetics of the adsorption processes of maleic acid and acrylic acid were well correlated with Langmuir models, suggesting the formation of monolayers of the organic acids on the alumina surfaces.[85] Taken together, these studies also indicate that increasing the numbers of carboxylic acids increases the adsorption rates and overall adsorption capacities of the carboxylic acids on alumina surfaces.[83–85] Morever, in the case of aromatic polycarboxylic acids, when the number of carboxylic groups on the benzene ring is equal, the adsorption kinetics and adsorption capacities are greater with the carboxylic groups positioned

adjacent to one another.[83,84] Finally, of paramount importance in the current research, Borah et. al found the adsorption of trimesic acid on the surface of alumina to be both thermodynamically favorable and in good agreement with the Langmuir model,[83] indicating that strong and facile adsorption occurs, resulting in the formation of a monolayer of trimesic acid on the alumina surface.

3.5 TMA-Alumina Adsorption Characteristics

A thorough search of the literature revealed that studies identifying and characterizing TMA-Alumina as a potent and selective adsorbent were performed exclusively by Saha, Chakraborty and Das.[65,86,87] These studies demonstrated powerful adsorption capabilities of TMA-Alumina for various adsorbates in simulated wastewater systems. Growing concerns with the pollution of aquatic reservoirs led the authors to evaluate the adsorption affinity of TMA-Alumina for iron,[88] copper[86] and phosphate,[65] three pollutants that are especially common in run-off from industrial manufacturing sectors.

Initial work performed by the research group showed that a treatment solution composed of 100 mg of TMA and 500 mL of methanol was ideal for providing an optimal coating of TMA on the alumina substrate.[86] Moreover, the initial work indicated that strong hydrogen bonding between TMA and the alumina surface was facilitated by the carboxylic groups on TMA and the hydroxyl groups on the metal oxides,[86] consistent with the outer sphere complexes that were previously mentioned.[83,84] SEM images obtained by the group, before and after TMA-treatment, showed that the TMA coated alumina was composed of aggregates of smaller crystallites (~1 μm) than the surface of the untreated alumina[86] and

powder XRD studies showed no noteworthy peaks in the XRD spectra, indicating that the TMA-coated alumina adsorbent was highly amorphous.[86]

Batch-mode studies assessing Copper (II) adsorption showed the adsorption behavior of Cu(II) to be dependent on temperature (adsorption decreased with increasing temperature), pH (adsorption decreased with decreasing pH up until pH 4-5), and the amount of adsorbent used (adsorption increased with increasing adsorbent dose).[86] Iron (III) adsorption was shown to be efficient and selective over Fe(II), with the highest adsorption capacities taking place in acidic solutions.[87] High adsorption of Fe (III) by TMA-Alumina was observed at all pH values up until the precipitation of Fe(III) ensued at a pH value of 3.0.[87] Ultimately, Saha et al. concluded in separate studies that the TMA-coating enhanced the adsorption efficiency of the alumina substrate by 60% for Cu(II) and 322.58% for Fe(III) versus untreated alumina and provided an adsorption that was spontaneous and thermodynamically favorable.[65,86] Moreover, the adsorption of Fe(III) and Cu(II) fit well to the Langmuir isotherm, indicating a monolayer adsorption process where binding sites had equivalent affinity for the adsorbates tested.[86,87]

Saha et al. observed efficient phosphate binding by TMA-Alumina over a broader pH range (1.0 – 8.0) than the other molecules previously described in this section. Mechanistically, the authors illustrated that adsorption was facilitated by hydrogen bonding that occurs between the phosphate species and the carboxyl moieties of the TMA molecules (Figure 3), in a manner dependent on the pH of the test solution.[65] The adsorption process is pH-dependent because the chemical species of phosphate and the extent of TMA dissociation

are heavily influenced by the solution pH and the respective pKa values of phosphate and trimesic acid.[65] Saha et al. observed adsorption kinetics which exhibited rapid initial adsorption of phosphate that gradually tapered as saturation of the trimesic acid constituents ensued. Moreover, the overall phosphate adsorption capacity was increased by the addition of extra phosphate to the test solution, indicative of the influential nature of the diffusion gradient on the adsorption behavior.[65] Finally, the chemically selective nature of the TMA-Alumina adsorbent was confirmed by Saha et al., with experimental results indicating that 90% of phosphate contained in a complex electrolyte solution was removed, without significant reductions of the other anions (Cl^-, Br^- and NO_3^-) that were also initially present.[65]

At the physiological pH of 7.40, which is relevant to the current research, the phosphate adsorption on TMA-Alumina mimics the diagram shown below (Figure 3).[65] In this physiological scenario, the predominant phosphate species are HPO_4^{2-} (80%) and $H_2PO_4^-$ (20%)[12] and the carboxyl groups of the TMA molecules are completely deprotonated. Although the results of these various selectivity studies have been reported, there are no indications in the literature that TMA-Alumina was considered for use in biological purification applications and no reported studies have been done to characterize adsorption in physiological solutions. Therefore, the current research will, in part, comprise the first studies of its kind that assess the adsorption characteristics of TMA-Alumina in scenarios relevant to hemoperfusion applications.

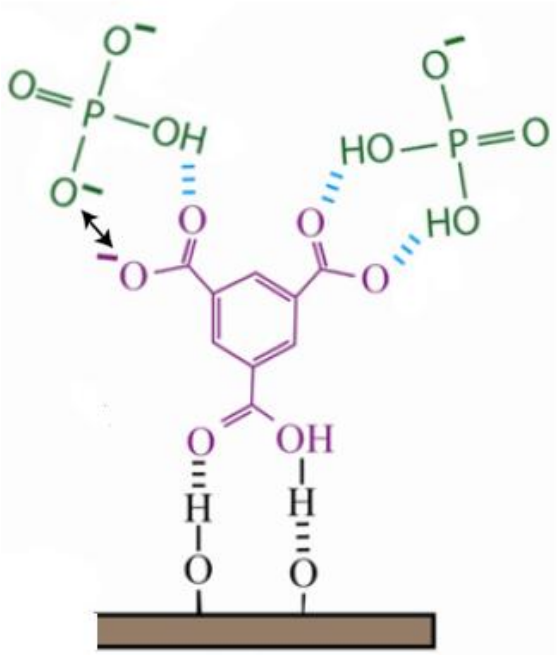

Figure 3. TMA species and phosphate adsorption observed at the physiological pH of 7.4. Representation adapted from.[65]

4. Objectives

The overarching aims of this research are to develop, characterize and evaluate a phosphate-selective hemoperfusion system that consists of TMA-Alumina hemoadsorbents immobilized on a hemocompatible textile scaffold. The ultimate end-goal of this work is to provide a safe and effective tool to augment the treatment regimens that are currently prescribed for managing hyperphosphatemia.

The specific objectives to achieve these ends are:

1. Characterize the properties of multiple alumina powders and compare their respective phosphate adsorption capabilities, following treatment

with trimesic acid. Select the most suitable candidate of these alumina powders for use in subsequent experiments.

2. Evaluate the efficacy of the grafting techniques of Carver® Press, Thermal Spray, SVI, and ALD for depositing alumina particles onto a textile substrate. Optimize the most favorable process, using the best alumina precursor from objective 1 (directly above).
3. Characterize the viable hemoperfusion system(s) that result(s) from objective 2 (directly above) and assess the phosphate adsorption capabilities in phosphate solutions and whole blood.
4. Evaluate the nature of adsorption in complex solutions and whole blood and determine the level of phosphate specificity.
5. Analyze the extent of particulate matter loss in blood from the viable hemoperfusion system(s), as a first look at biocompatibility.

5. Experimental Work

This chapter covers the materials and methods used in the fabrication of the TMA-Alumina hemoperfusion systems, the characterization of these systems and their raw material powders, and the experimental evaluations of adsorption behavior and biocompatibility of TMA-alumina grafted fabrics.

5.1 Materials

5.1.1 Alumina Powders

Three alumina powders of varying type and morphology were utilized in this research in order to identify an optimal hemoadsorbent formulation and to suit the unique requirements of each method used for uniting alumina and textile substrate. Two of the alumina powders were basic alumina chromatography powders that were activated and displayed a Brockmann activity of I. The first of these chromatography powders was procured from Acros Organics (Acros Organics, CAS:AC18999-0051)[1] and consisted of irregularly shaped particles with diameters ranging from 50-200 μm and a reported surface area of 135-165 m^2/g. Similarly, the second alumina chromatography powder, obtained from Selecto Scientific (Selecto Scientific, CAS:157024)[2], was comprised of irregular shaped particles of 63-150μm diameters and an overall surface area of roughly 115m^2/g. A third alumina powder sample, Al-1110 HP (Praxair Surface Technologies, CAS:EM8 56773)[3], which is uniquely formulated for thermal spraying applications, was procured from Praxair Surface Technologies and is a spherical powder of particle sizes ranging from 5 – 22 μm. For simplicity and disambiguation, the two chromatography alumina powders are identified henceforth by the names of their respective manufacturers (Acros Organics and Selecto Scientific). The remaining alumina powder sample is hereafter identified by its intended application (Thermal Spray). Additionally, a variant of the Selecto Scientific chromatography

[1] 1 Reagent Lane, Fair Lawn, NJ 07410, USA
[2] 3980 Lakefield Court, Suwanee, GA 30024, USA
[3] Rue de Veyrot 25 1217, Meyrin, Switzerland

alumina powders, obtained by the exposure of this powder type to a ball-milling process (discussed later), was also utilized in this research. The properties specific to each of these powder types can be seen in the following table (Table 3).

Table 3. Physical properties and chemical compositions of the raw alumina powders, as reported by the respective manufacturers.

Aluminum Oxide Powder Formulation	Manufacturer	Bulk Morphology	Particle Size (μm)	Surface Area (m^2/g)	pH	Composition
Basic, Brockmann I, for chromatography	Acros Organics	Powder (irregular)	50 - 200	135 - 165	9 – 10 (in 10% aq. suspension)	> 99% Al_2O_3, < 0.4% Na_2O, < 300 ppm Fe_2O_3, < 300 ppm SiO_2
Alumina B Super I	Selecto Scientific	Powder (irregular)	63 - 150	~115	9.8 (in 10% aq. suspension)	> 99% Al_2O_3
Milled Alumina B Super I	Selecto Scientific	Powder (irregular)	5 - 20		9.8 (in 10% aq. Suspension)	> 99% Al_2O_3
Thermal Spray (Al-1110 HP)	Praxair Surface Technologies	Powder (spherical)	5 - 22			99.3% Al, crushed and fused

5.1.2 Substrates

Polyester fabrics, specifically designed for medical filtration applications, were utilized to provide a chemically inert and physically robust platform for the deposition of TMA-alumina hemoadsorbents. This textile substrate, Saaticare PES 41/14 (Saatitech, CAS:PES4114)[4], was procured from Saatitech and is composed of precision-woven monofilament poly(ethylene terephthalate) fibers, which create a uniform network of well-defined mesh openings.[89] The physical properties that are specific to these PET filtration fabrics can be seen in Table 4. The SaatiCare PES 41/14 filtration fabric is designed for medical filtration applications and is certified to USP Class VI, indicating that the fabric is not biologically reactive.[90] Due to the

[4] 247 Route 100, Somers, NY 10589, USA

necessarily high level of quality control and sterility involved in the manufacturing of the filtration fabrics, each fabric was rinsed in only deionized water for 60 seconds and dried in a vacuum oven at 50°C prior to use, unless otherwise noted.

Table 4. Technical specifications of the SaatiCare PES 41/14 filtration fabric, purchased from SaatiTech.

Mesh Opening (µm)	Open Area (%)	Mesh Count (n/inch)	Thread Diameter (µm)	Thickness (µm)	Porosity (%)
41	14	229	60	2.5	51

5.2 Grafting Methods

Various grafting methods were employed in order to firmly secure the micro-sized hemoadsorbents to the underlying material substrate and thus mitigate potential losses of particulate matter during the hemoperfusion procedure. Two deposition processes based on the physical linkage of alumina particles to the fabric substrate were explored during this research. These processes made use of a heated Carver® press and a flame-spraying technique, respectively, to physically adhere alumina particles to the PET fabrics with the aid of heat application. Two chemical grafting processes, atomic layer deposition and sequential vapor infiltration, were also explored during this research in an effort to provide robust linkages of alumina powders to PET fabrics via covalent bonding. Following the utilization of these processes to produce alumina-coated filtration fabrics, the efficacy of each grafting method was compared against one another by evaluating images produced by scanning electron microscopy, assessing the overall alumina masses added by each process

and by assaying the phosphate adsorption capabilities of each assembly after TMA-treatment.

5.2.1 Carver® Press

A standard manual bench-top laboratory heat press (Carver®, Model C)[5] was utilized to physically join alumina powders to PET filtration textile substrates. The Carver® press (Figure 4) is an apparatus that consists of a set of heated steel plates, with one fixed to an adjustable platform that can be raised and lowered and the other remaining stationary and fixed to the outside frame of the apparatus. The adjustable platform can be manually raised and lowered via the action of a hydraulic jack mechanism. When the platform is fully raised, both steel plates contact one another, creating a clamping force of up to 24,000 pounds (9071.85 kg). A pressure gauge is connected to the hydraulic system to provide accurate pressure readings for reproducible grafting operations. The temperature of the heated plates can be individually tailored by the manual adjustment of temperature controllers, which are linked to heating elements adjoined to the steel plates, and temperatures up to 650°F can be achieved.

The pressure reading that is displayed on the pressure gauge of the hydraulic Carver® press system is not directly indicative of the pressure that is applied to the sample, which is sandwiched between the steel plates (Figure 4). Rather, the analog pressure gauge displays the magnitude of the hydraulic pressure (P_{gauge}) that is present inside the hydraulic unit of the Carver® press at any given time. As the hydraulic jack handle is manually pumped, the

[5] 1569 Morris Street, P.O.Box 544, Wabash, IN 46992-0554, USA

pressure in the hydraulic system is increased, exerting a distributed force on the hydraulic ram that interfaces with the hydraulic fluid in the system. This resulting distributed force can be calculated by multiplying the hydraulic pressure indicated on the pressure gauge (P_{gauge}) by the surface area of the hydraulic ram (A_{ram}), as in Equation 1. As this distributed force acts on a rigid metal cylinder, it can be simplified to a concentrated upward force that is applied at the center of the hydraulic ram (F_{ram}). The upward-acting force (F_{ram}) causes the hydraulic ram to move upward until the displacement of the hydraulic ram reaches a maximum, as contact is made between the heated steel plate on the bottom, adjustable platform and the heated steel plate on the upper-most, stationary platform. Once the hydraulic ram can no longer be displaced, the force acting on the hydraulic ram (F_{ram}) by the mounting hydraulic pressure exerts a force on the contiguous steel plate. With further displacement prohibited, the upward force acting on the hydraulic ram (F_{ram}) is then applied directly to the adjacent square-shaped steel plate, creating pressure between the rigid steel plates (P_{plate}), and therefore applying this same pressure to the sample contained therein. The resulting pressure within the plates is a function of the surface area of the steel plate (A_{plate}) and can be calculated by dividing the upward force of the hydraulic ram by the total surface area of the steel plate (A_{plate}) as shown in Equation 2. In the same manner, the pressure applied to the sample (P_{plate}) can be expressed as a function of the other three aforementioned variables (P_{gauge}, A_{ram} and A_{plate}), as illustrated in Equation 3.

$$F_{ram} = (P_{gauge})*(A_{ram}) \quad \text{(Equation 1)}$$

$$P_{plate} = (F_{ram})/(A_{plate}) \quad \text{(Equation 2)}$$

$$P_{plate} = P_{gauge}*(A_{ram}/A_{plate}) \quad \text{(Equation 3)}$$

The cylindrical hydraulic ram has a radius of 1.02397 in. (2.6008 cm), meaning that the surface area of the ram that contacts the steel plate (A_{ram}) is 3.294 in.^{2} (25.316 cm^2). Moreover, the square-shaped steel plate has length and width dimensions of 6 in. (15.24cm), correlating to a surface area (A_{plate}) of 36 in.^{2} (232.258 cm^2). By plugging these surface area values in to Equation 3, a ratio can be calculated which allows for the pressure exerted on the fabric sample by the plate to be easily calculated by simply multiplying the pressure read from the pressure gauge (P_{gauge}) by this surface area ratio (A_{ram}/A_{plate}). Consequently, the pressure exerted by the plates on the fabric sample is the pressure displayed on the pressure gauge scaled by a factor of 0.0915 (Equation 5).

$$(A_{ram}/A_{plate}) = (3.294in^2/36in^2) = 0.0915 \quad \text{(Equation 4)}$$

$$P_{plate} = P_{gauge}*(0.0915) \quad \text{(Equation 5)}$$

In this research, the temperatures of the steel plates were initially varied between 300°F, 400°F and 500°F (148.9 °C, 204.4°C and 260°C) to determine which temperature produced the highest grafting yields and to assess how the application of each temperature affects the underlying fabric substrate. It was determined that fabrics Carver® pressed with alumina at 300°F, 400°F and 500°F (148.9 °C, 204.4°C and 260°C) showed measured alumina

depositions of 86.5mg, 138.7mg and 304.2mg, respectively. Despite accompanying dimensional and morphology changes, the 500°F (260°C) temperature was selected for use in all subsequent grafting operations due to the much greater alumina additions observed. Two additional thin, removable steel plates (15.24cm x 15.24cm) were utilized to sandwich the fabric samples and accompanying alumina powders, thereby holding all components in place during the subsequent grafting operations. Alumina powders (Acros Organics) were sprinkled on the top surface of one of the removable steel plates, providing a thin coverage of alumina on the steel surface. An appropriately sized PET filtration fabric sample (either 6cm x 9cm or 10cm x 10cm, depending on the experimental scenario in which the fabric was to be used) was then placed on top of the alumina powder layer. A second layer of alumina powder (Acros Organics) was then placed on top of the PET filtration fabric, ensuring thin coverage of the entire fabric surface area. Finally, the remaining thin, steel plate was placed on top of the alumina-fabric conglomeration. The fixed Carver® press plates were heated to 500°F (260°C) and the plates sandwiching the fabric and alumina powders were placed on the bottom fixed steel plate. The adjustable platform was then manually jacked up until the hydraulic pressure gauge read 4500 psi (31026.41 kPa), correlating to a pressure of 411.75 psi (2838.92 kPa) exerted on the sample sandwiched between the steel plates. The Carver® press was maintained at this pressure for 90 seconds and the removable steel plates, and accompanying alumina and fabric, were immediately removed. The PET fabric, with newly grafted alumina powders, was promptly taken out from between the two steel plates and allowed to cool for 60 seconds. This process,

beginning with the addition of alumina powders to the steel plate surface, was repeated two more times to ensure that three Carver® press cycles were executed.

After the completion of three Carver® press cycles, the fabric samples were washed with deionized water to remove residual, non-adhered alumina particles. The alumina-coated fabric was submerged in deionized water and manually agitated for 30 seconds. This process was repeated three times before the alumina-coated fabric was placed in a vacuum oven at 50°C to dry overnight.

Each fabric sample was massed once prior to the addition of alumina powders and the execution of the Carver® press protocol, again following each successive Carver® press cycle, and one last time after drying in the vacuum oven.

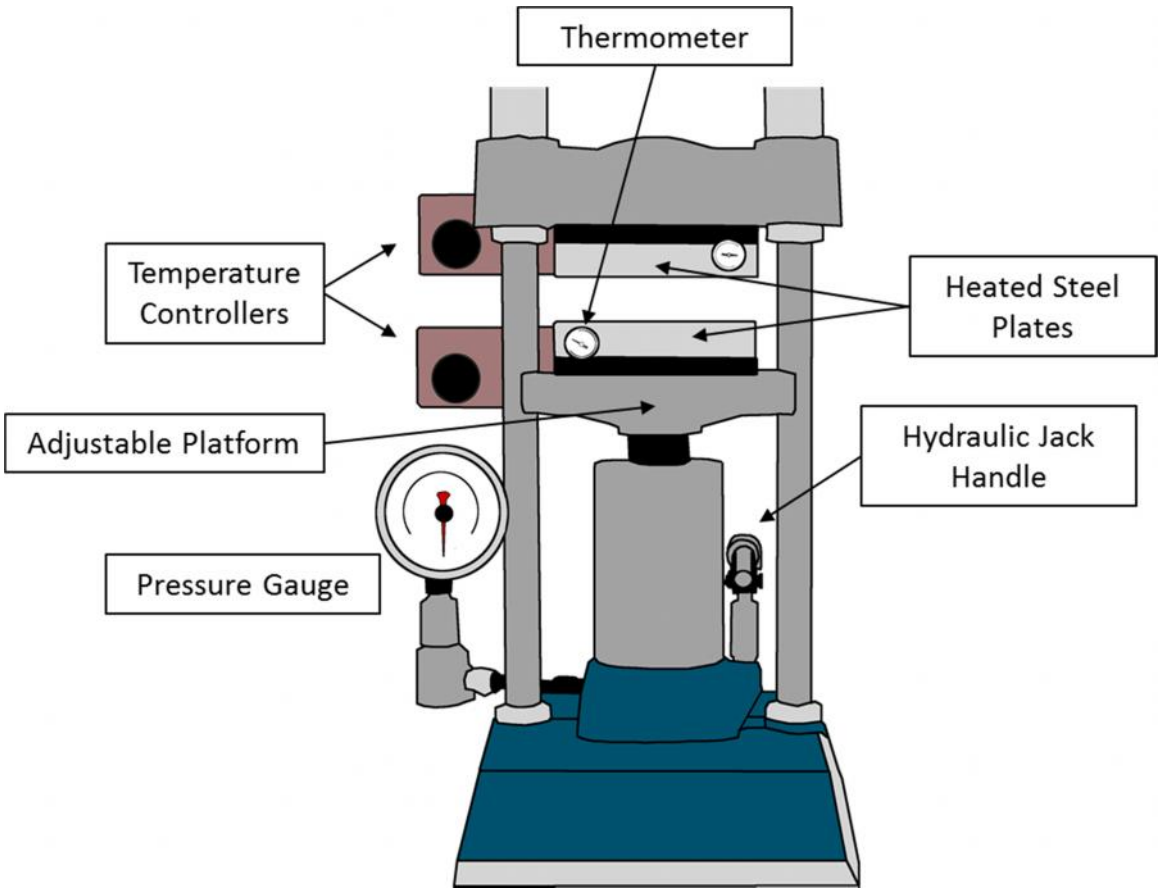

Figure 4. Schematic representation of the Carver® press apparatus utilized to graft alumina particles to PET filtration fabrics.

5.2.2 Flame-Spraying

A flame spraying technique, performed by the Center for Thermal Spray Research at Stony Brook University, was studied in order to evaluate the process's efficacy as a potential grafting method for uniting alumina powders materials with PET filtration fabrics. Two separate types of alumina (thermal spray and milled, Selecto Scientific) were individually grafted to the PET filtration fabrics through the use of a single powder flame spraying process (Figure 5). Alumina powder samples were loaded into the hopper of the flame spray

gun where oxygen or compressed air accelerated the powders toward the nozzle of the flame-spray torch. Once in the nozzle, the alumina powders were exposed to the oxygen-acetylene fueled flame where the accompanying heat transformed each particle into a semi-molten state. The semi-molten powders were then ejected toward the mounted PET filtration fabric where they were deposited onto the monofilament fibers of the substrate. The flame spray process made use of a low-velocity combustion powder spray with an approximate spray velocity of 40 m/s. The use of a reduced powder spray velocity mitigated deleterious effects that typically accompany the high-velocity impacts of ceramic particles on polymer substrates. Moreover, the flame-spray technique utilized a tailored ratio of acetylene and oxygen fuel sources to provide a constant flame-temperature of 2200°C, which is low relative to that of other common thermal spray variations. This reduced temperature also helped in maintaining dimensional stability and minimizing melting of the PET substrate.

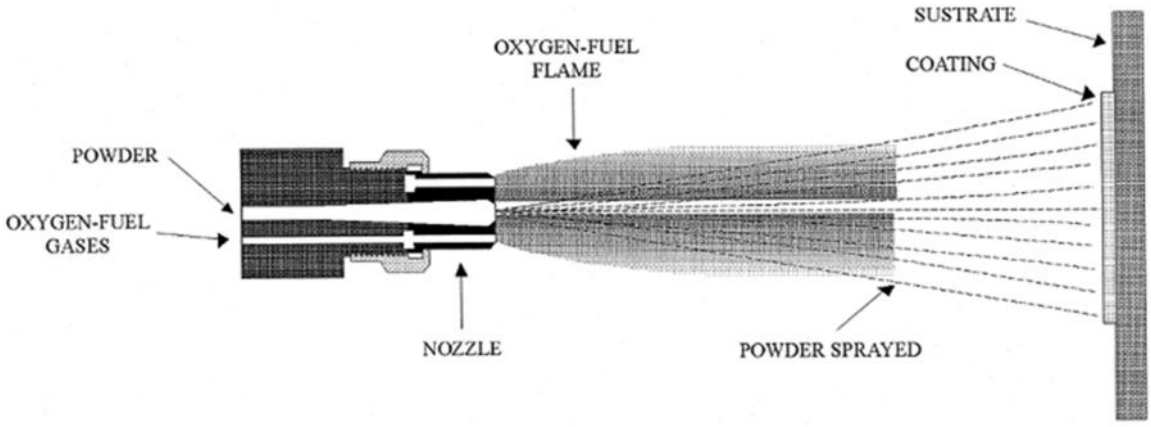

Figure 5. Schematic representation of the general flame-spray process used for grafting alumina powders to the PET filtration fabrics. Figure reprinted from [91]

5.2.2.1 Milling of Selecto Scientific Alumina Powders for Flame-Spraying

Commercially available chromatography powders, such as those mentioned above, are generally larger in diameter and more variable in particle size than thermal spray powders. Due to the need for powders to flow through the narrow channels found within thermal spray guns, only powders with specific particle sizes and particle size distributions are compatible with thermal spraying operations. Moreover, as larger powders require hotter flames to partially melt the individual particles, their use in this research would invariably melt the PET substrate. Therefore, in order to provide a powder sample with high surface area and basic character that could also be used in the thermal spraying process, the Selecto Scientific alumina powders were subjected to a ball-milling process that was performed by Union Process[6]. The ball milling operation was carried out using dry grinding in a 1-SDG batch attritor with a 1.5 gallon aluminum oxide tank, operating at 350 rpm and 0.80 horsepower. The grinding media used were 3/8" aluminum oxide balls and identical operations were performed two times for durations of 30 minutes each. The resulting powder that was produced from the milling operations displayed drastically reduced particle sizes and tighter particle size distributions, as analyzed by a Microtrac laser particle analyzer. The average particle size of the powders changed from 129.9 μm prior to the milling operation down to 19.67 μm after completion of the process. Also following the milling operation, 80% of the milled, Selecto Scientific powders were of particle sizes

[6] 1925 Akron-Peninsula Road, Akron, OH 44313, USA

between 1 µm and 29.00 µm. The milled powders were sieved using a 20 µm sieve but otherwise used as supplied, following ball-milling, for the flame-spray grafting experiments.

5.2.3 Atomic Layer Deposition and Sequential Vapor Infiltration Reactor

Grafting of alumina by atomic layer deposition (ALD) and sequential vapor infiltration (SVI) was carried out using a custom-designed viscous flow tube reactor (Figure 6). The reaction chamber is composed of a stainless steel tube that is 90 cm in length and 20 cm in diameter and is sealed with a vacuum flange. Prior to initiation of the ALD and SVI processes, an Alcatel 2021 SD mechanical pump was used to pump the reaction chamber down to vacuum conditions at a base pressure of < 20 mTorr. During both the ALD and SVI procedures, Nitrogen gas (Airgas National Welders, 99.999% N_2)[7] was used to provide a dry and chemically inert gas for delivery of the reactive components and for the subsequent purging of the reaction vessel of all reactive components. Prior to delivery of the Nitrogen gas to the reactor, an Entegris Gatekeeper inert gas purifier was used to remove any residual impurities and to ensure moisture content of the reaction vessel remained below 10 parts per trillion. The flow-rate of the N_2 gas was controlled using an MKS flow controller, allowing for the application of a precise mass-flow rate of 300 standard cubic centimeters per minute (sscm). Through the application of this mass-flow rate and the action of the mechanical pump, an internal pressure of 1 Torr was achieved within the reaction vessel during the ALD and SVI processes. Omegalux fiberglass heating tapes were utilized to achieve an internal reaction vessel temperature of 60°C. The trimethylaluminum (Strem

[7] 4301 Capital Boulevard, Raleigh, NC 27604, USA

Chemicals, Inc., CAS: 75-24-1, 98% purity)[8] and high purity water (Sigma Aldrich, biotechnology performance grade, CAS: 7732-18-5)[9] reagents were delivered to the N_2 gas flow through the use of Swagelok ALD pneumatic valves, with the valve sequencing controlled by a customized LabView™ program.

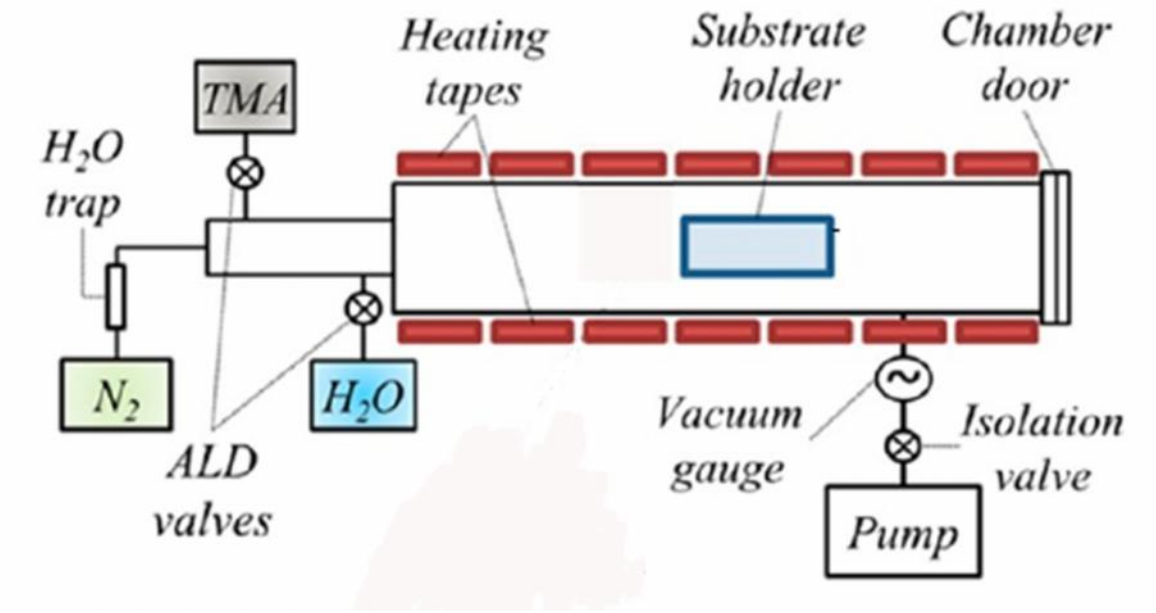

Figure 6. Schematic representation of the reaction vessel used for the experimental grafting of alumina to PET filtration fabrics via atomic layer deposition and sequential vapor infiltration.[92]

5.2.3.1 Atomic Layer Deposition

The atomic layer deposition process is a cyclical procedure comprised of the step-wise exposure of vaporized reactants to a material surface, which results in the self-limited growth of the reaction product distal to the material surface.[92] The process is initiated by the introduction of a vaporized reactant that provides surface functionalities that can react

[8] 7 Mulliken Way, Newburyport, MA 01950-4098, USA
[9] 3050 Spruce Street, St. Louis, MO 63103, USA

with the material surface and the next vapor, once introduced. An intermediate purging step using an inert gas is utilized for clearing out the residual initial reactants, prior to the introduction of the next vaporized chemical.

In the atomic layer deposition procedure used in this research, the reaction chamber was maintained at a temperature of 60°C and a pressure of 1 Torr. The reaction vessel was initially purged by the application of N_2 gas for 300 seconds, followed by the execution of 100 deposition cycles and a final purge with N_2 gas for 150 seconds (Figure 7). One deposition cycle consisted of the initial introduction of the trimethylaluminum dose for 0.3 seconds, followed by a purge with N_2 gas for 45 seconds, a subsequent dose of high-purity water for 0.3 seconds, and a cycle-ending N_2 purge for 60 seconds.

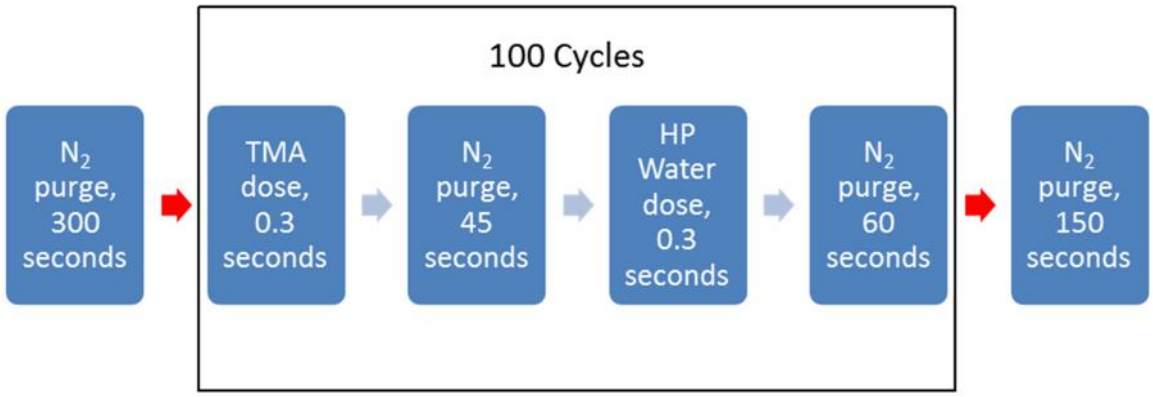

Figure 7. Process diagram of the atomic layer deposition process used to chemically graft alumina to PET filtration fabrics.

5.2.3.2 Sequential Vapor Infiltration

The sequential vapor infiltration process also makes use of step-wise introductions of trimethylaluminum and high-purity water precursors to the reaction chamber with the use of intermediate purging steps. However, the sequence of vapor exposure and exposure times used for SVI differs from that utilized in the ALD process. Furthermore, in SVI hold steps are used to increase the overall exposure of the reactants to the material substrate and the process does not alternate between exposures of each chemical species.[92]

In this research, the reaction chamber was maintained at a temperature of 60°C and a pressure of 1 Torr. The SVI process was initiated by purging the reaction chamber with inert N_2 gas for 300 seconds. Immediately following the initial purge step, 30 cycles that consisted of TMA dosing for 0.5 seconds, followed by a 30 second hold-step and then a 30 second N_2 purge were executed. Immediately following the 30-cycle TMA dose, 30 cycles, which consisted of high-purity H_2O dosing for 0.2 seconds, followed by a 30 second N_2 purge were performed. Finally, the SVI process was completed by one last purge step with N_2 gas for 120 seconds. An illustration of this process is provided in Figure 8 below.

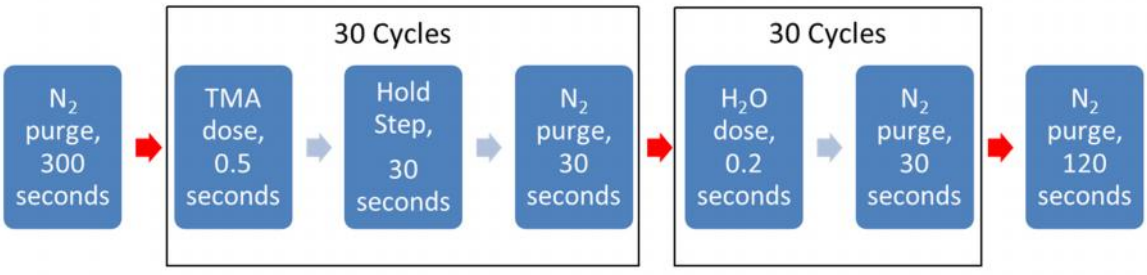

Figure 8. Process diagram of the sequential vapor infiltration process used to chemically graft alumina to PET filtration fabrics.

5.3 Scanning Electron Microscopy

Untreated alumina powder samples, TMA-treated samples of Acros Organics alumina powders, and PET filtration fabric substrates grafted with alumina by the various grafting methods described above were characterized by scanning electron microscopy (SEM). Samples were prepared for scanning electron microscopy by first sputter coating with a gold-palladium alloy using an Anatech Hummer 6.2 sputter coater. Following sputter coating, all SEM images, excluding the milled, Selecto Scientific alumina powder samples, were obtained by a FEI Phenom scanning electron microscope[10] using an acceleration voltage of 5 kV. Due to their smaller size and the need for greater magnifications, SEM images of the milled, Selecto Scientific alumina powder samples were obtained using a Hitachi S3200 variable pressure scanning electron microscope[11] with an acceleration voltage of 20 kV.

5.4 Grafting Yield Measurements

Masses were obtained for each fabric, both before and after the application of alumina through the chosen grafting method, by massing dried samples on a laboratory balance. Grafting yields were calculated for each alumina-coated fabric by subtracting the initial measured mass of the fabric sample by the final measured mass obtained after the completion of the utilized grafting process. The resulting grafting yields allowed for comparison of the relative effectiveness of each grafting method and aided in the selection of the most viable method for producing optimized hemoperfusion fabrics.

[10] 5350 NE Dawson Creek Drive, Hillsboro, OR 97124, USA
[11] 1375 North 28th Avenue, P.O. Box 612208, Dallas, TX 75261-2208, USA

5.5 Trimesic Acid Surface Treatment

Trimesic Acid (TMA) was coated onto the surfaces of alumina powders by scaling-up the reaction scheme outlined by Saha et al.[86] Trimesic acid (Acros Organics, CAS: 105355000)[12] was procured from Acros Organics and LC/MS-grade Methanol (Fisher Scientific, CAS: A456-500, 99.9% purity)[13] was procured from Fisher Scientific. 2.5g of TMA was dissolved in 500mL of methanol in a boiling flask with continuous stirring to provide the treatment solution. Powders were treated by the addition of 25g of each alumina powder type to the flask in a continuous fashion. Due to uncertainties in the effects of subsequent heat treatments on TMA-treated powders, the material substrates were first grafted with alumina and then exposed to the TMA treatment by submerging the alumina-coated fabrics in 100mL of the TMA-methanol solution. Regardless of the material type to be treated, the solution pH was maintained at ~2.5, a value close to the pK_{a1} of TMA, by the addition of hydrochloric acid. Once the material had been added to the reaction mixture and the pH had been stabilized at 2.5, the mixture was placed on an oscillating shaker and continuously agitated for a period of at least 6 hours. After this duration had elapsed, the material contents of the boiling flask were vacuum filtered and rinsed with methanol and deionized water to remove any unreacted trimesic acid. The resulting TMA-treated material was placed in a vacuum oven at 40°C to dry overnight.

[12] 1 Reagent Lane, Fair Lawn, NJ 07410, USA
[13] 300 Industry Drive, Pittsburgh, PA 15275, USA

5.6 X-ray Photoelectron Spectroscopy

X-Ray Photoelectron Spectroscopy (XPS) was carried out to investigate changes in the surface chemical composition of Acros Organics alumina powders that resulted from the application of the trimesic acid treatment. XPS data was obtained from a Riber LAS-3000 with MgKα excitation (1254 eV). Energy calibration was established by referencing to adventitious Carbon (C1s line at 284.9 eV binding energy). A takeoff angle of ~75° from surface was used with an X-Ray incidence angle of ~20° and an x-ray source to analyzer angle of ~55°. The base pressure in the analysis chamber was on the order of 10^{-10} Torr. Data obtained from the XPS investigation was analyzed by CASA XPS software, allowing for the calculation of percent atomic compositions of the alumina powder surface.

5.7 Bench-top Phosphate Adsorption Studies – Phosphate Solution

5.7.1 Phosphate Test Solution

Stock solutions of a 100 mg/L phosphate test solution were created by thoroughly mixing 143.68mg of potassium phosphate (Fisher Scientific, CAS: 7778-77-0)[14] with 1000 mL of deionized water. Test solutions of 10, 20, 40, 60, 80 and 100 mg/L phosphate were prepared from the stock solution by diluting the stock solution at ratios of PO_4 stock solution:Deionized water of 10:90, 20:80, 40:60, 60:40, 80:20 and 100:0, respectively. In the bench-top studies, a test solution volume of 50mL was used for experiments designed to evaluate adsorption characteristics of the powder samples; while a volume of 80mL was used for experiments involving fabrics, to ensure that the fabric-based adsorbent system

[14] 300 Industry Drive, Pittsburgh, PA 15275, USA

was complete submerged in the test solution throughout the experiment. In the studies which utilized the hemoperfusion circuit, a test solution volume of 1L was used. Prior to experimental use, the pH of each test solution was adjusted to a physiological pH of 7.4 by the incremental addition of sodium hydroxide or hydrochloric acid, as appropriate.

5.7.2 Phosphate Colorimetric Assay

In order to accurately assess the phosphate concentrations present in the experimental test solutions, a colorimetric assay kit was purchased from Biovision (Biovision, CAS: K410-500)[15]. The colorimetric assay exploits malachite green and ammonium molybdate reagents, which form a chromogenic complex with phosphate ions that are present in solution (Figure 9). Following uptake of phosphate, the reagent complex emits an intense absorption band of light at a wavelength of 650nm that can be subsequently measured with a spectrophotometer.[93] By utilizing the provided phosphate standard and plating samples of precise volumes that fall within the linear range of the calibration standard curve, the phosphate concentration of test solutions cans be calculated from the absorbance values yielded from the spectrophotometric analysis of the assay. The lower level detection limit of the assay is approximately 1 µm and phosphate concentrations between 1µm and 1 mM can be directly determined.[93]

[15] 155 South Milpitas Blvd., Milpitas, CA 95035, USA

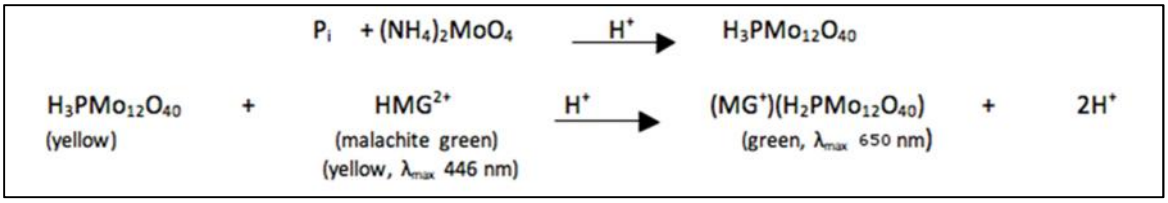

Figure 9. Chemical equations governing the complexation of inorganic phosphate (Pi) with ammonium molybdate and the ensuing formation of the malachite green-phosphomolybdate complex, with both steps occurring under acidic conditions.[93]

5.7.3 Experimental Bench-top Adsorption Assay

After preparation, an appropriate volume of phosphate test solution, at the desired concentration, was added to a clean 250mL plastic container. A 1mL sample ("pre") was taken from the container using a new 3mL syringe (Becton Dickinson, CAS: 305269)[16] and the sample was then transferred to a new 2.0 mL microcentrifuge tube for later analysis, with filtering of particulate matter done through a 0.22µm syringe-driven filter tip. Following the collection of this initial sample, the fabric or powder sample to be tested was inserted into the plastic container and the plastic container was placed into a shaking water bath (Thermo Scientific Precision Coliform Incubator Bath) that was maintained at a constant temperature of 37°C and a shaking speed of 135 rpm. Additional samples of 1mL volume were taken from the plastic container at the pre-determined intervals of t = 0, 10, 25, 50, 75, 100, 120, 150, 180, 200 and 240 minutes in order to establish kinetic profiles of phosphate adsorption. Collected samples were plated in duplicate along with calibration standards and analyzed using the Biovision Colorimetric Assay Kit and a Genios (Tecan) plate-reader in absorbance mode using a wavelength of 650nm. Absorbance values for

[16] 1 Becton Drive, Franklin Lakes, NJ 07417, USA

samples and standards were averaged between replicates and a set of calculations were made, referencing calibration standards, to determine the phosphate concentration that was present in the experimental solution at each time point and the extent of phosphate adsorption that occurred due to exposure of the solution to TMA powders or TMA-alumina. Absorbance values yielded from the spectrophotometer for the samples were fit to the calibration curve (derived from absorbance values for the standards) to determine the molar concentration (nM) of phosphate present in each sample. The resulting molarities were multiplied by the molar mass of phosphate and divided by the volume present in each well of the 96-well plate, yielding a ng/µL concentration, before final conversion of the units to mg/L. After multiplying the mg/L concentrations by the volume used in the respective experiment, a value indicative of the mass of phosphate present in each sample was yielded. All values of mass present after the initiation of the experiment were subtracted from the "pre" sample to yield data on the mass of phosphate removed (mg) at each time point. By dividing these phosphate mass reduction values (mg) by the amount of adsorbent used (g), phosphate adsorption capacities (mg/g) were derived. The phosphate adsorption capacity defines the mass of phosphate (mg) that was adsorbed from solution by a given mass of adsorbent (g) and can be used to compare the phosphate removal capabilities of similar systems that use varying masses of the same adsorbent.

5.8 Bench-top Phosphate Selectivity Studies

Hemoperfusion is only a viable treatment option for hyperphosphatemia if the adsorptive action of the hemoperfusion system is phosphate selective and devoid of the tendency to

remove non-target electrolytes and substances. In order to determine the selective or non-selective nature of adsorption exhibited by the TMA-alumina hemoperfusion fabrics, it was necessary to evaluate adsorption behavior in solutions that are more complex than the phosphate solution described above. For this reason, fabricated TMA-alumina fabrics were tested in a lactated Ringer's solution. Moreover, as patient blood is a complex and viscous solution consisting not only of electrolytes, but also cells and proteins, it was most pertinent to evaluate the adsorption behavior of these fabrics when exposed to whole blood samples.

5.8.1 Lactated Ringer's Solution

Lactated Ringer's solution, composed of 130 mEq of sodium ion, 109 mEq of chloride ion, 28 mEq of lactate, 4 mEq of potassium ion, and 3 mEq of calcium ion was procured from hospital central supply at the University of North Carolina at Chapel Hill[17]. The solution had an initial pH of 6.5 and was therefore adjusted to pH 7.4 through the incremental addition of sodium hydroxide, to more accurately mimic the physiological conditions of human blood. As lactated Ringer's solution is inherently devoid of phosphate, aliquots of the solution were spiked with potassium phosphate to achieve initial phosphate concentrations of 10 mg/L, 20 mg/L and 30 mg/L. The experiments to evaluate phosphate selectivity in a complex electrolyte solution were performed using the same protocol as the bench-top experiments described above, only instead using these phosphate-spiked lactated Ringer's solutions. The composition of lactated Ringer's solution, prior to the addition of potassium phosphate, is shown in Table 5.

[17] 101 Manning Drive, Chapel Hill, NC 27514

Table 5. Constituents of the Lactated Ringer's Solution and concentrations of each component.

Sodium (Na+) (mmol/L)	**Chloride (Cl-)** (mmol/L)	**Lactate** (mmol/L)	**Potassium** (mmol/L)	**Calcium** (mmol/L)
130.0	109.0	28.0	4.0	1.5

5.8.2 Bovine Whole Blood – Full Chemistry Panels

Heparinized bovine whole blood was purchased from Quad Five[18] in 1 liter aliquots with 50 units of heparin added to each liter prior to shipping. Once received, all whole blood samples were refrigerated until experimental use. In order to assess the level of phosphate selectivity exhibited by the TMA-alumina hemoperfusion fabrics when exposed to whole blood, bench-top experiments were performed using 50mL aliquots of each heparinized whole blood type. Blood volumes of 50mL were added to separate conical tubes and a 3mL sample was drawn from each tube by a 3mL syringe (Becton Dickinson, CAS: 305269), prior to the addition of the hemoperfusion fabrics. Each collected sample was transferred to a 5mL BD Rapid Serum Tube (Becton Dickinson, CAS: 368774)[19], in order to yield plasma for subsequent blood chemistry analyses. Immediately after collecting these initial samples, the appropriate hemoperfusion fabric samples were added to the respective conical tubes and the conical tubes were sealed and placed on a rotating tube inverter (Figure 10). The rotating tube inverter was allowed to rotate at 30 inversions per minute (15 rpm) for 60 minutes, before a final 3mL sample was taken from each tube and placed in a new Rapid Serum Tube for blood chemistry analysis.

[18] 361 Rothiemay Road, Ryegate, Montana 59074, USA
[19] 1 Becton Drive, Franklin Lakes, NJ 07417, USA

Figure 10. Photograph of the experimental set-up used for the phosphate selectivity experiments performed with heparinized bovine whole blood.

Following the collection of blood samples from the aforementioned experiment, the blood samples were spun down in a swinging bucket centrifuge at 1700xG for 10 minutes, which yielded plasma for use in laboratory analysis. The resulting plasma samples were delivered to the UNC-McLendon Core Laboratory, where a myriad of tests were performed to determine the concentrations of glucose, albumin, total protein, chloride, potassium, sodium, bicarbonate, phosphorus, creatinine, urea, calcium and magnesium present in each collected sample. Each of these analyte concentrations were measured using a Vitros 5600 Integrated Analyzer (Ortho Clinical Diagnostics)[20], using separate colorimetric,

[20] 100 Indigo Creek Drive, Rochester, NY 14626, USA

potentiometric or enzymatic assay slides. Details of the testing procedures that were used in assays of analyte concentration can be seen in the table below (Table 6).

Table 6. Details of slides used in conjunction with the Vitros 5600 analyzer to assay the analyte concentrations of plasma samples submitted to McClendon Labs at UNC-Chapel Hill.

Analyte Measured	Test Type	Reagents	Wavelength for Analysis (nm)
Glucose	Colorimetric	Glucose oxidase & Peroxidase	540
Albumin	Colorimetric	Bromcresol Green	630
Total Protein	Colorimetric	Cu^{2+}-Azo Dye Complex	670
Magnesium	Colorimetric	Chelator & Formazan Dye Derivative	
Calcium	Colorimetric	Arsenazo III	680
Urea	Colorimetric	Urease & Ammonia Indicator	670
Bicarbonate	Enzymatic Endpoint	Phosphenolpyruvate Carboxylase, Malate Dehydrogenase, Phosphoenolpyruvate, Nicotinamide, adenine dinucleotide	340
Phosphorus	Colorimetric	Ammonium Molybdate & p-methylaminophenol	670
Creatinine	Potentiometric	Silver & Silver Chloride	-
Chloride	Potentiometric	Silver and Silver Choride	-
Sodium	Potentiometric	Silver, Silver Chloride, Sodium Chloride, Methyl Monensin	-
Potassium	Potentiometric	Silver, Silver Chloride, Sodium Chloride, Potassium Chloride, Valinomycin	-

5.9 – Hemoperfusion Circuit Phosphate Adsorption Studies

After the efficacy of the TMA-Alumina grafted fabrics was proven in a bench-top setting, it was necessary to test the fabrics in a more dynamic setting that was applicable to the intended end-use hemoperfusion application. For this reason, a test device was designed

and fabricated to house the TMA-Alumina hemoadsorbent fabrics. The test-device was inserted into a simulated hemoperfusion circuit that was constructed based on an experimental dialysis circuit,[94] with several modifications.

5.9.1 – Hemoperfusion Test Device

The hemoperfusion test device, which housed the TMA-Alumina hemoadsorbent fabrics, was designed with fluid chamber geometries that were based on the reverse-engineering of existing flat-plate dialyzers (Figure 11).[95,96] The test device (Figure 12, Figure 13, and Figure 14) consists of a two-part polycarbonate structure, with a quasi-diamond internal cavity comprising the volume for fluid flow (Figure 12); a set of 10 fabric-spacers composed of expanded Polytetrafluoroethylene (ePTFE) for separating test fabrics from one another (Figure 13); and polycarbonate hose-barbs for inlet and outlet ports that allow passage of the circulating fluid into and out of the test device (Figure 13). The test device was used in experimental studies to house the TMA-alumina fabrics and provide a vehicle for providing fluid exposure to the TMA-treated hemoperfusion fabrics. The device provided a high degree of blood compatibility, laminar flows, and an internal structure conducive to the spreading of blood-flow across the entire surface area of the hemoperfusion fabrics (Figure 13).

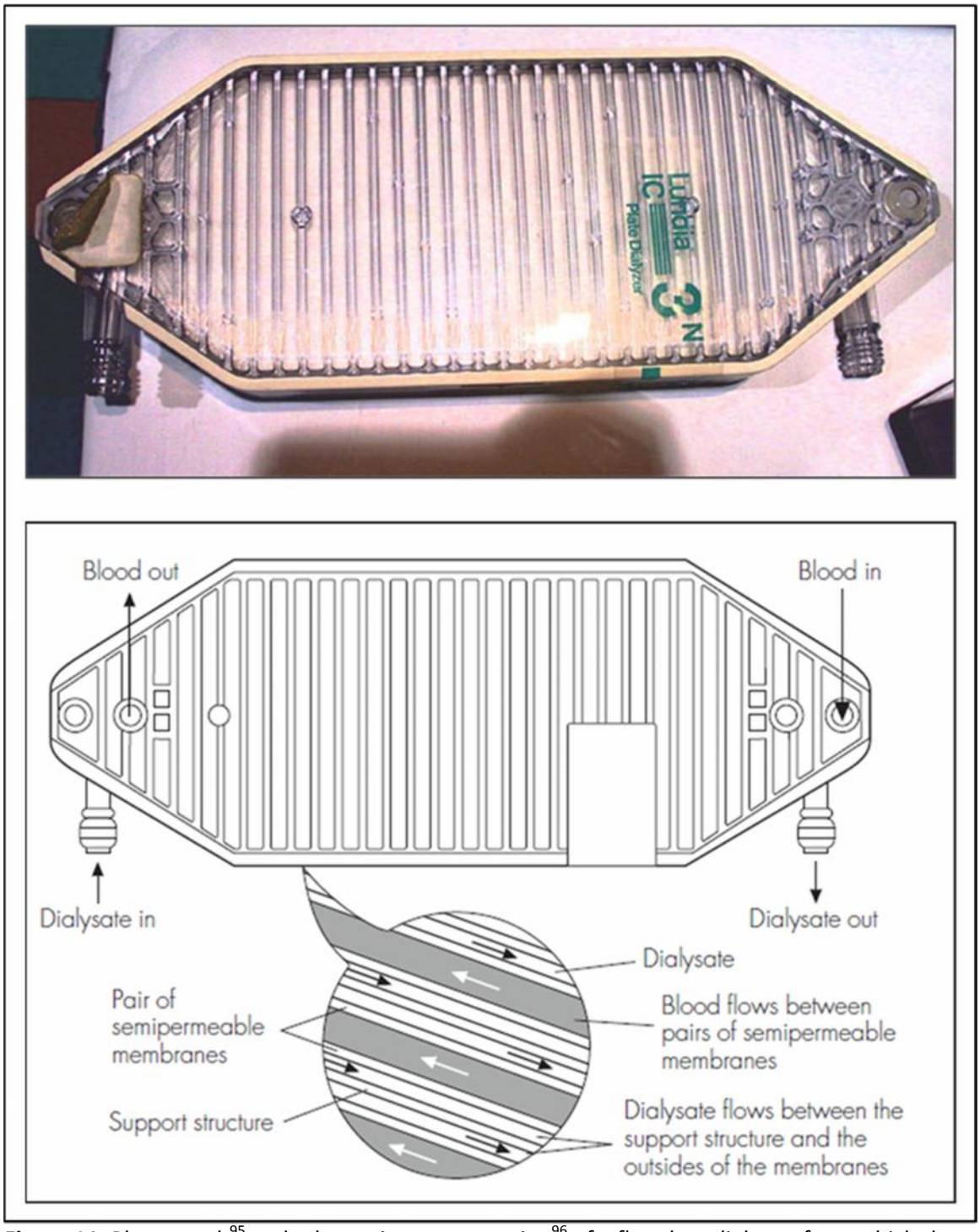

Figure 11. Photograph[95] and schematic representation[96] of a flat plate dialyzer, from which the design of the functional geometries of the hemoperfusion test device were based.

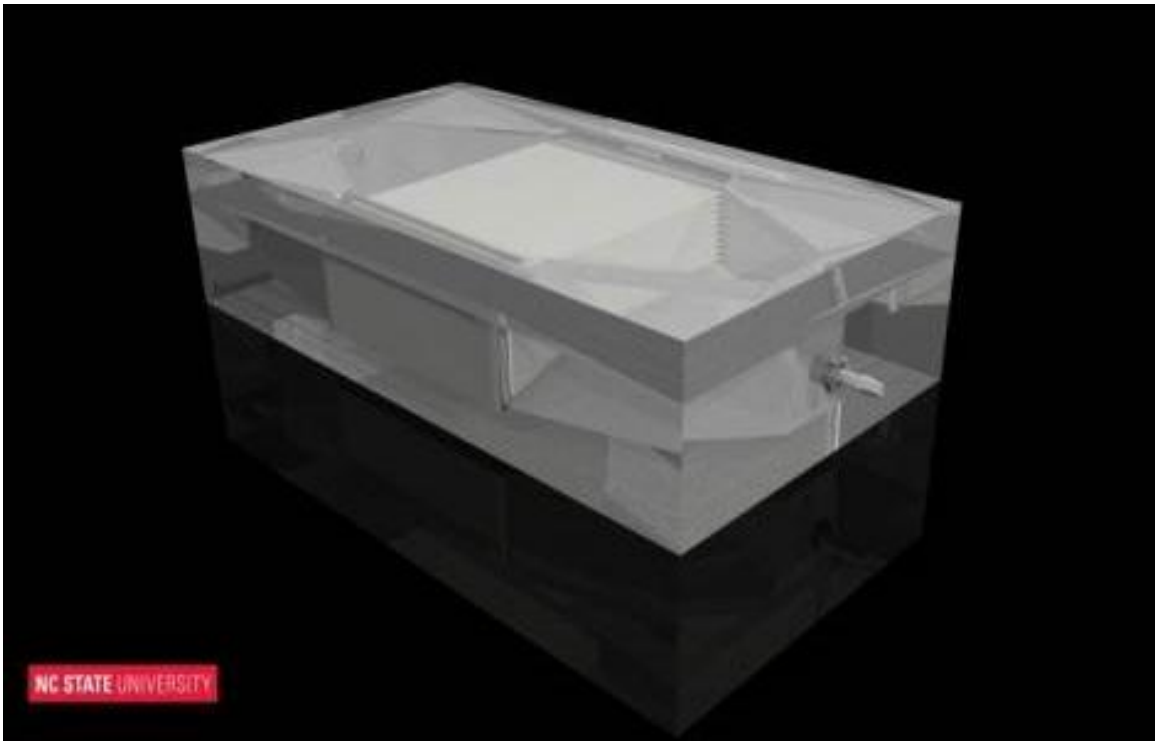

Figure 12. Rendering of the hemoperfusion test device, showing the assembled test device containing 10 TMA-alumina hemoperfusion fabrics.

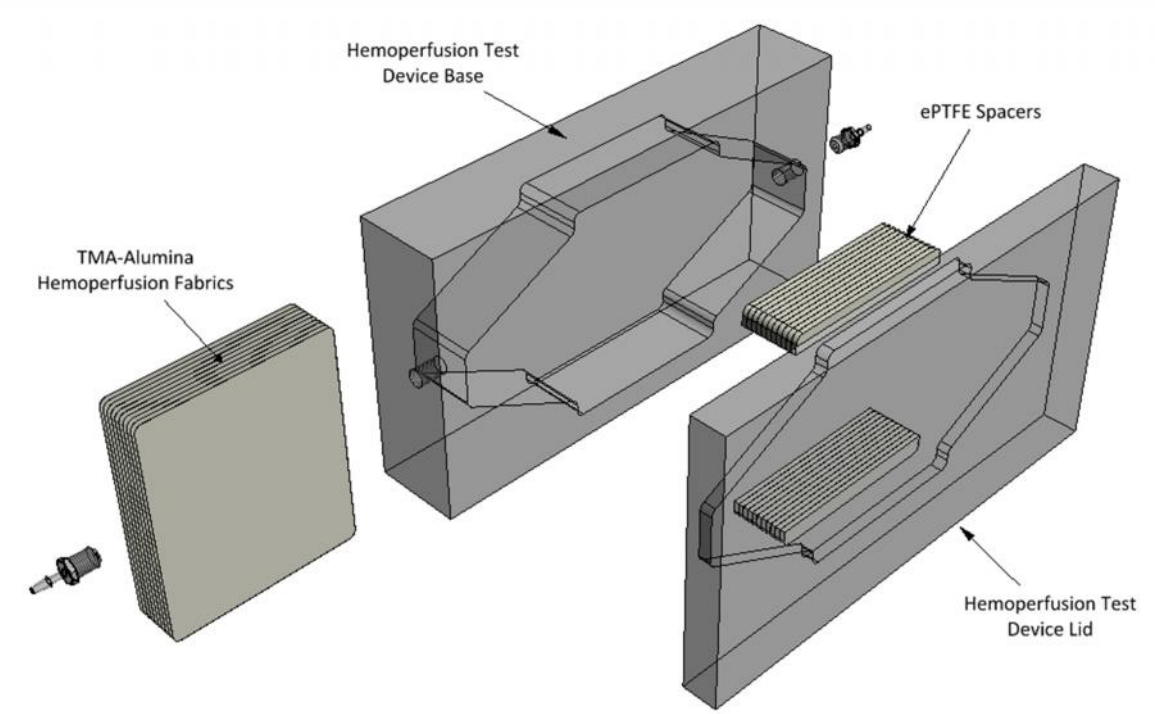

Figure 13. Exploded view of the hemoperfusion test device, showing the disassembled components.

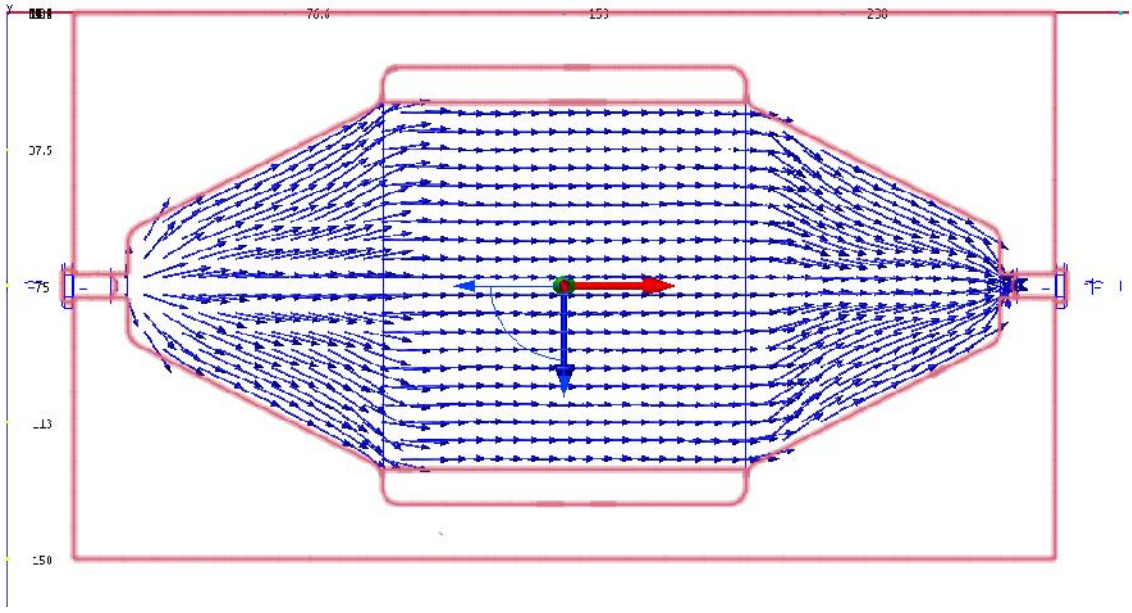

Figure 14. Top view of the assembled hemoperfusion test device. The results of a computational fluid dynamics simulation are displayed, illustrating the flow-paths of circulating blood.

5.9.2 – Hemoperfusion Circuit Design

A simulated circuit designed to mimic typical hemoperfusion systems was constructed in order to evaluate the efficacy of the TMA-Alumina hemoperfusion fabrics in a more clinically relevant setting. The circuit (Figure 15) was composed of a polypropylene Erlenmeyer flask that served as a blood/solution reservoir, an FH100 peristaltic pump (Thermo Scientific, 72-300-000)[21], the fabricated hemoperfusion test device, and a 3-way luer-lock stopcock that served as a sampling port. All of these components were connected by silicon tubing (Thermo Scientific, 72-300-025)[22] of a 4.8mm internal diameter that is blood compatible and designed for heavy-wear applications. In order to maintain a physiologic temperature of 37°C and provide adequate mixing of the contents, the polypropylene Erlenmeyer flask was submerged in a shaking water bath (Thermo Scientific Precision Coliform Incubator Bath)[23] that was set at 37°C and 90 rpm.

[21] 28W092 Commercial Ave, Barrington, IL 60010, USA
[22] 28W092 Commercial Ave, Barrington, IL 60010, USA
[23] 28W092 Commercial Ave, Barrington, IL 60010, USA

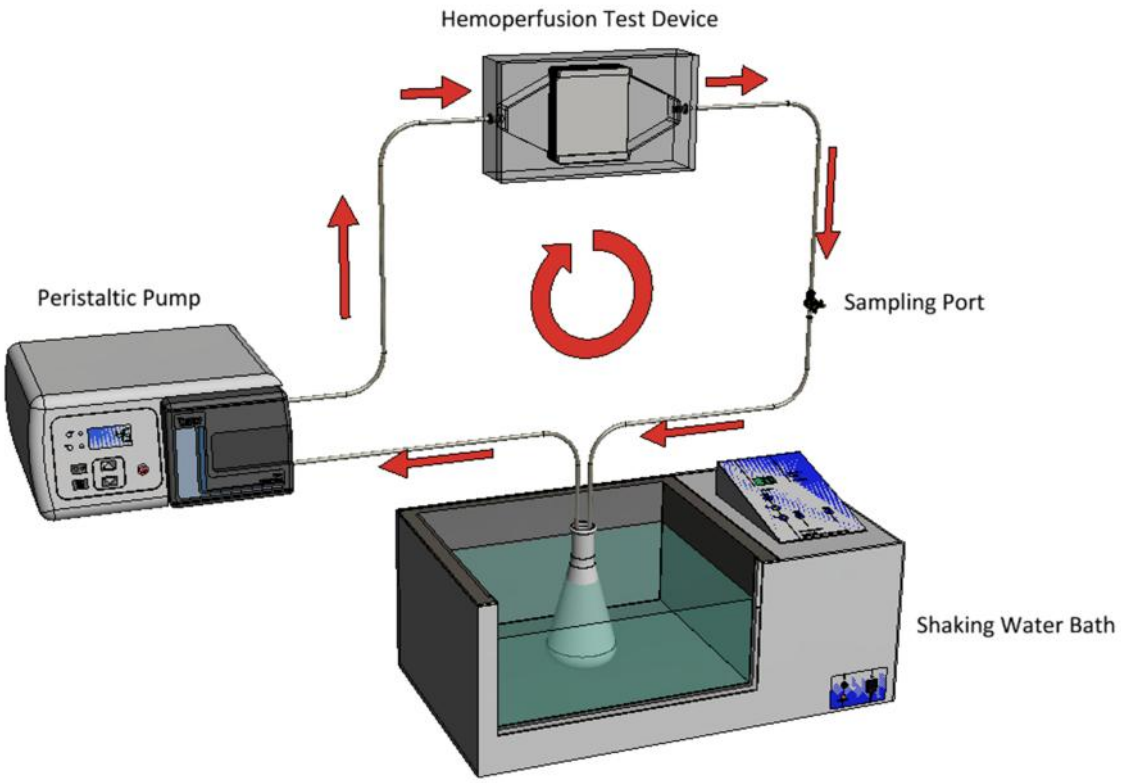

Figure 15. Perspective view of the hemoperfusion circuit design, modeled with Autodesk Inventor 2013.

5.9.3 – Phosphate Adsorption Experiments

Phosphate adsorption experiments conducted in the simulated hemoperfusion circuit made use of both phosphate solution and heparinized bovine whole blood as circulating test solutions that would be exposed to TMA-alumina fabrics. The phosphate solution and heparinized bovine blood are the same as used in the bench-top phosphate adsorption experiments and the phosphate selectivity studies, respectively. In a given experiment, 1 liter of either phosphate solution or heparinized bovine whole blood was poured into the polypropylene reservoir and a varying number (from 5-10) of TMA-alumina hemoperfusion

fabrics were inserted into the hemoperfusion test device. The polypropylene reservoir was inserted into the shaking water bath, where the water was maintained at 37°C. The polypropylene reservoir and the hemoperfusion test device were secured in place and the silicon tubing was used to connect all of the circuitry components in an orientation shown in Figure 15. The peristaltic pump was set to a speed of 45rpm, which correlated to a volumetric flow rate of 150 mL/min. Prior to initiating pumping of the test solution through the circuit, an initial sample was drawn from the reservoir to give a base-line measurement of the initial phosphate concentration. The shaking mechanism on the shaking water bath was then started and the peristaltic pump was also started, allowing the test fluid to flow out of the polypropylene reservoir, past the peristaltic pump, through the hemoperfusion test device (and over the TMA-alumina hemoperfusion fabrics) and finally through the stop-cock sampling port before returning to the polypropylene reservoir (Figure 15). Immediately after the circulating test fluid first returned to the polypropylene reservoir (after the first complete pass through the circuit), the pump was stopped and a 3mL sample was taken from the sampling port through the use of a 3mL luer-lock syringe (Becton Dickinson, CAS: 305269)[24]. After closing the sampling port, the peristaltic pump was re-started and the test solution was again allowed to circulate through the hemoperfusion circuit until the next sampling time point was reached. Samples were taken at time points consisting of t = 0, 10, 25, 50, 75, 100, 120, 150, 180, 200, 240 minutes. Phosphate solution samples were transferred to clean microcentrifuge tubes and analyzed via the Phosphate Colorimetric

[24] 1 Becton Drive, Franklin Lakes, NJ 07417, USA

Assay (Biovision, CAS: K410-500)[25], as described in the section describing bench-top phosphate adsorption experiments. Blood samples were transferred to new Rapid Serum Tubes (Becton Dickinson, CAS: 368774)[26] and analyzed by McLendon Clinical Laboratories using the Vitros 5600 Integrated Analyzer, as described earlier.

5.10 – Alumina Shedding/Aluminum Dissociation Studies

The extent of alumina shedding and/or aluminum dissociation was assessed experimentally in bench-top studies where TMA-Alumina hemoperfusion fabrics were continuously exposed to circulating heparinized bovine whole blood or heparinized human whole blood. Heparinized human whole blood was purchased from Valley Biomedical[27] in 500 mL aliquots with 50 units of heparin added to each liter prior to shipping. Bovine whole blood was procured from Quad Five, as previously mentioned.

In an effort to prevent mechanical abrasion during the experimental set-up or during execution of the testing procedure, polycarbonate frames were fabricated from Lexan, as shown in Figure 16. Initial experiments showed that the addition of these polycarbonate frames to experimental tubes did not produce increased aluminum measurements from the ICP-MS analyses.

Prior to the initiation of the experimental protocol, 50mL volumes of heparinized bovine whole blood and heparinized human whole blood were inserted into separate 50mL conical tubes. A sample was withdrawn from each of these conical tubes by drawing 3mL of blood

[25] 155 South Milpitas Blvd., Milpitas, CA 95035, USA
[26] 1 Becton Drive, Franklin Lakes, NJ 07417, USA
[27] 121 Industrial Drive, Winchester, VA 22602

into a 3mL luer-lock syringe (Becton Dickinson, CAS: 305269)[28]. Each sample was then transferred to a plastic trace element tube (Becton Dickinson, CAS: 368380)[29] and served to provide a baseline measurement for the initial aluminum concentration of the heparinized whole blood. The frames, with TMA-alumina fabrics fixed therein, were then inserted into each 50mL blood-filled conical tube. The conical tubes were then sealed and secured to the rotating tube inverter. The tube inverter was then rotated at a speed of 15rpm (providing 30 inversions of the conical tubes each minute) for a 60 minute duration. After 60 minutes had elapsed, the tube inverter was stopped and a final blood sample was drawn from each tube and transferred to a new plastic trace element tube.

[28] 1 Becton Drive, Franklin Lakes, NJ 07417, USA
[29] 1 Becton Drive, Franklin Lakes, NJ 07417, USA

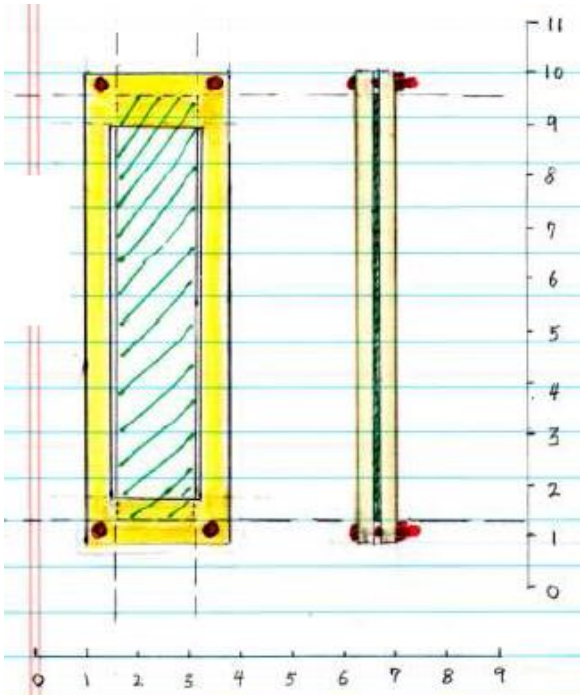

Figure 16. Concept sketch of frames used to hold each fabric sample during the alumina shedding/aluminum dissociation tests.

The collected blood samples were shipped to the Mayo Clinic Medical Laboratory in Rochester, MN to analyze the aluminum trace metal content present in each sample. Once received, the blood samples were centrifuged to yield plasma and then the resulting plasma samples were subjected to a 1:10 dilution with an aqueous acidic diluent. The aluminum content of each sample was measured by Ion Coupled Plasma-Mass Spectroscopy, performed on an Elan 6000 DRC ICP-MS instrument. The Elan 6000 DRC ICP-MS consists of an inductively coupled plasma-mass spectrometer (ICP-MS) and a dynamic reaction cell, which utilizes bandpass tuning to remove chemical moieties that interfere with aluminum quantification and maximize analyte sensitivity. External calibration solutions were created through the serial dilution of 1000 µg/mL aluminum stock solutions, with concentrations

ranging from 0 to 50 ng/mL. These calibration standards allowed the quantification of known aluminum concentrations, and provided a linear relationship between the signal intensity and aluminum concentrations of the standards. The calibration standard was subsequently applied for calculating the concentrations of aluminum in serum samples from the measured signal intensities. As was done for the serum samples, the calibrating standards, along with blanks, were diluted with an aqueous acidic diluent before analysis. The standards, blanks and blood samples were aspirated into a pneumatic nebulizer and directed to a hot plasma discharge by a flow or argon. In this plasma, the samples were vaporized, atomized and then ionized. To reduce analyte interference produced by polyatomic ions, an NH_3 gas was introduced to the test cell, which chemically reacted with interfering species and allowed for the removal of these species from the ion beam. The chemically scrubbed gas that resulted was transferred to a quadrupole mass spectrometer, where ions were filtered based on their mass to charge ratio and counted by a detector that continuously scanned the mass range of 1-263 daltons to quantify aluminum ion counts (in ppb) found within the gas. After correcting these ion counts to account for dilutions and sample volumes used in the analysis, aluminum concentrations were derived.

6. Results

6.1 Scanning Electron Microscopy

The images that directly follow, yielded from scanning electron microscopy analyses, reveal the surface morphology and particle sizes of the untreated alumina powders. Figure 17 – Figure 19 serves to show the similarities in surface structure of the untreated Acros Organics and Selecto Scientific alumina powders and the alterations in surface structure and particle sizes due to the ball-milling operation that was used to produce the milled, Selecto Scientific powders.

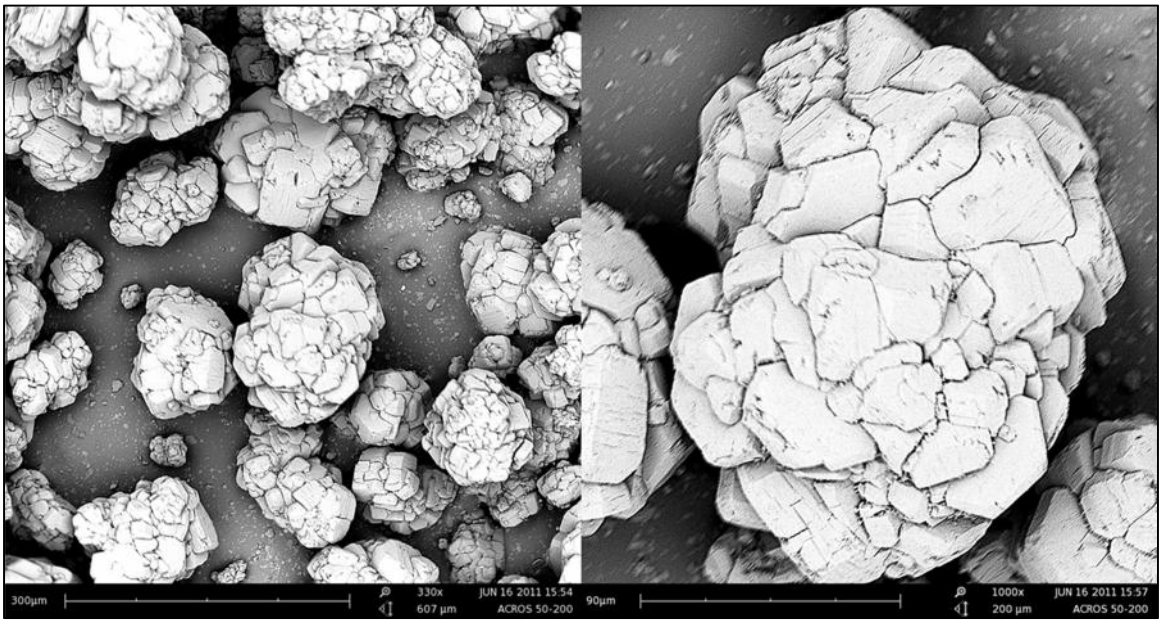

Figure 17. SEM image of untreated alumina powders (Acros Organics). Left: 330x magnification; Right: 1000x magnification.

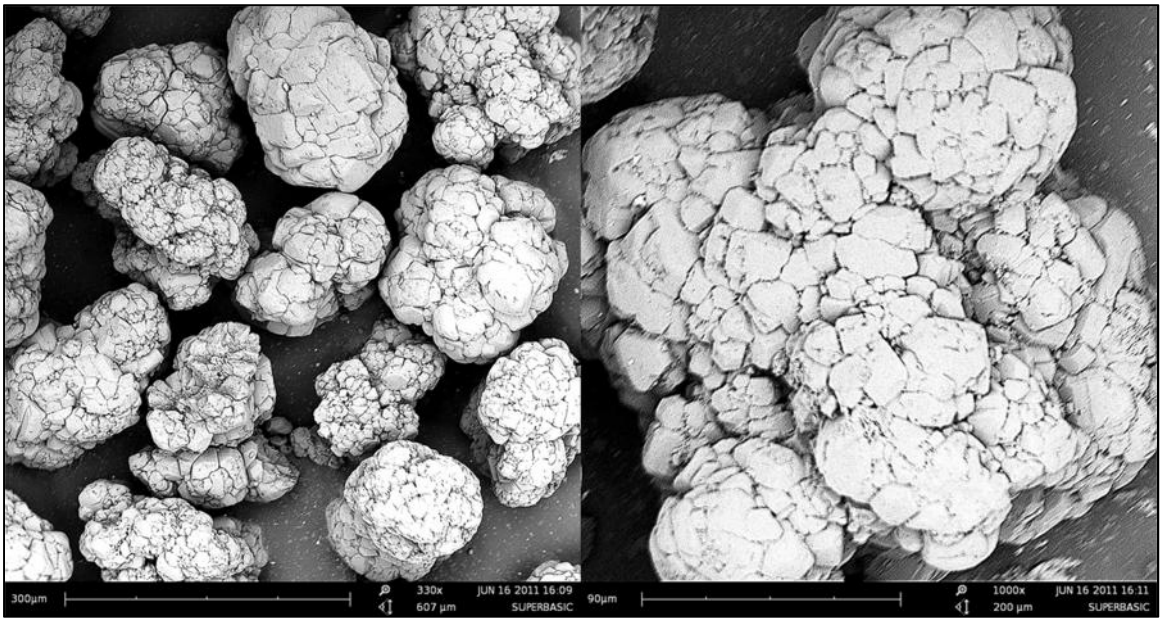

Figure 18. SEM images of untreated alumina powders (Selecto Scientific). Left: 330x magnification; Right: 1000x magnification.

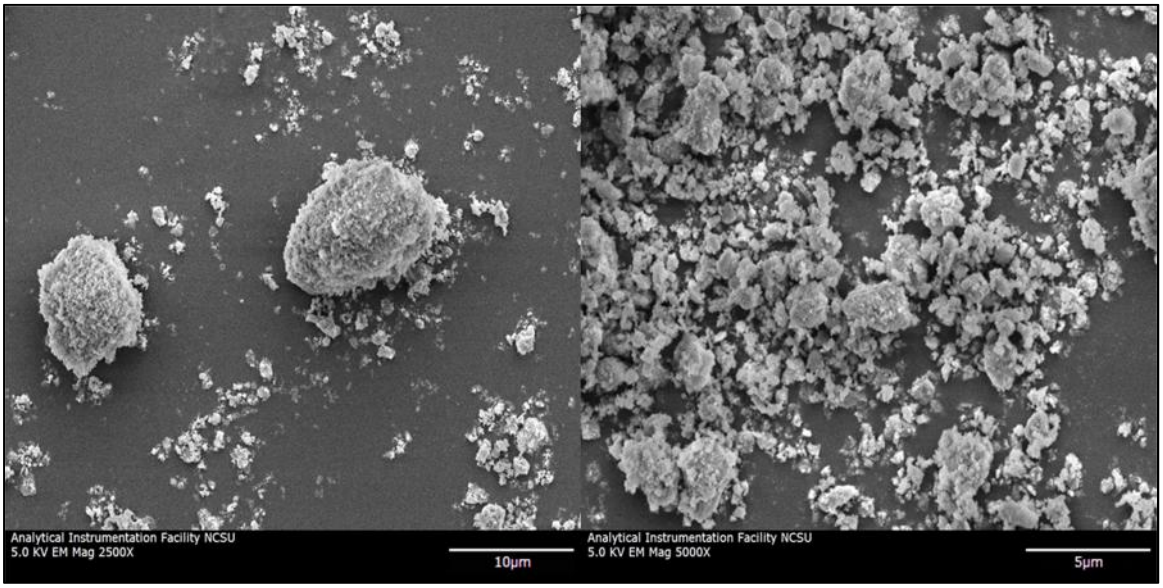

Figure 19. SEM images of untreated alumina powders (milled, Selecto Scientific). Left: 2500x magnification; Right: 5000x magnification.

Figure 20 presents two different magnifications of SEM images of Acros Organics alumina particles, prior to TMA-alumina treatment (left) and following treatment by TMA (right). From the comparison, it can be seen that no significant differences in surface morphology were detected at these magnifications due to the application of the TMA-treatment.

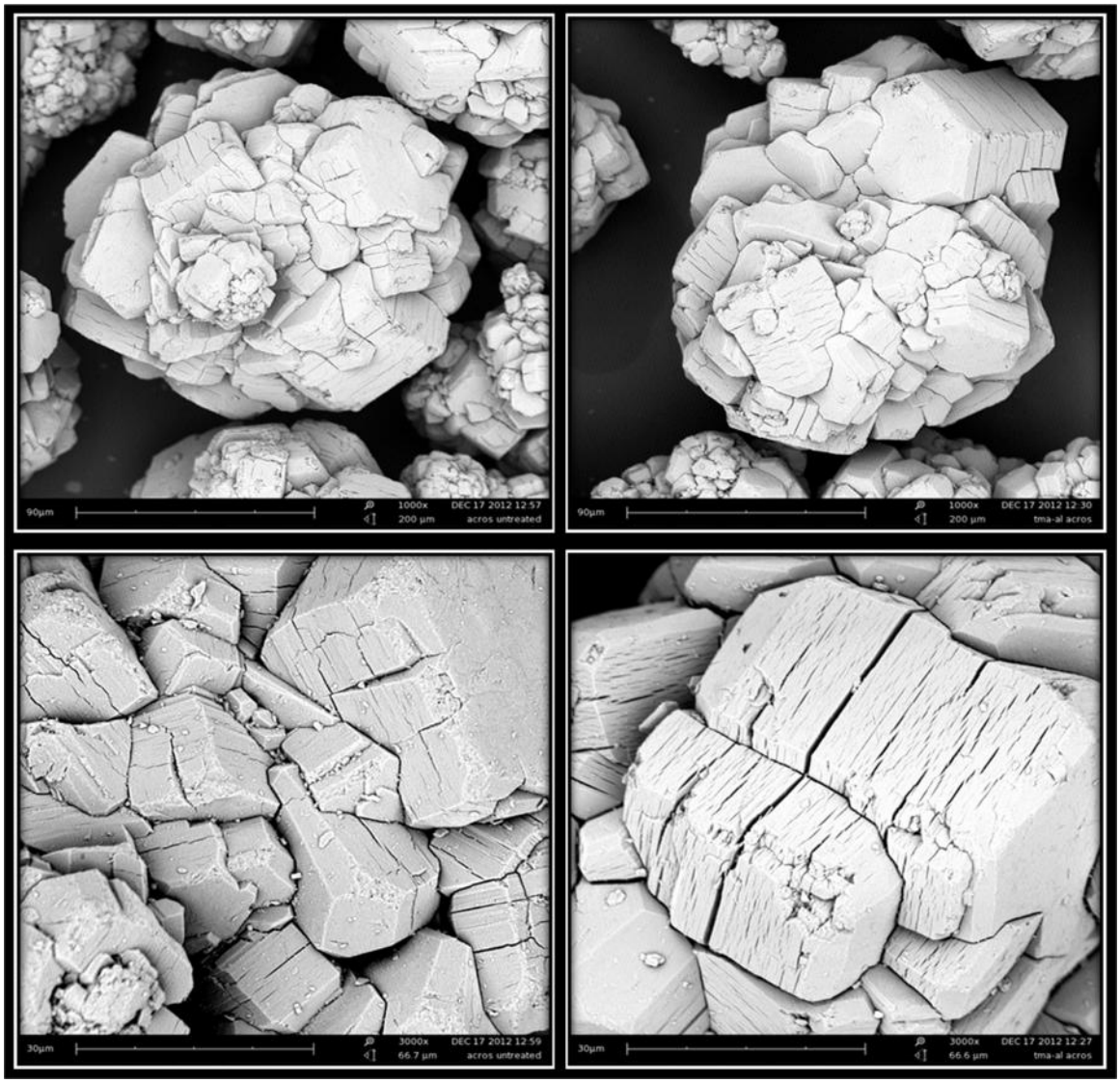

Figure 20. SEM image of untreated alumina (Acros Organics) and TMA treated alumina (Acros Organics). Top left: [untreated alumina, 1000x magnification]; Top Right: [alumina treated with TMA, 1000x magnification]; Bottom left: [untreated alumina, 3000x magnification]; Bottom right: [alumina treated with TMA, 3000x magnification].

Figure 21 presents the scanning electron microscopy results of the Carver® pressing operations used to graft Acros Organics alumina powders to the PET filtration fabrics. Clear morphological differences in the PET filtration fabrics due to variances in temperature during the procedure are displayed, with the original porosity of the substrate further diminishing with increases in Carver® pressing temperatures. Moreover, the Acros Organics alumina powders are visibly fractured during the Carver® pressing operation and cover a large fraction of the fabric samples pressed at each temperature.

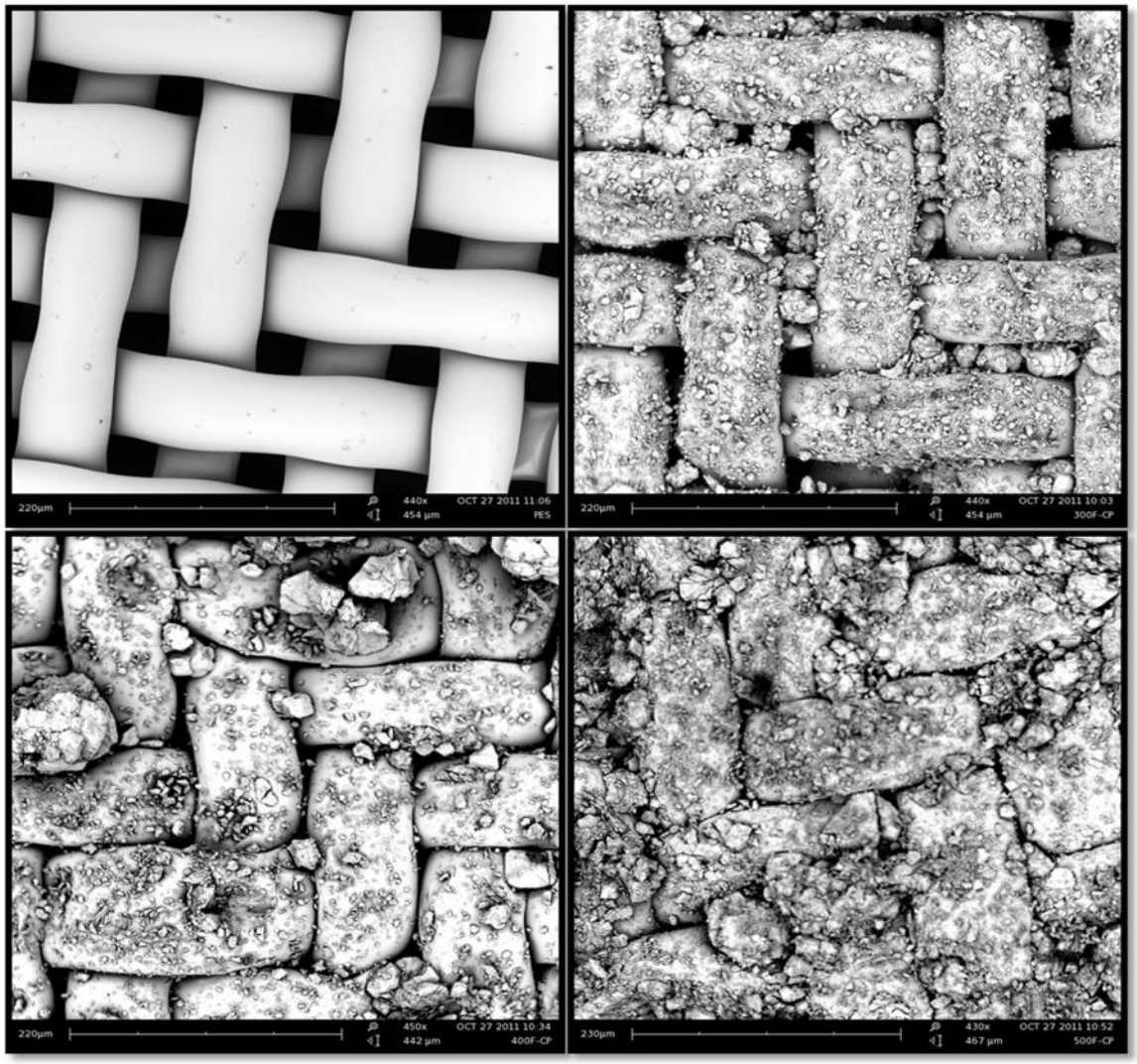

Figure 21. SEM Images of alumina powders Carver® pressed to PET blood filtration fabrics at ~450x magnification. Top left: untreated PET fabric; Top right: alumina powders (Acros Organics) Carver® pressed @ 300°F (148.9 °C); Bottom left: alumina powders (Acros Organics) Carver® pressed @ 400°F; Bottom right: alumina powders (Acros Organics) caver-pressed @ 500°F.

Figures 22 and 23 display the SEM images of the surface alterations induced by the flame-spraying of thermal spray powders to PET filtration fabrics. Figure 22 depicts changes in the PET filtration fabric structure induced by the contact of molten alumina particles and shows that the grafting efficiency was high, with a sufficient fraction of the PET surface covered by

alumina particles. Figure 23 shows a range of magnifications of the flame-sprayed PET filtration fabrics and illustrates that the spherical particles embed into the PET via a localized melting phenomenon.

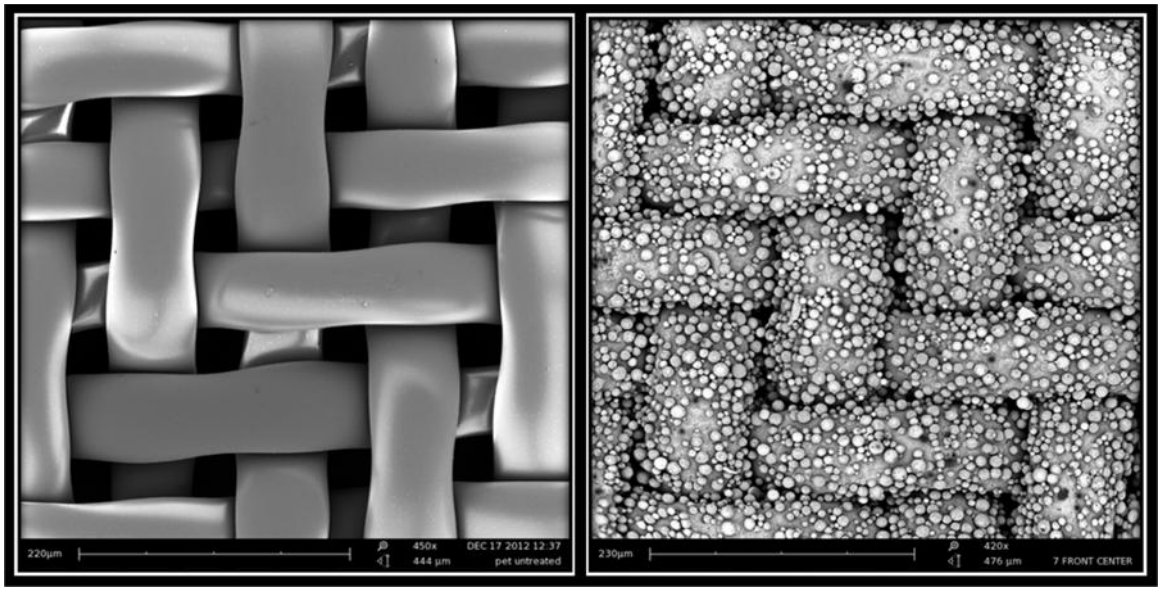

Figure 22. SEM images of untreated PET blood filtration fabrics (control) and PET blood filtration fabrics with alumina (thermal spray powders) grafted via flame spraying (FS-PET). Left: [Surface of untreated PET fabric (control), 450x magnification]; Right: [Surface of Flame-sprayed PET fabric (Thermal Spray Powders), 420x magnification].

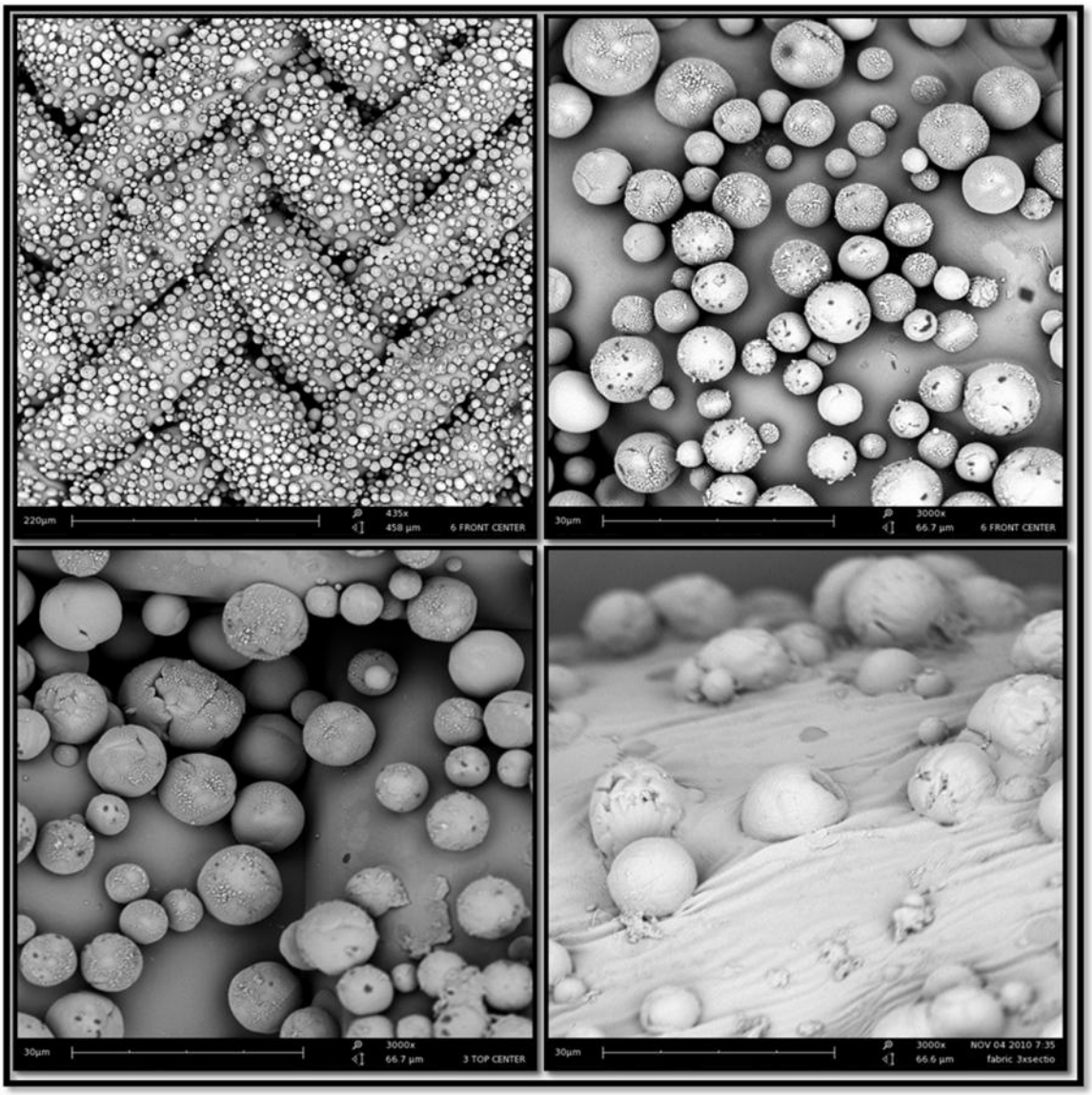

Figure 23. SEM images of alumina powders (thermal spray) grafted to PET blood filtration fabrics via flame spraying. Top left: [450x magnification surface]; Top Right: [3000x magnification surface]; Bottom left: [3000x magnification surface]; Bottom right: [3000x magnification surface, angled perspective].

Figure 24 displays the surface alterations induced by the flame-spraying of milled, Selecto Scientific powders to PET filtration fabrics. The SEM images show that the grafting efficiency

was poor, with the majority of the fraction of the PET surface remaining unaltered following the application of the flame-spraying operation using this milled alumina powder type.

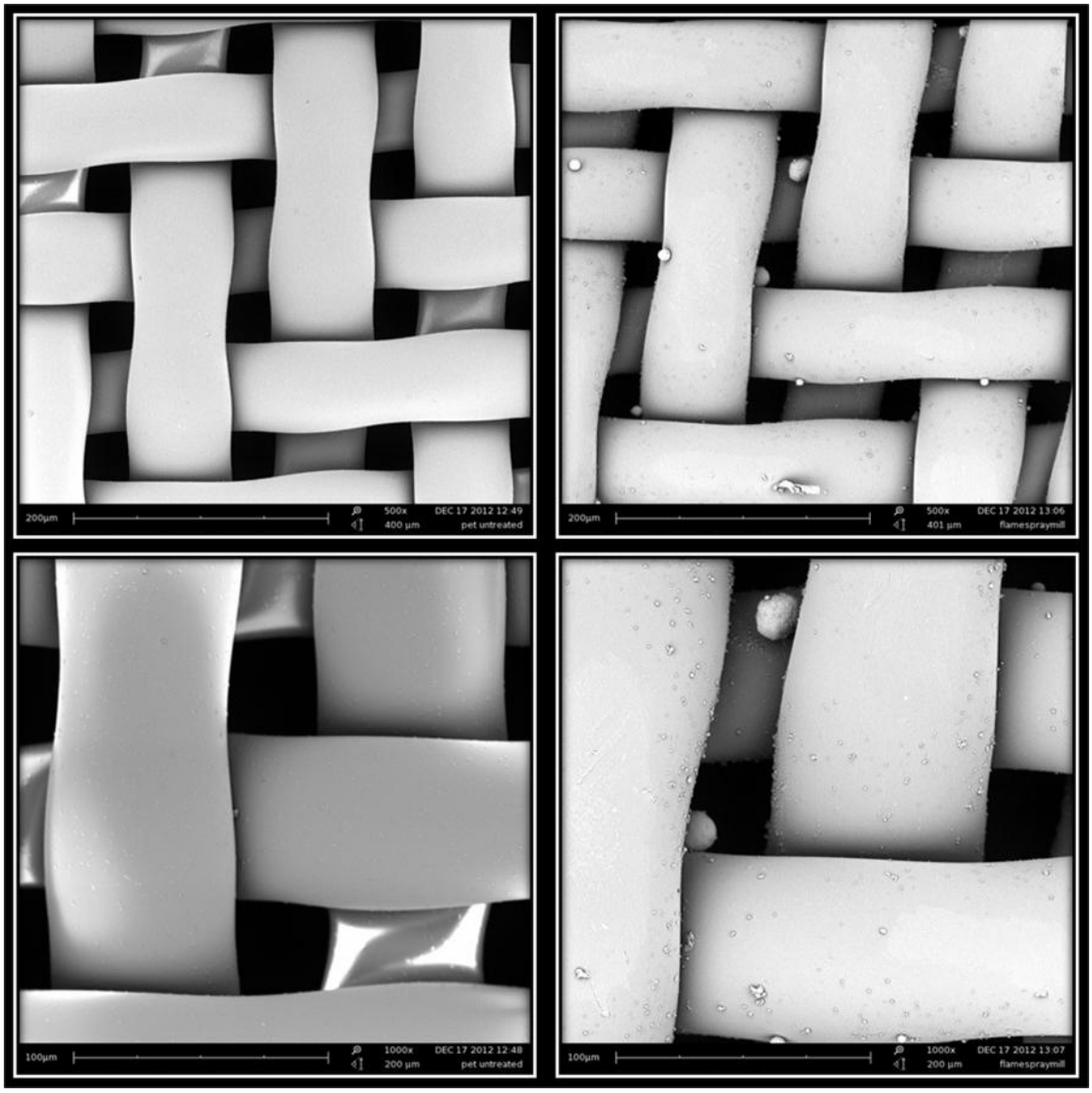

Figure 24. SEM images of untreated PET blood filtration fabrics (control) and PET blood filtration fabrics with alumina (milled, Selecto Scientific) grafted via flame-spraying. Top left: [500x magnification surface of PET control]; Top Right: [500x magnification surface of flame-sprayed PET]; Bottom left: [1000x magnification surface of PET control]; Bottom right: [1000x magnification surface of flame-sprayed PET].

Figure 25 presents the surface alterations caused by the grafting of alumina to PET filtration fabrics by atomic layer deposition. The SEM images show that the porosity of the underlying PET substrate was largely unchanged but that the grafting efficiency of alumina was poor, with the majority of the PET fiber surfaces absent of alumina following the application of the atomic layer deposition process.

Figure 26 illustrates the fabric surface alterations caused by the grafting of alumina by sequential vapor infiltration. The images show that the porosity of the underlying substrate was largely unchanged but that the surface layers of the PET fibers were significantly etched during the SVI process. Despite obvious alterations in the fiber surface, the grafting efficiency of alumina was poor, with the majority of PET surface absent of alumina.

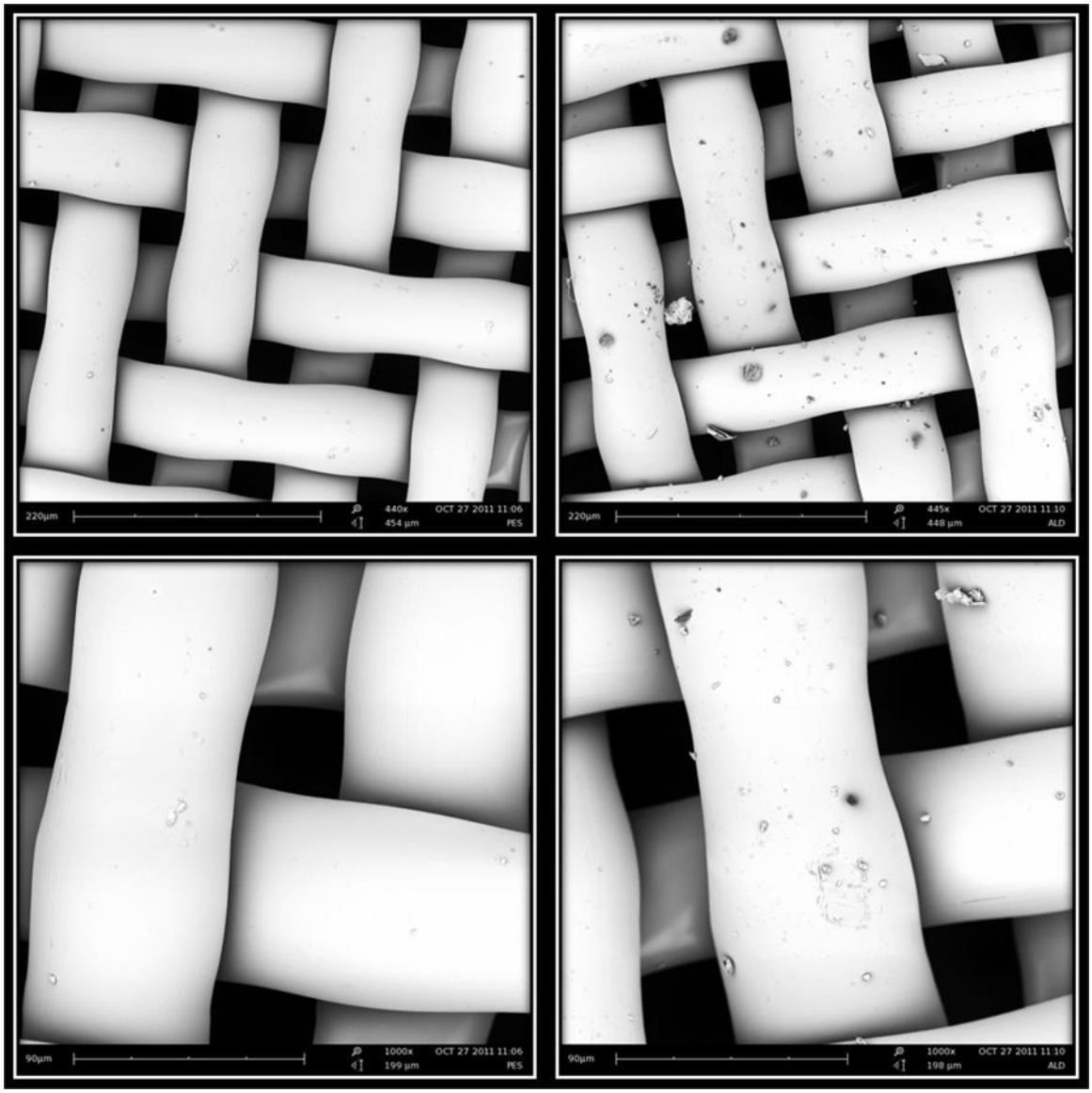

Figure 25. SEM images of untreated PET blood filtration fabrics (control) and PET blood filtration fabrics with alumina grafted via atomic layer deposition (ALD-PET). Top left: [440x magnification surface of PET control]; Top Right: [440x magnification surface of ALD-PET]; Bottom left: [1000x magnification surface of PET control]; Bottom right: [1000x magnification surface of ALD-PET].

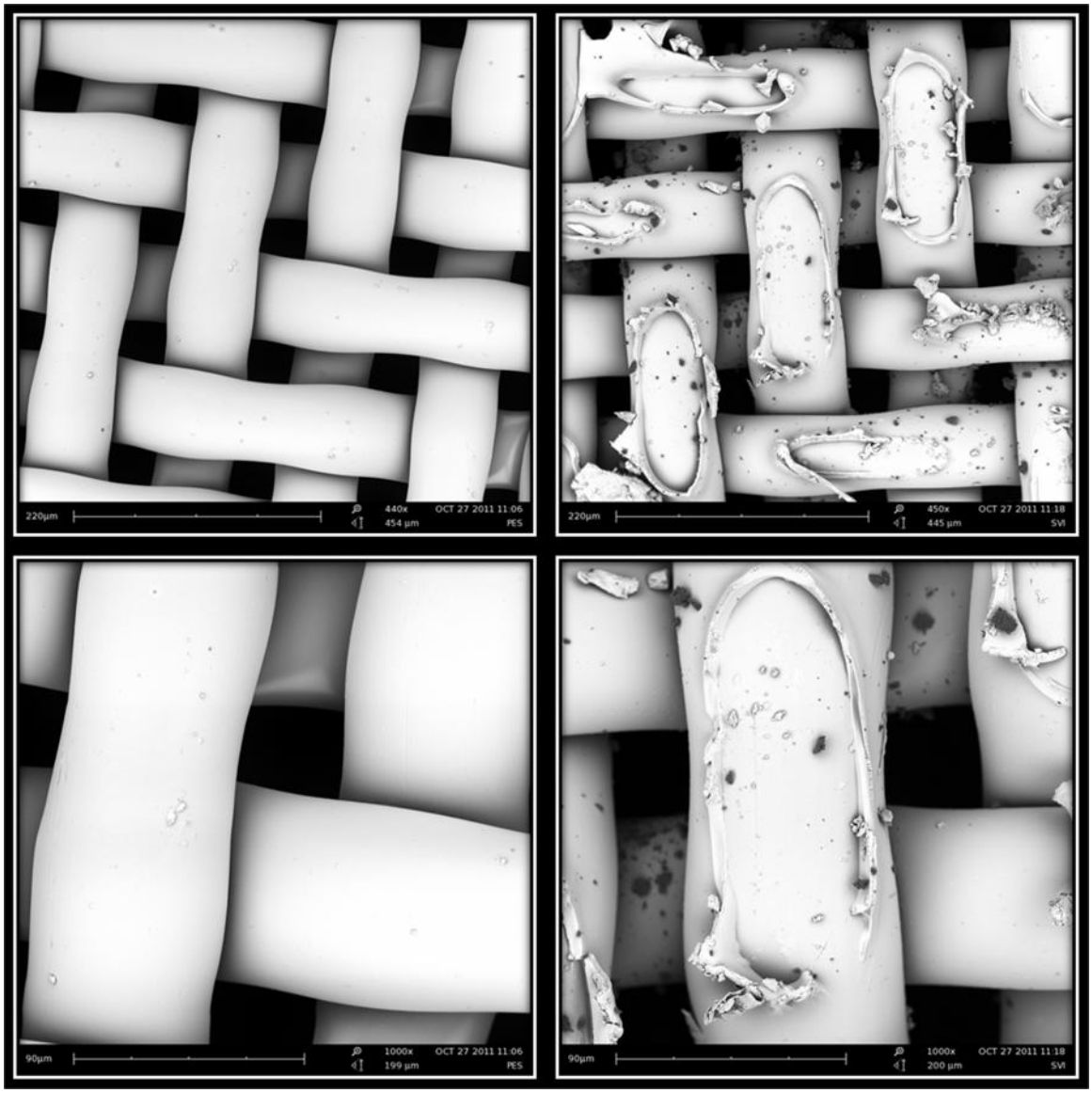

Figure 26: SEM images of untreated PET blood filtration fabrics (control) and PET blood filtration fabrics with alumina grafted via sequential vapor infiltration (SVI-PET). Top left: [440x magnification surface of PET control]; Top Right: [440x magnification surface of SVI-PET], Bottom left: [1000x magnification surface of PET control]; Bottom right: [1000x magnification surface of SVI-PET].

6.2 Alumina Grafting Yields

Table 7 displays the masses of alumina grafted to the PET filtration fabric substrates by all Carver® pressing operations and by the preliminary trials utilizing flame-spraying, atomic layer deposition and sequential vapor infiltration. As different experimental undertakings required differing sizes of fabrics, Table 7 also displays a calculated value which normalizes the mass of alumina grafted by the total surface area of the fabric substrate. Although a 51% porosity is inherent to the PET filtration fabrics, the surface area that is calculated for this purpose does not account for this porosity and is instead based only on the macroscopic dimensions of the fabric samples used (not indicative of the true surface area). Consequently, the surface area reported (cm^2) is calculated by multiplying the measured length (cm) and width (cm) of the fabrics, and is multiplied by two to reflect the use of each side for adhering alumina particles. The results indicate that despite the use of identical procedures and process parameters for all Carver® pressing operations, the amount of hemoadsorbent mass grafted to each PET filtration fabric substrate per unit surface area (mg/cm^2) by Carver® pressing was subject to significant variability. Still, the Carver® press method proved to impart the largest masses of alumina to the fabric substrates of all methods that were explored within this research. For this reason, the Carver® press method was identified as the best performing grafting method and was selected for use in the subsequent fabrication of all hemoperfusion assemblies. The average alumina mass grafted per unit surface area for all fabrics that were Carver® pressed with Acros Organics alumina powders is also displayed in Table 7.

Table 7. Surface areas, grafting yields, and masses gained per cm^2 for all alumina-modified fabrics used and all grafting methods explored within the scope of this research. All grafting yield data for fabrics Carver® pressed with alumina were pressed at 500°F (260°C) and 411.75psi (2833.92 kPa), as previously described.

Entry No.	Grafting Method	Alumina Type Used	Surface Area of Fabric Sample (cm^2)	Hemoadsorbent Grafting Yield (g)	Hemoadsorbent Mass Grafted per Surface Area (mg/cm^2)
1	Carver® Press	Acros Organics	200.0	0.346	1.73
2	Carver® Press	Acros Organics	200.0	0.328	1.64
3	Carver® Press	Acros Organics	200.0	0.350	1.75
4	Carver® Press	Acros Organics	200.0	0.595	2.97
5	Carver® Press	Acros Organics	200.0	0.326	1.63
6	Carver® Press	Acros Organics	200.0	0.333	1.66
7	Carver® Press	Acros Organics	200.0	0.486	2.43
8	Carver® Press	Acros Organics	200.0	0.180	0.90
9	Carver® Press	Acros Organics	200.0	0.656	3.28
10	Carver® Press	Acros Organics	200.0	0.248	1.24
11	Carver® Press	Acros Organics	200.0	0.308	1.54
12	Carver® Press	Acros Organics	200.0	0.262	1.31
13	Carver® Press	Acros Organics	200.0	0.261	1.31
14	Carver® Press	Acros Organics	200.0	0.277	1.39
15	Carver® Press	Acros Organics	200.0	0.292	1.46
16	Carver® Press	Acros Organics	200.0	0.274	1.37
17	Carver® Press	Acros Organics	200.0	0.090	0.45
18	Carver® Press	Acros Organics	200.0	0.362	1.81
19	Carver® Press	Acros Organics	200.0	0.263	1.32
20	Carver® Press	Acros Organics	200.0	0.602	3.01
21	Carver® Press	Acros Organics	200.0	0.336	1.68
22	Carver® Press	Acros Organics	200.0	0.228	1.14
23	Carver® Press	Acros Organics	200.0	0.417	2.09
24	Carver® Press	Acros Organics	200.0	0.305	1.52
25	Carver® Press	Acros Organics	200.0	0.173	0.86
26	Carver® Press	Acros Organics	200.0	0.243	1.22
27	Carver® Press	Acros Organics	200.0	0.373	1.87
28	Carver® Press	Acros Organics	200.0	0.261	1.31
29	Carver® Press	Acros Organics	200.0	0.443	2.22
30	Carver® Press	Acros Organics	200.0	0.659	3.30

Table 7. Continued

31	Carver® Press	Acros Organics	200.0	0.196	0.98
32	Carver® Press	Acros Organics	200.0	0.322	1.61
33	Carver® Press	Acros Organics	200.0	0.354	1.77
34	Carver® Press	Acros Organics	200.0	0.339	1.70
35	Carver® Press	Acros Organics	200.0	0.345	1.73
36	Carver® Press	Acros Organics	200.0	0.352	1.76
37	Carver® Press	Acros Organics	108.0	0.220	2.04
38	Carver® Press	Acros Organics	108.0	0.243	2.25
39	Carver® Press	Acros Organics	108.0	0.314	2.91
40	Carver® Press	Acros Organics	108.0	0.308	2.85
41	Carver® Press	Acros Organics	108.0	0.326	3.02
42	Carver® Press	Acros Organics	108.0	0.399	3.69
43	Carver® Press	Acros Organics	108.0	0.3042	2.82
44	Carver® Press	Acros Organics	54.0	0.139	2.57
45	Carver® Press	Acros Organics	54.0	0.158	2.93
46	Carver® Press	Acros Organics	54.0	0.150	2.78
			AVERAGES	0.321	1.93
47	Thermal Spray	Thermal Spray Formulation	54.0	0.041	0.76
48	Thermal Spray	milled, Selecto Scientific	54.0	0.007	0.13
49	Atomic Layer Deposition	ALD Al_2O_3	108.0	NONE DETECTED	0.00
50	Sequential Vapor Infiltration	SVI Al_2O_3	108.0	NONE DETECTED	0.00

6.3 Bench-top Phosphate Adsorption Studies on Powders – Phosphate Solution

According to the results of the phosphate adsorption assay, both the TMA-treated Acros Organic alumina powders and the untreated Acros Organic alumina powders displayed favorable phosphate adsorption capabilities when tested in a ~30 mg/L phosphate solution in a bench-top setting (Figure 27 - Figure 31). The TMA-treatment was shown to improve

the phosphate adsorption capacity of the Acros Organics alumina powders by 49.16% after 4-hours, in comparison to the untreated Acros Organics powders (Figure 31).

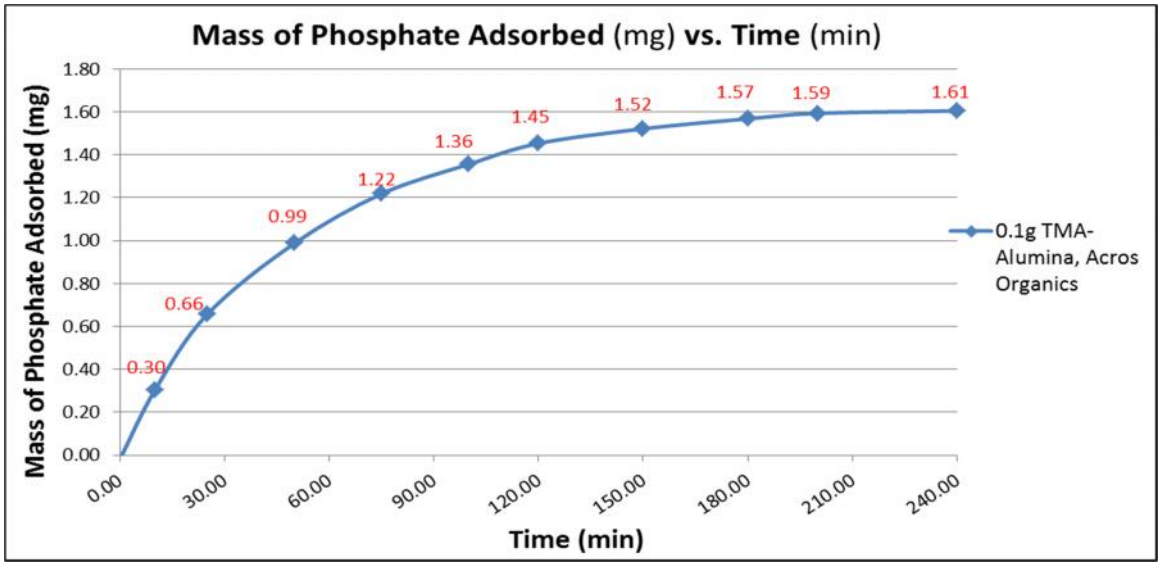

Figure 27. Mass of phosphate removed from phosphate solution (50 mL, initial PO_4 concentration of 33.33 mg/L) by 0.1g of TMA treated alumina powders (Acros Organics) over 4-hour duration.

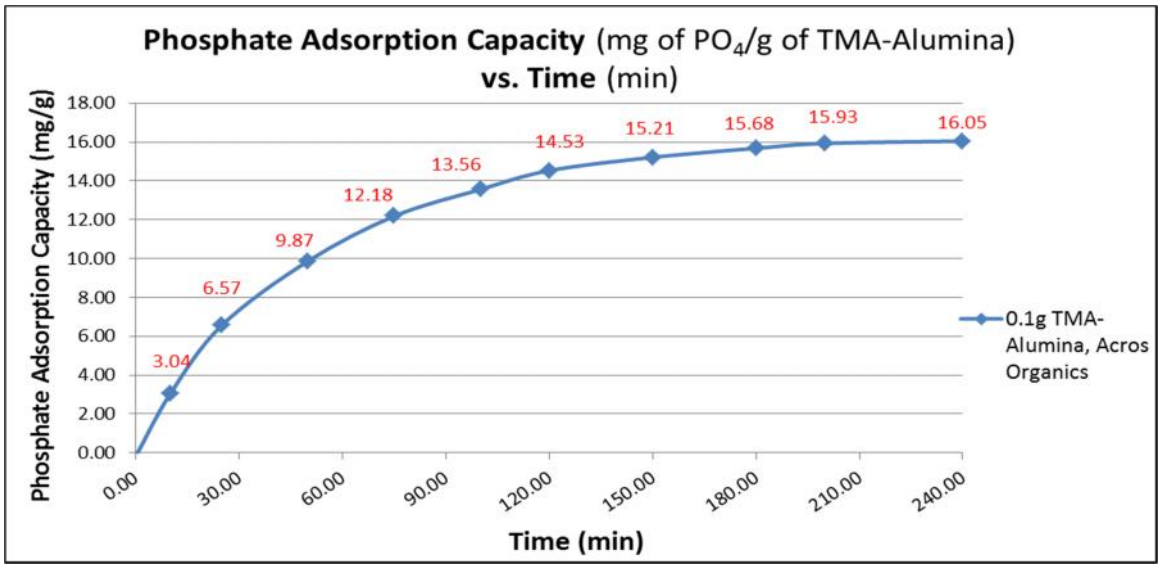

Figure 28. Phosphate adsorption capacity of TMA treated alumina powders (Acros Organics) in phosphate solution (50 mL, initial PO_4 concentration of 33.33 mg/L) over 4-hour duration.

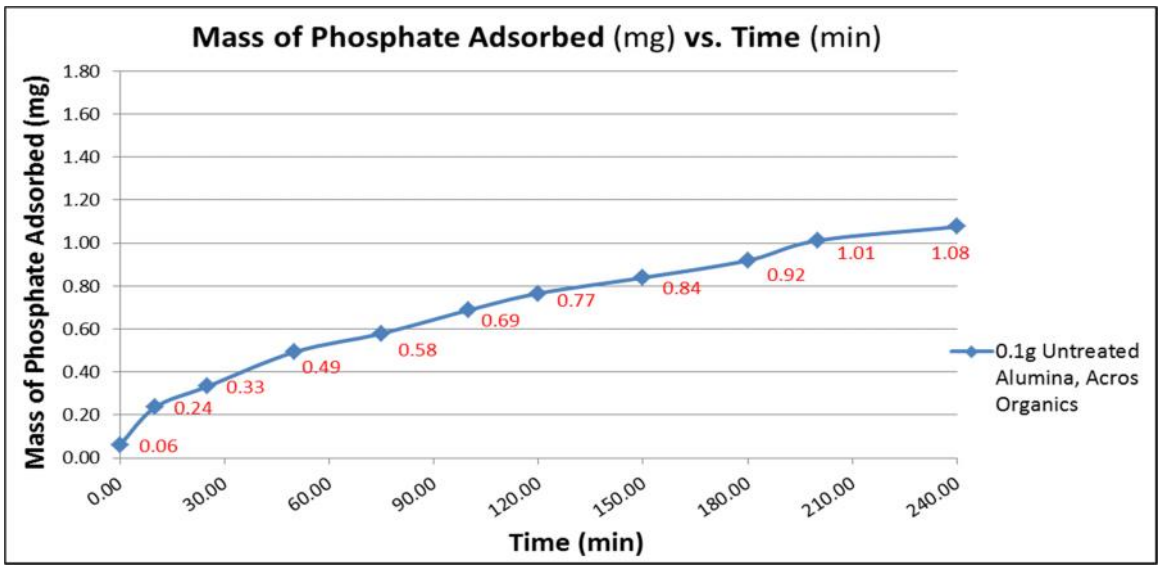

Figure 29. Mass of phosphate removed from phosphate solution (50 mL, initial PO_4 concentration of 33.85 mg/L) by 0.1g of untreated alumina powders (Acros Organics) over 4-hour duration.

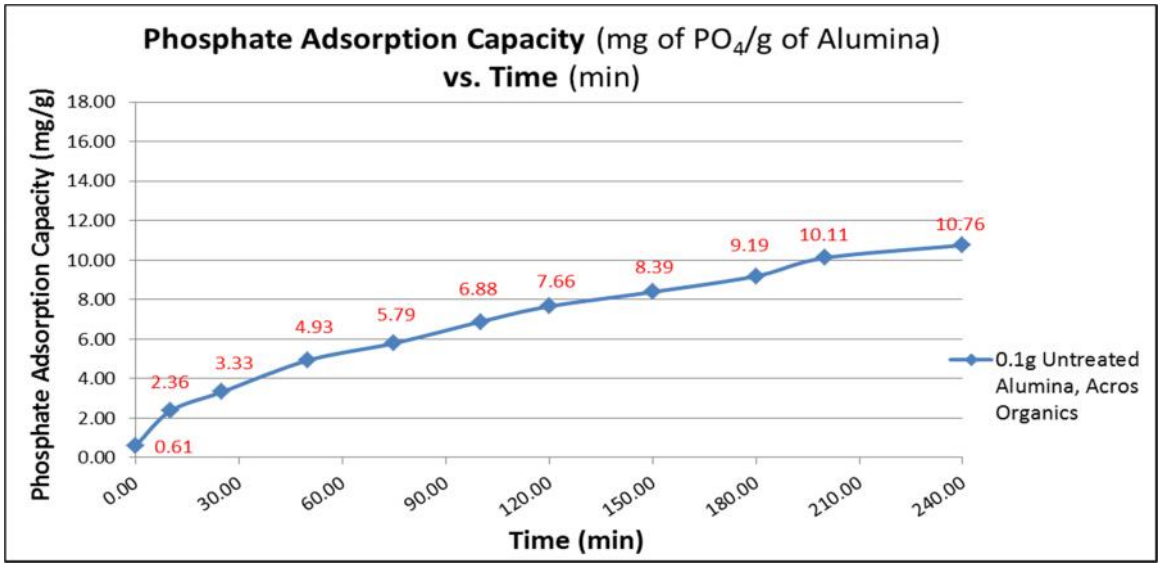

Figure 30. Phosphate adsorption capacity of untreated alumina powders (Acros Organics) in phosphate solution (50 mL, initial PO_4 concentration of 33.85 mg/L) over 4-hour duration.

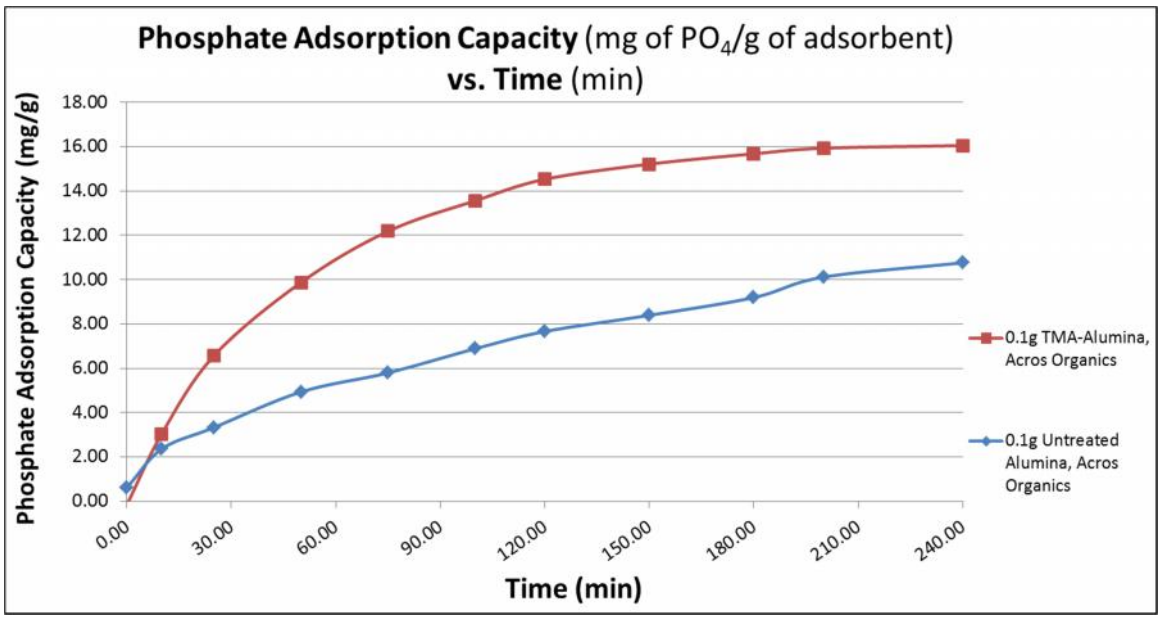

Figure 31. Comparison of phosphate adsorption capacities of TMA treated alumina powders (Acros Organics) and untreated alumina powders (Acros Organics) in phosphate solution (50 mL, initial PO_4 concentration of ~30 mg/L) over 4-hour duration.

According to the results of the phosphate assay, both the TMA-treated Selecto Scientific alumina powders and the untreated Selecto Scientific alumina powders displayed favorable phosphate adsorption capabilities when tested in a ~30 mg/L phosphate solution in a bench-top setting (Figure 32 – Figure 26). The TMA-treatment was shown to improve the phosphate adsorption capacity of the Selecto Scientific alumina powders by 79.49% after 4-hours, in comparison to the untreated Selecto Scientific powders (Figure 36). While the increase in the adsorption capacity due to the application of the TMA-treatment was substantially greater for the Selecto Scientific alumina powders than the Acros Organics alumina powders, the overall magnitudes of the phosphate mass removed and the adsorption capacity of the TMA-treated Acros Organics alumina powders was greater than that of the TMA-treated Selecto Scientific alumina powders.

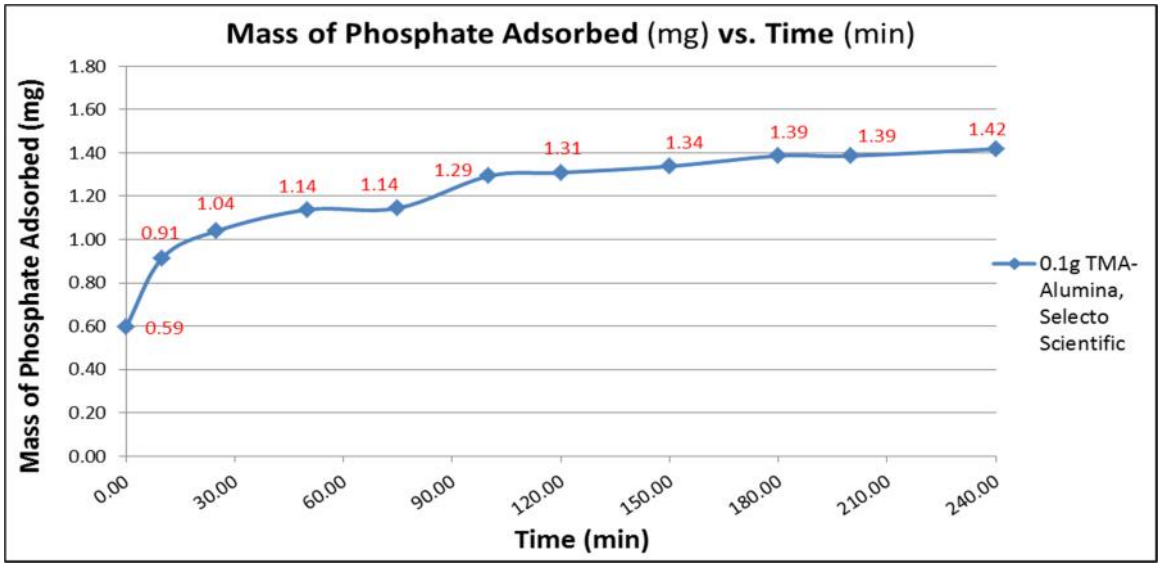

Figure 32. Mass of phosphate removed from phosphate solution (50 mL, initial PO_4 concentration of 32.07 mg/L) by 0.1g of TMA treated alumina powders (Selecto Scientific) over 4-hour duration.

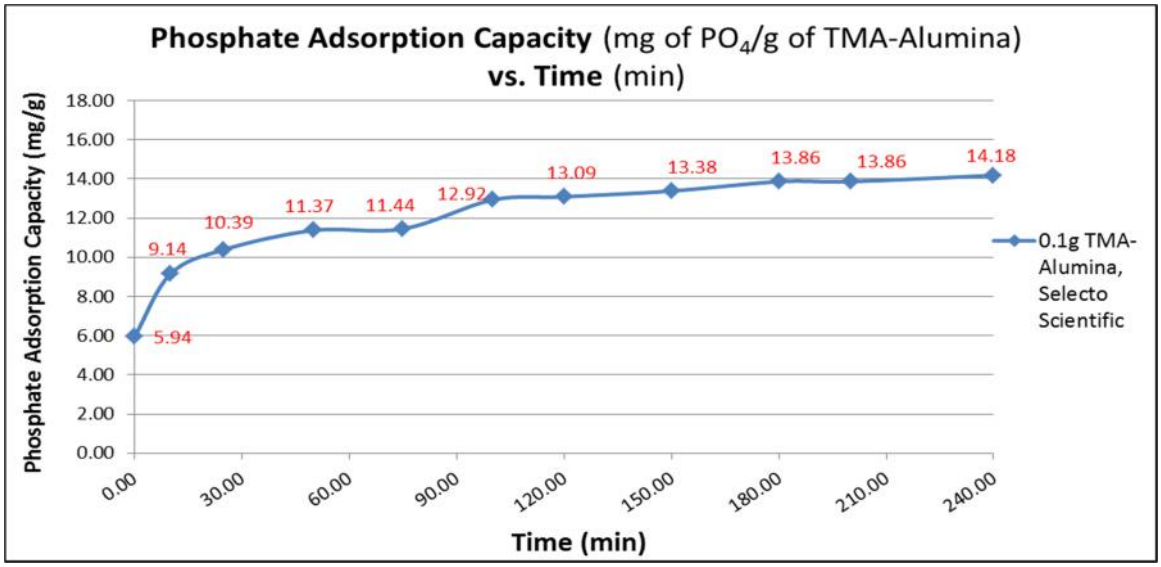

Figure 33.: Phosphate adsorption capacity of TMA treated alumina powders (Selecto Scientific) in phosphate solution (50 mL, initial PO_4 concentration of 32.07 mg/L) over 4-hour duration.

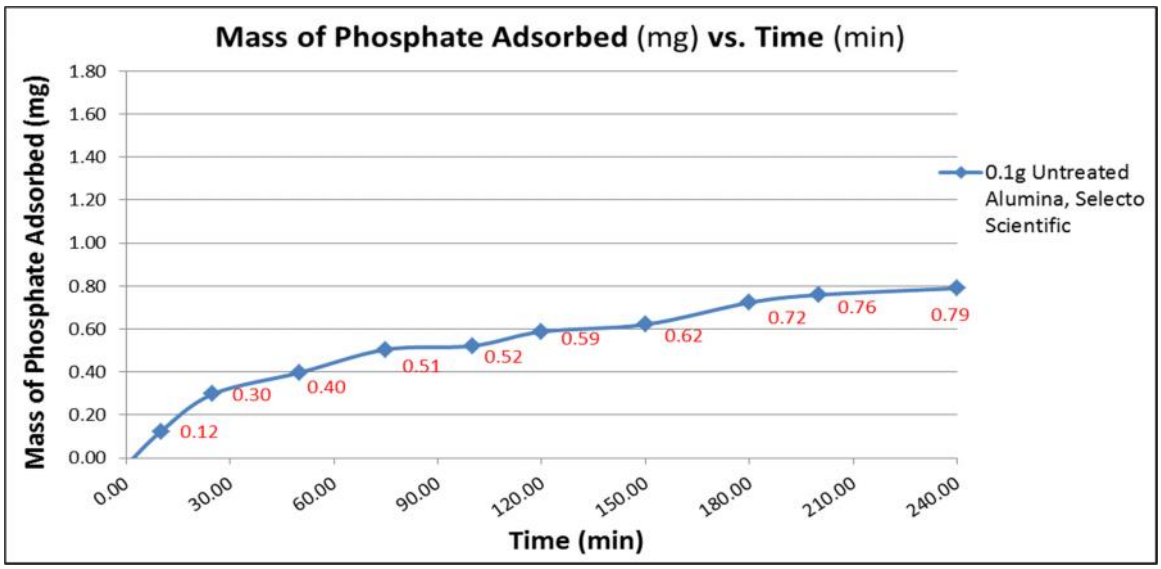

Figure 34. Mass of phosphate removed from phosphate solution (50 mL, initial PO_4 concentration of 34.10 mg/L) by 0.1g of untreated alumina powders (Selecto Scientific) over 4-hour duration.

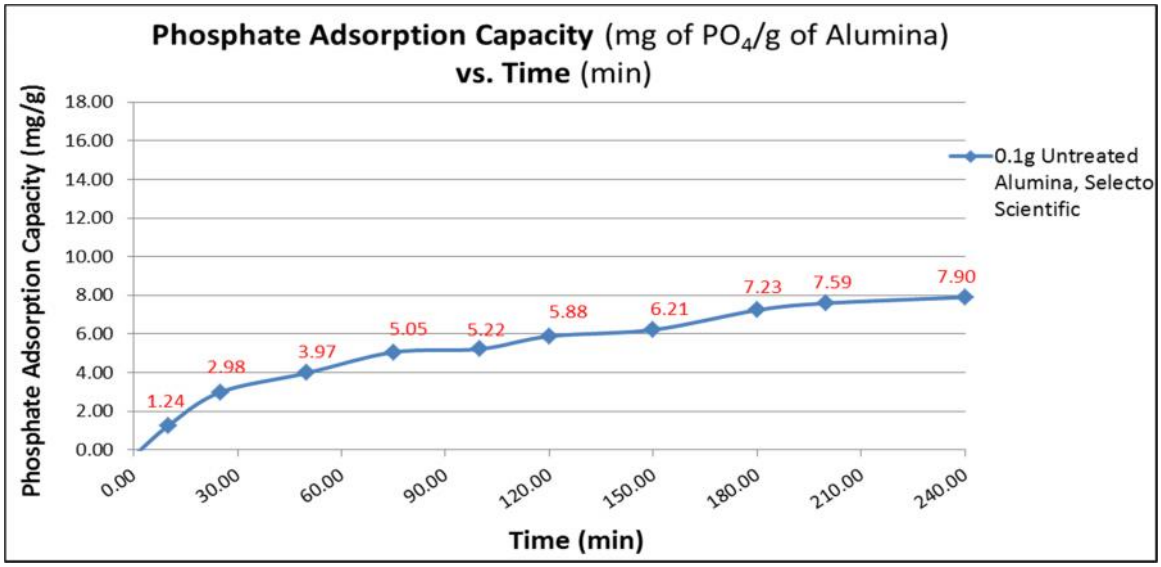

Figure 35. Phosphate adsorption capacity of untreated alumina powders (Selecto Scientific) in phosphate solution (50 mL, initial PO_4 concentration of 34.10 mg/L) over 4-hour duration.

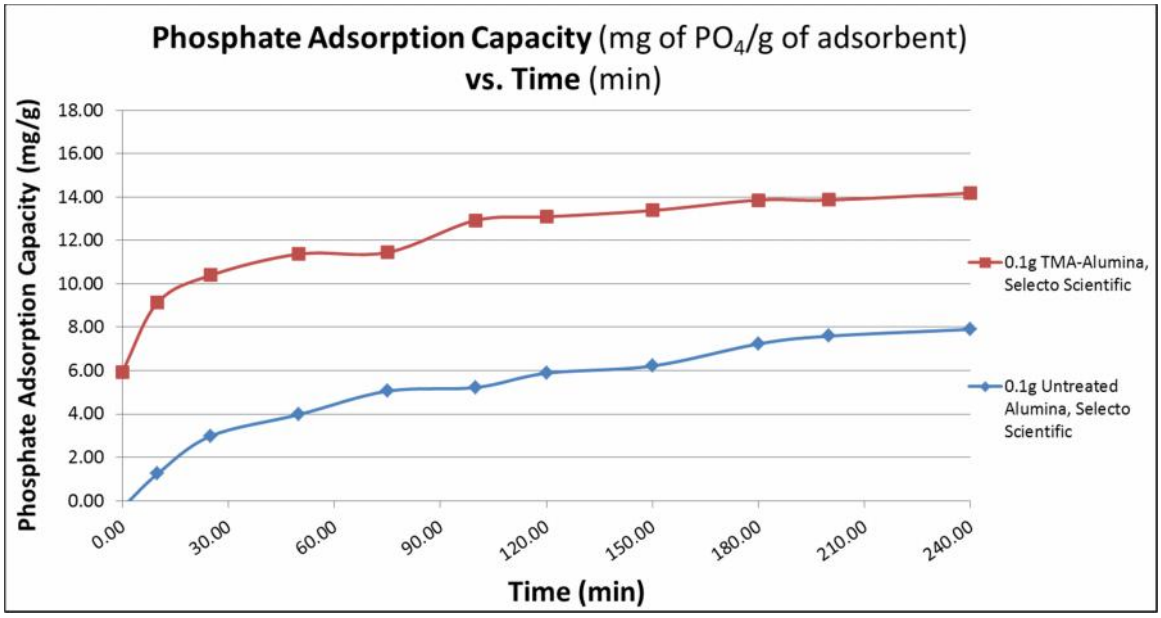

Figure 36. Comparison of phosphate adsorption capacities of TMA treated alumina powders (Selecto Scientific) and untreated alumina powders (Selecto Scientific) in phosphate solution (50 mL, initial PO_4 concentration of ~30 mg/L) over 4-hour duration.

According to the results of the phosphate assay, neither the TMA-treated Thermal Spray alumina powders nor the untreated Thermal Spray alumina powders displayed favorable phosphate adsorption capabilities when tested in a ~30 mg/L phosphate solution in a bench-top setting (Figure 37 - Figure 41). As a result of the fluctuating non-specific physisorption and desorption of phosphate to the surface of both TMA-treated and untreated thermal spray alumina powders, the phosphate concentrations measured by the phosphate assay were shown to irregularly oscillate around the x-axis. In both cases, the oscillating non-zero values of phosphate mass adsorbed (Figure 37 and Figure 39) were shown to reflect values below the lower-level of detection of the colorimetric assay and consequently, the extent of phosphate adsorption displayed by both the TMA-treated and the untreated thermal spray alumina powders was deemed insignificant.

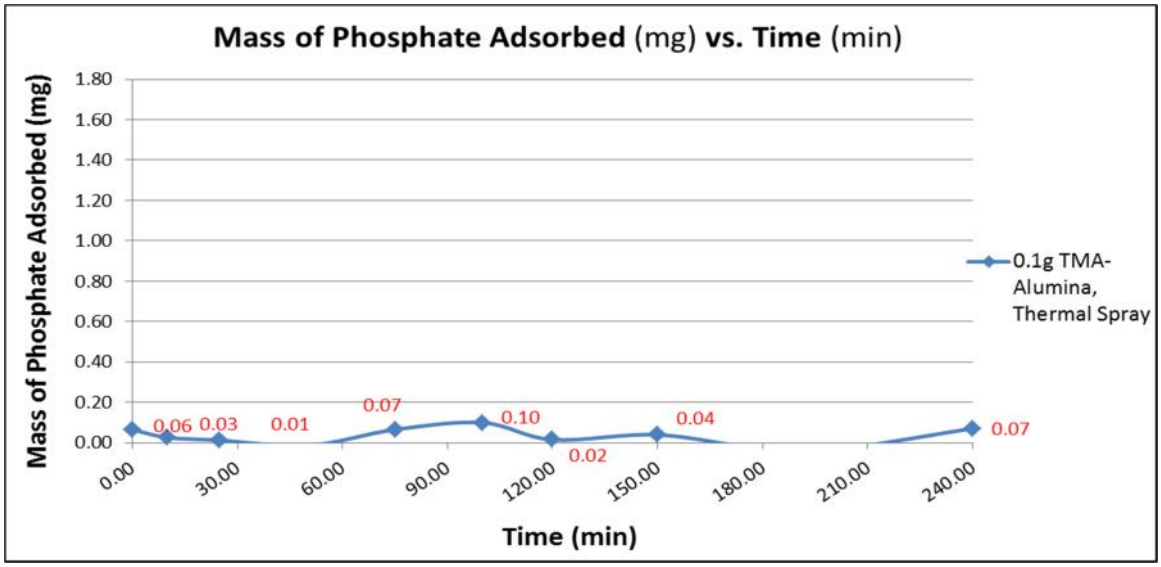

Figure 37. Mass of phosphate removed from phosphate solution (50 mL, initial PO_4 concentration of 30.40 mg/L) by 0.1g of TMA treated alumina powders (Thermal Spray) over 4-hour duration.

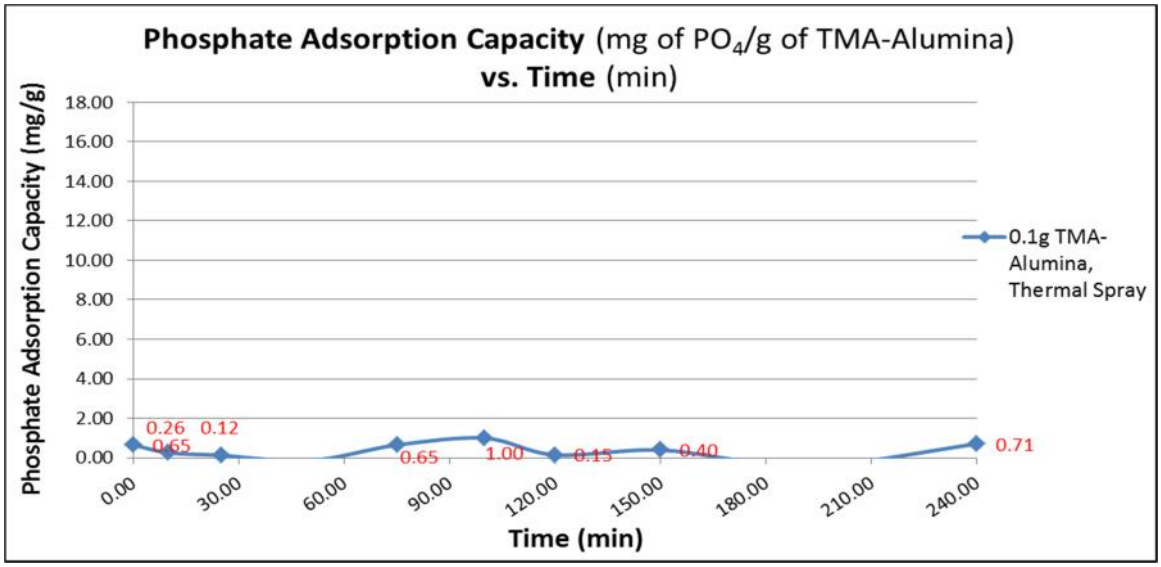

Figure 38. Phosphate adsorption capacity of TMA-treated alumina powders (Thermal Spray) in phosphate solution (50 mL, initial PO_4 concentration of 30.40 mg/L) over 4-hour duration.

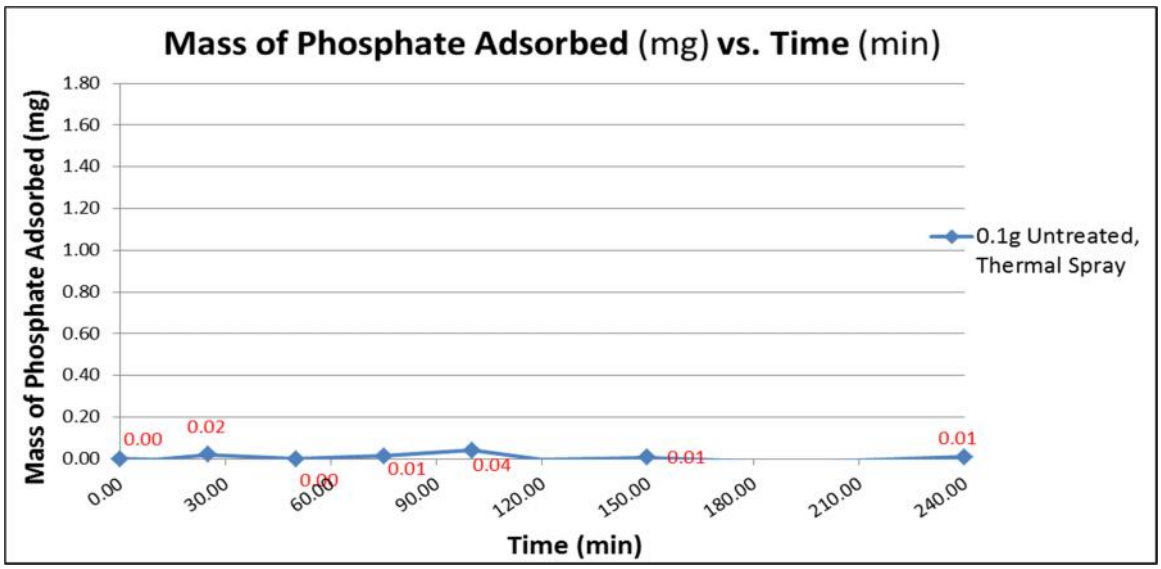

Figure 39. Mass of phosphate removed from phosphate solution (50 mL, initial PO_4 concentration of 30.47 mg/L) by 0.1g of untreated alumina powders (Thermal Spray) over 4-hour duration.

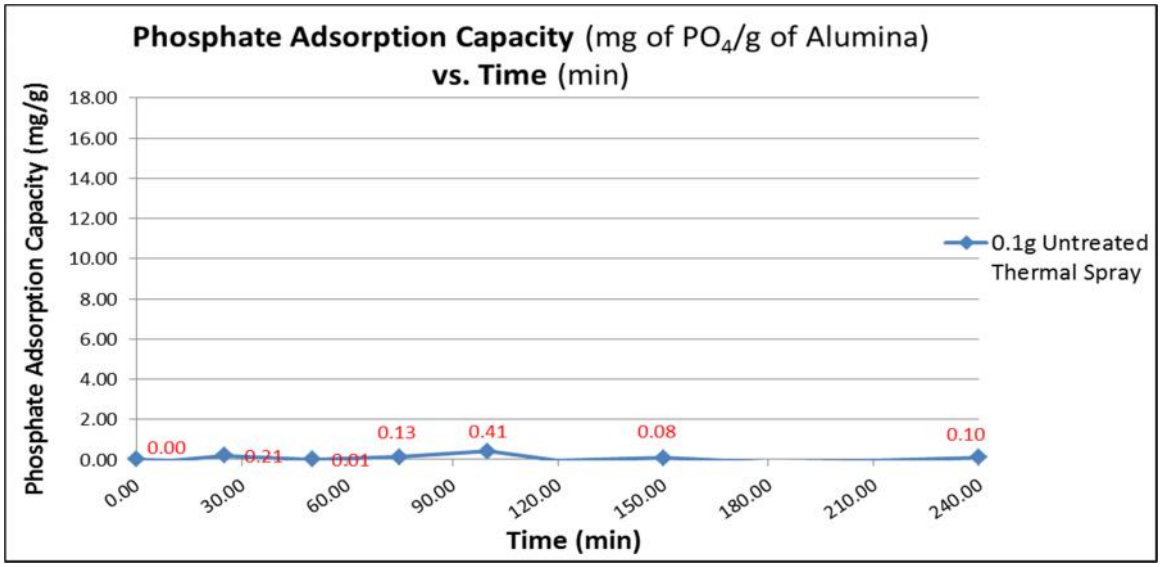

Figure 40. Phosphate adsorption capacity of untreated alumina powders (Thermal Spray) in phosphate solution (50 mL, initial PO_4 concentration of 30.47 mg/L) over 4-hour duration.

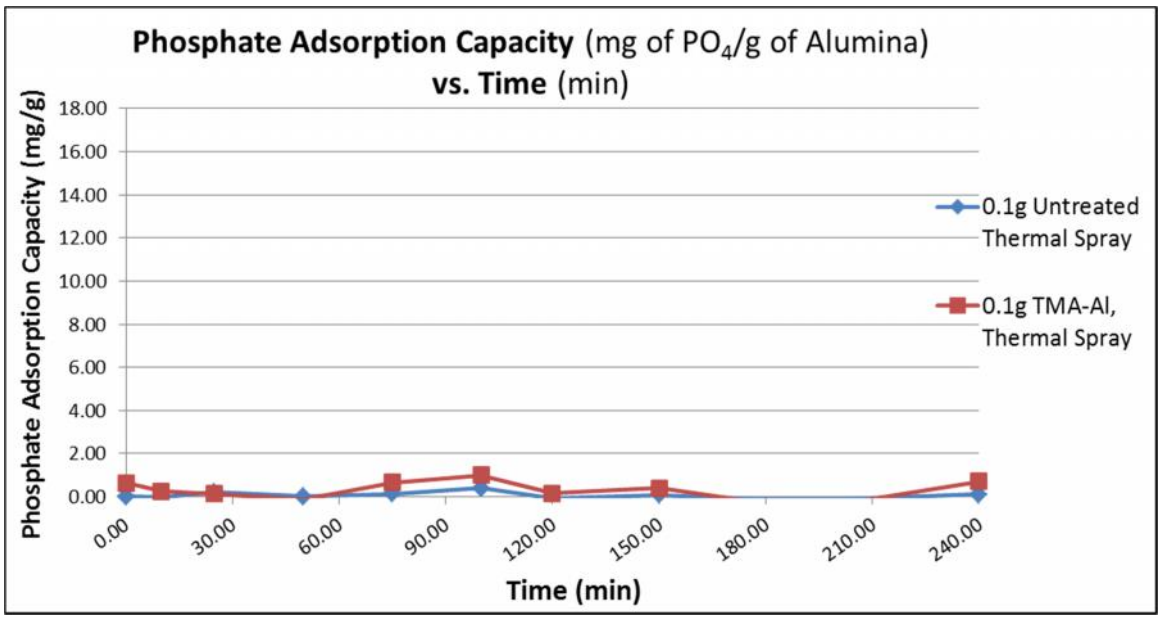

Figure 41. Comparison of phosphate adsorption capacities of TMA treated alumina powders (Thermal Spray) and untreated alumina powders (Thermal Spray) in phosphate solution (50 mL, initial PO_4 concentration of ~30 mg/L) over 4-hour duration.

A ball-milling operation was employed in an effort to yield an alumina powder of a particle size-range appropriate for use in flame-spraying operations that was also more conducive to phosphate adsorption following TMA-treatment than the original thermal spray powders. This milled variant of the Selecto Scientific alumina powders displayed high phosphate adsorption capabilities when tested in a ~30 mg/L phosphate solution in a bench-top setting (Figure 42 – Figure 43). The overall phosphate adsorption capacity observed for the milled, Selecto Scientific alumina powders after 4-hours was slightly higher, but in close agreement with that of the un-milled, TMA-treated Selecto Scientific powders (Figure 34 and Figure 42).

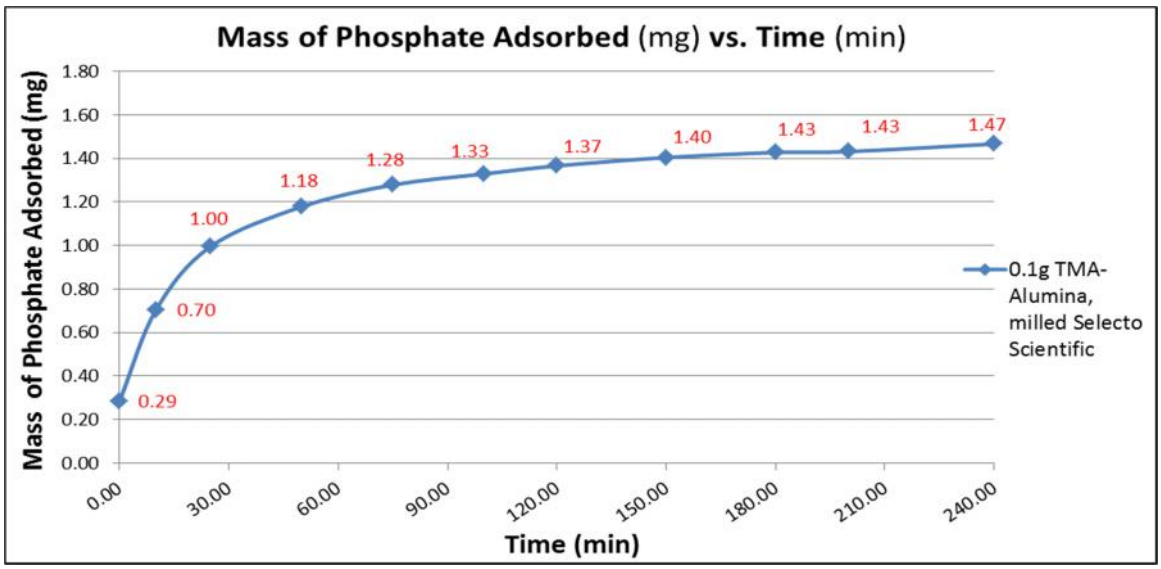

Figure 42. Mass of phosphate removed from phosphate solution (50 mL, initial PO_4 concentration of 34.63 mg/L) by 0.1g of TMA treated alumina powders (milled, Selecto Scientific) over 4-hour duration.

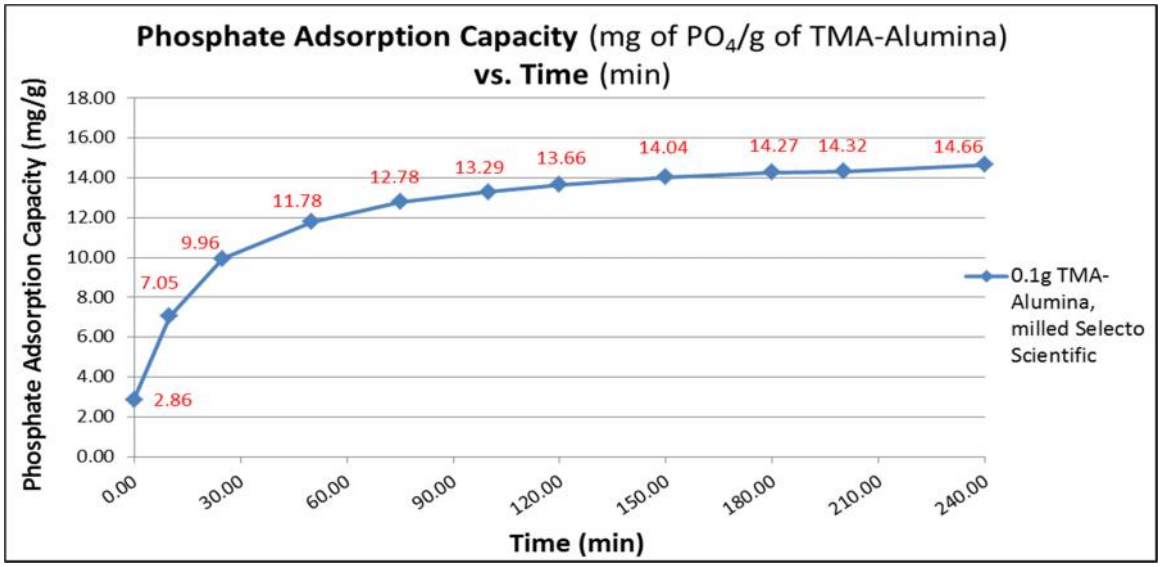

Figure 43. Phosphate adsorption capacity of TMA treated alumina powders (milled, Selecto Scientific) in phosphate solution (50 mL, initial PO_4 concentration of 34.63 mg/L) over 4-hour duration.

The TMA-treated Acros Organics alumina powder formulation proved to deliver the greatest levels of phosphate adsorption of all of the TMA-treated adsorbents tested in ~30

mg/L phosphate solution in the bench-top experiments (Figure 44 and Figure 45). Based on these results, the Acros Organics powders were reasoned to be the best performing alumina powders and were consequently selected for use in all subsequent adsorbent characterization and Carver® Press grafting procedures.

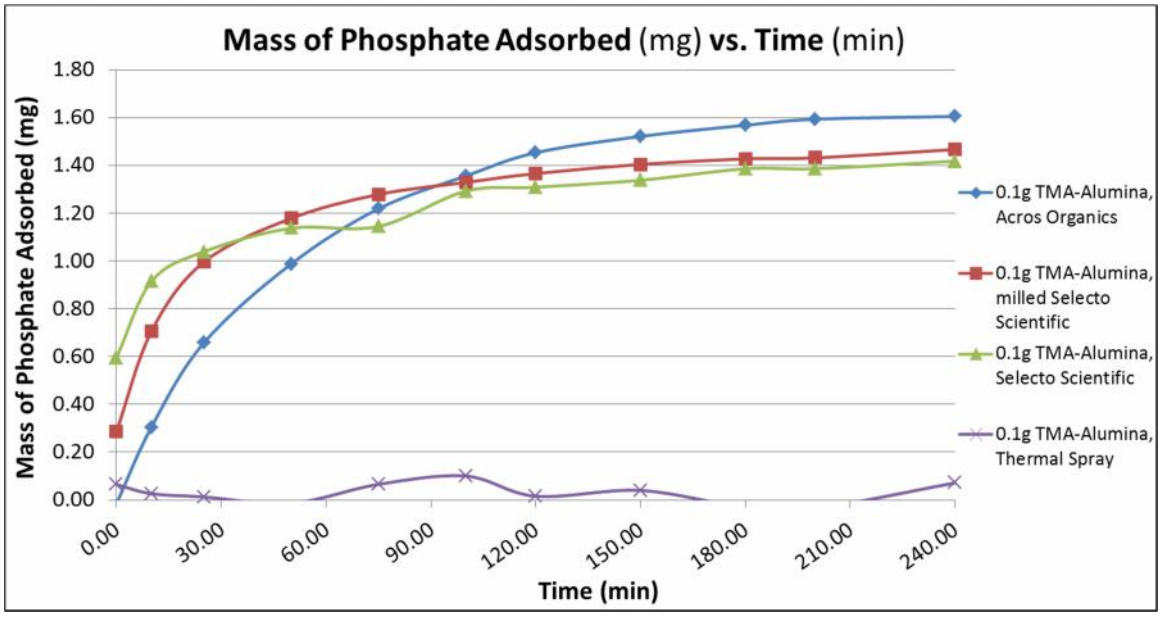

Figure 44. Comparison of phosphate masses removed from phosphate solutions (50 mL, initial PO_4 concentrations of ~30 mg/L) by 0.1g of various TMA treated alumina powders over 4-hour duration.

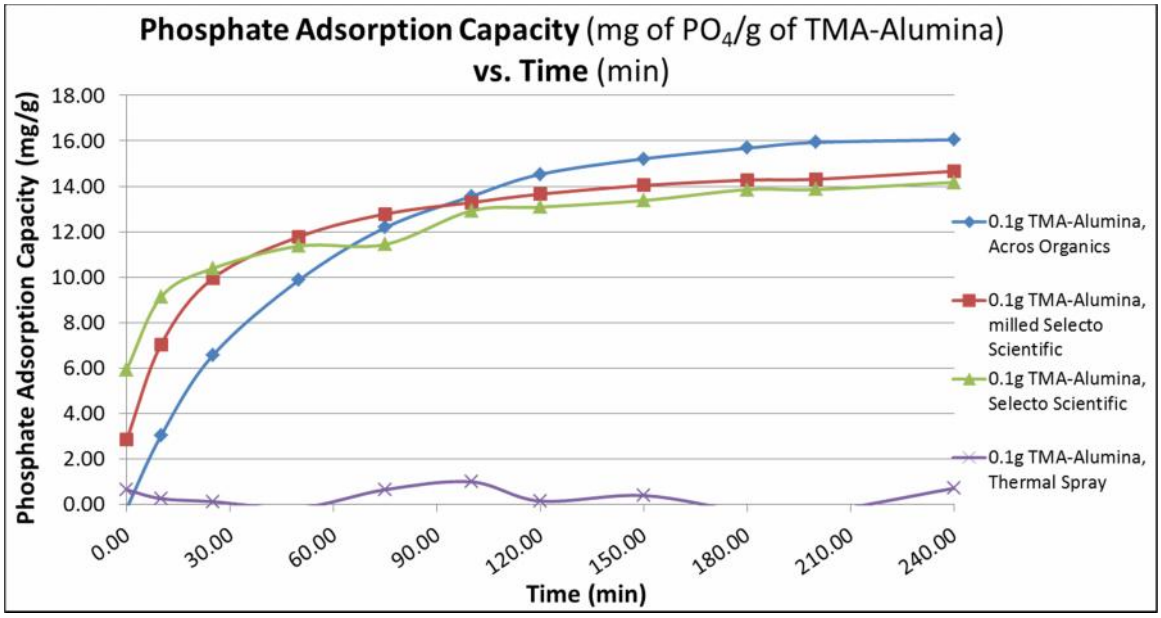

Figure 45. Comparison of phosphate adsorption capacities of various TMA treated alumina powders in phosphate solutions (50 mL, initial PO_4 concentrations of ~30 mg/L) over 4-hour duration.

6.4 X-ray Photoelectron Spectroscopy

From the results of X-ray Photoelectron Spectroscopy analyses, which measured the surface compositions of the untreated and TMA-treated Acros Organics alumina powders, the elemental compositions of the treated and untreated powder samples can be seen (Table 8, Figure 46 and Figure 47). The percentage elemental compositions of oxygen and aluminum were shown to decrease and the percentage elemental compositions of carbon were shown to increase, following the application of the TMA-treatment. Moreover, the O:Al ratio was shown to increase following the TMA-treatment.

Table 8. Surface composition of alumina powders before and after TMA treatment, as measured by X-ray Photoelectron Spectroscopy.

Sample	% Oxygen	% Carbon	% Aluminum	O:Al Ratio
Alumina Powders (Acros Organics), **prior to TMA-Treatment**	**60.2**	**5.0**	**34.9**	**1.77**
Alumina Powders (Acros Organics), **following TMA-Treatment**	**57.1**	**12.5**	**30.4**	**1.88**

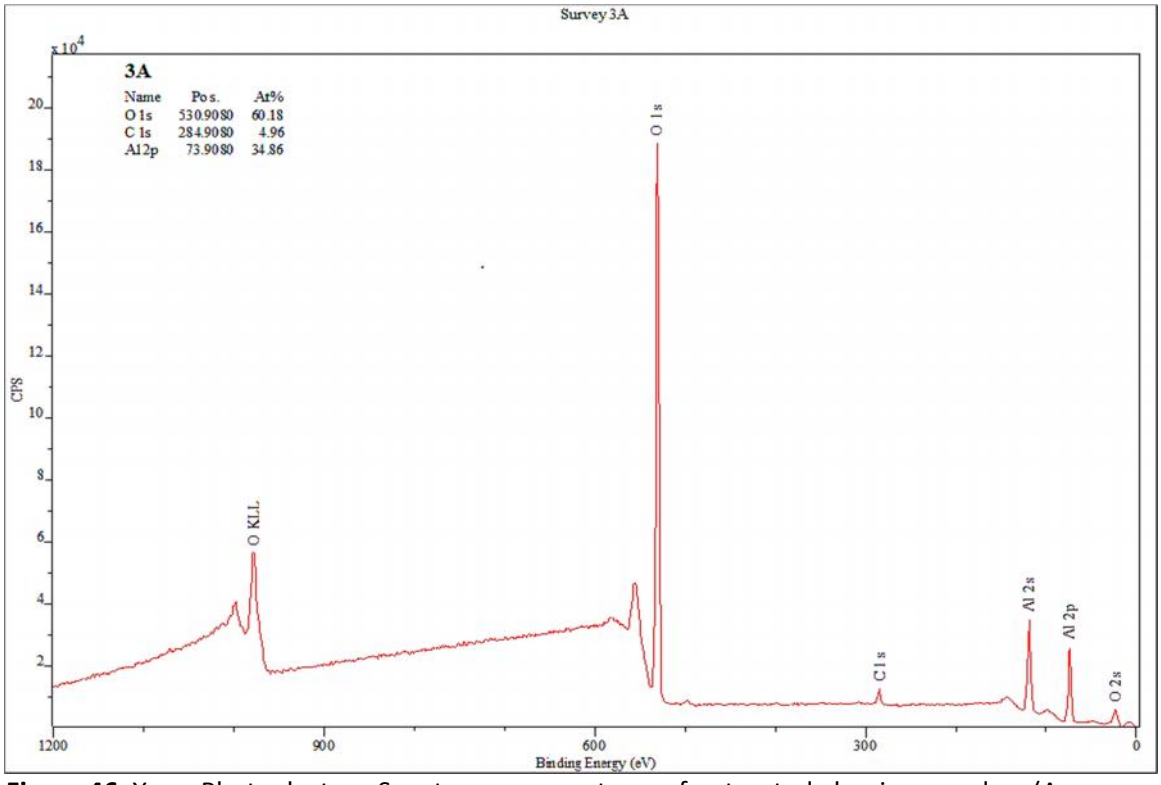

Figure 46. X-ray Photoelectron Spectroscopy spectrum of untreated alumina powders (Acros Organics).

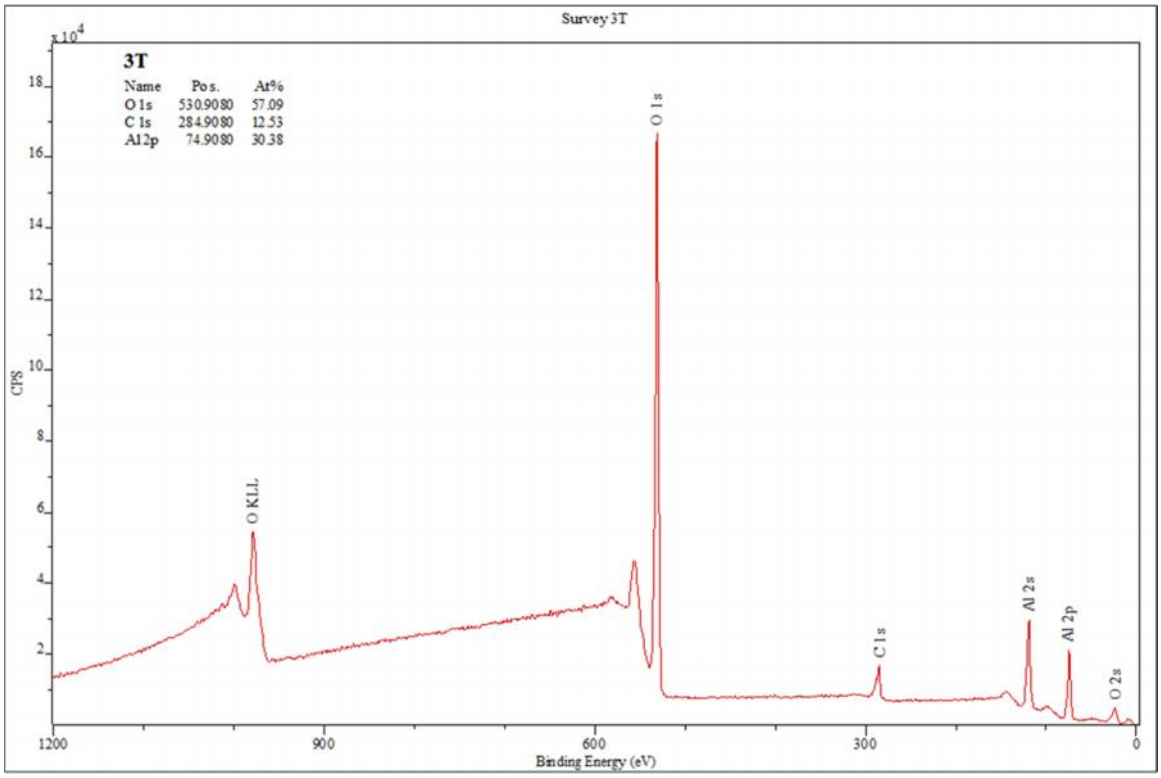

Figure 47. X-ray Photoelectron Spectroscopy spectrum of alumina powders (Acros Organics) following TMA treatment.

6.5 Bench-top Phosphate Adsorption Studies on Fabrics – Phosphate Solution

The phosphate adsorption capacities of fabrics grafted with TMA-alumina via Carver® pressing (Acros Organics alumina) and flame-spraying (thermal spray alumina) in phosphate solutions of various initial phosphate concentrations are graphed in Figure 37 and Figure 38, respectively. While the adsorption afforded by the TMA-treated Acros Organics alumina powders on fabrics was lower than that measured for the TMA-treated powders alone (Figure 28), the Carver® pressed alumina fabrics were consistently shown to reduce the measured phosphate levels in solution (Figure 48). In contrast, the thermal sprayed PET fabrics were shown by the phosphate adsorption assay to provide a very low level of

phosphate adsorption from phosphate solution (Figure 49). The phosphate concentrations measured by the phosphate colorimetric assay and the subsequently calculated phosphate adsorption capacities of the TMA-treated flame-spray powders (thermal spray powders) were therefore shown to irregularly vacillate around the x-axis, much in the same way as that observed for the TMA-treated thermal spray powders alone.

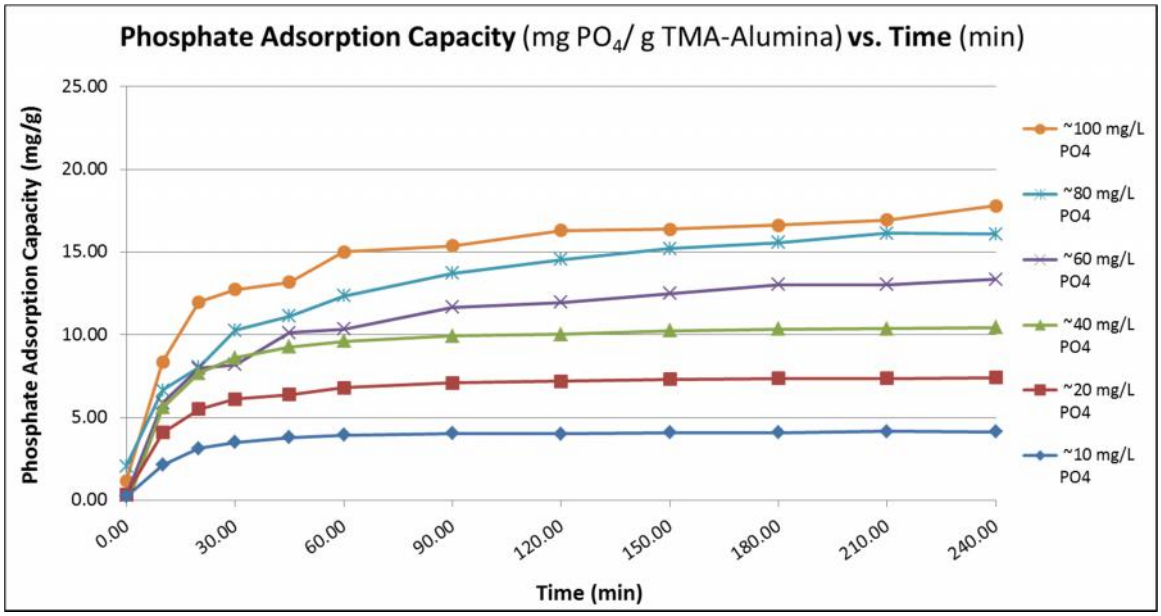

Figure 48. Comparison of phosphate adsorption capacities of TMA-Alumina impregnated fabric samples (Carver® pressed, Acros Organics) phosphate solutions (80 mL, initial PO_4 concentrations of ~10, ~20, ~40, ~60, ~80, ~100 mg/L) over 4-hour duration. Alumina masses grafted on fabric samples used in experiments of 0.220g, 0.243g, 0.314g, 0.308g, 0.326g, and 0.399g respectively.

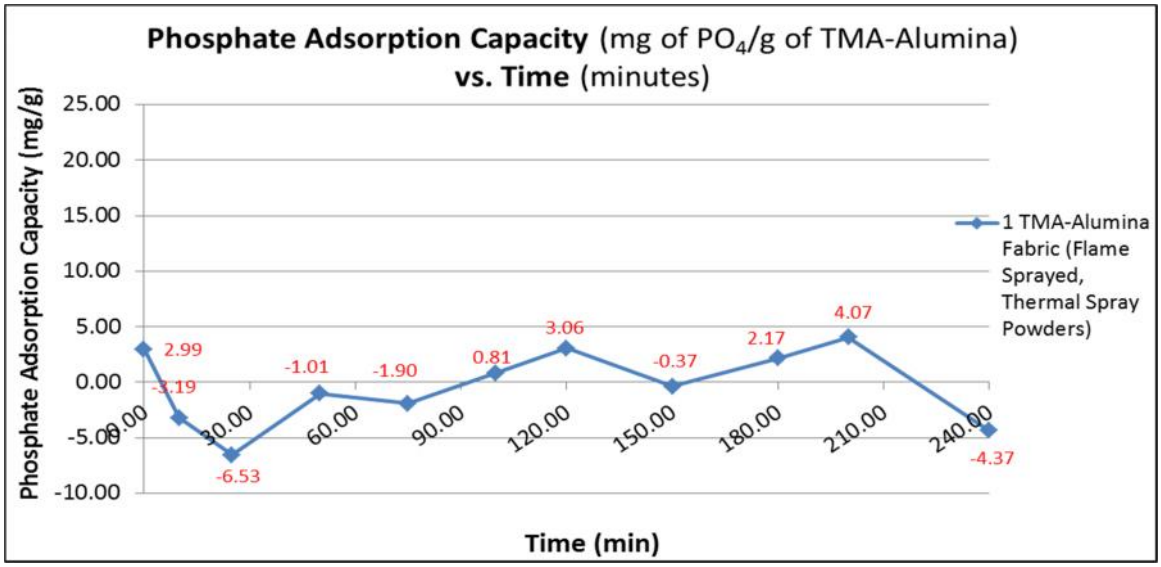

Figure 49. Phosphate adsorption capacity of 1 TMA-Alumina impregnated fabric (Flame Sprayed, Thermal Spray Powders) in 80mL of ~20 mg/L phosphate solution. PET blood filtration fabrics grafted with a total of 0.041g of TMA-Alumina hemoadsorbent and exposed to phosphate solution for 4 hours.

6.6 Phosphate Selectivity Studies

6.6.1 Lactated Ringer's Solution

The phosphate adsorption capacities by assemblies of TMA-alumina (Acros Organics) Carver® pressed onto PET filtration fabrics in phosphate-spiked lactated Ringer's solution are shown in Figure 39 below. Despite the presence of other electrolytes in the lactated Ringer's solution, the phosphate adsorption capacities at 4-hours (Figure 50) were similar to that observed in the solution containing only phosphate ions (Figure 48). These results serve to illustrate preliminary trials that indicated phosphate selectivity in a physiologically relevant solution.

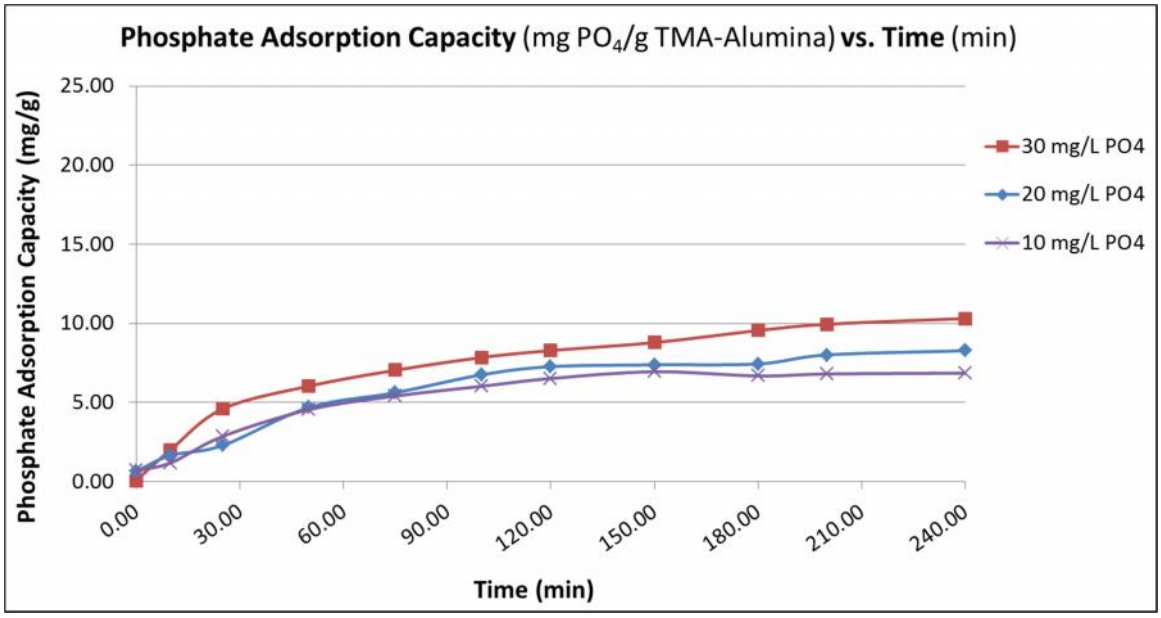

Figure 50. Comparison of phosphate adsorption capacities of TMA-Alumina grafted fabric samples (Carver® pressed, Acros Organics) in Lactated Ringer's solution (80mL, spiked with PO_4 concentrations of ~10, ~20 and ~30 mg/L) over 4-hour duration. Alumina masses grafted on fabric samples used in experiments of 0.0461g, 0.0341g and 0.0497g respectively.

6.6.2 Bovine Whole Blood

Results of full chemistry panels ran on bovine blood samples exposed to TMA-alumina Fabrics (Carver® pressed, Acros Organics) are shown in Table 9. These results show that the prolonged exposure of bovine blood to Carver® pressed TMA-alumina (Acros Organics) fabrics resulted in high reductions of phosphate concentrations, moderate reductions of calcium concentrations and mild reductions in chloride and bicarbonate concentrations from analyzed plasma. Moreover, these results indicate that small increases in the plasma sodium, potassium, albumin, glucose and total protein concentrations were measured.

Table 9. Results of blood chemistry panels from bench-top tests with heparinized bovine whole blood exposed to TMA-Alumina grafted PET filtration fabrics (Carver® pressed, Acros Organics) for 60 minutes. Red values indicate reductions in measured analyte concentrations; green values indicate increased analyte concentrations. Alumina mass grafted to fabric used in experiment of 0.158g.

	Samples Tested			Net Change After 60 Minute Experiment	
	Bovine Whole Blood, Initial	Bovine Whole Blood (control), t = 60 minutes	Bovine Whole Blood + TMA-Alumina Fabric (carver-pressed, Acros Organics), t = 60 minutes	Bovine Whole Blood (control)	Bovine Whole Blood + TMA-Alumina Fabric (carver-pressed, Acros Organics)
Glucose (mg/dL)	61	61	64	0	3
Total Protein (g/dL)	6.8	7.0	7.2	0.2	0.4
Albumin (g/dL)	3.1	3.3	3.4	0.2	0.3
Cl- (mEq/L)	93	93	91	0	-2
K+ (mEq/L)	6.8	6.8	6.9	0.0	0.1
Na+ (mEq/L)	133	133	136	0	3
Bicarbonate (mmol/L)	30	28	25	-2	-5
Phosphorus (mg/L)	82	83	33	1	-49
Creatinine (mg/dL)	0.92	0.92	0.81	0.00	-0.11
Urea, BUN (mg/dL)	14	15	15	1	1
Calcium (mg/dL)	9.4	9.6	6.7	0.2	-2.7
Magnesium (mEq/L)	1.5	1.7	1.5	0.2	0.0

6.7 Hemoperfusion Simulation Circuit Adsorption Studies

6.7.1 Phosphate Solution

The results of the simulated hemoperfusion experiments with 1 liter of circulating phosphate solutions exposed to Carver® pressed TMA-alumina (Acros Organics) fabrics are shown directly below (Figures 51 – 57).

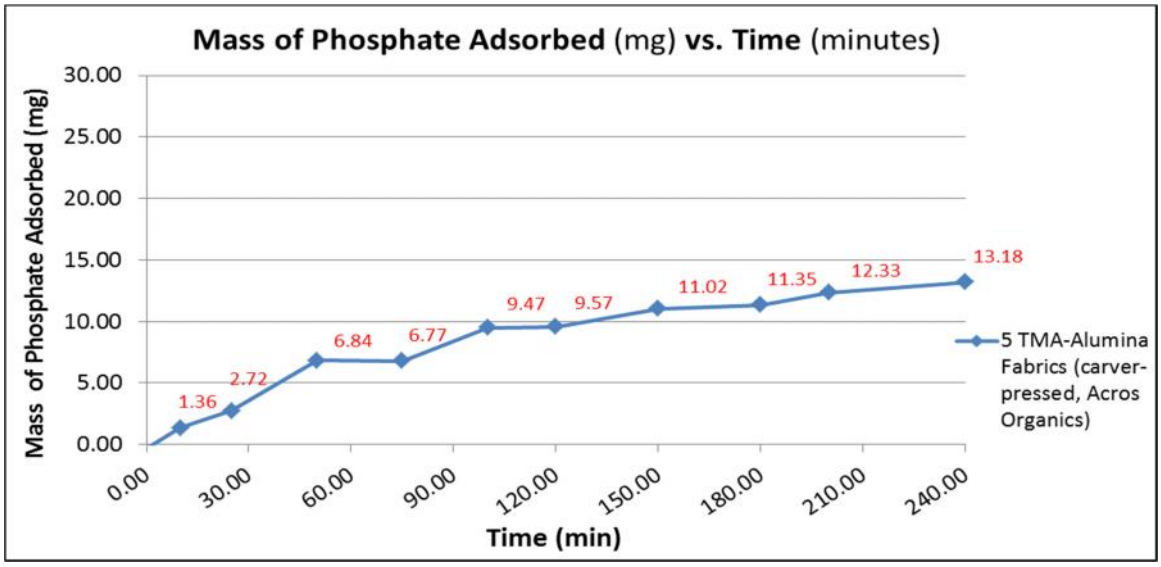

Figure 51. Mass of phosphate adsorbed from 1L of ~30 mg/L phosphate solution by 5 TMA-Alumina grafted fabric samples (Carver® pressed, Acros Organics). PET blood filtration fabrics grafted with a total of 1.400g of TMA-Alumina hemoadsorbent, loaded into test cell and exposed to circulating phosphate solution for 4 hours.

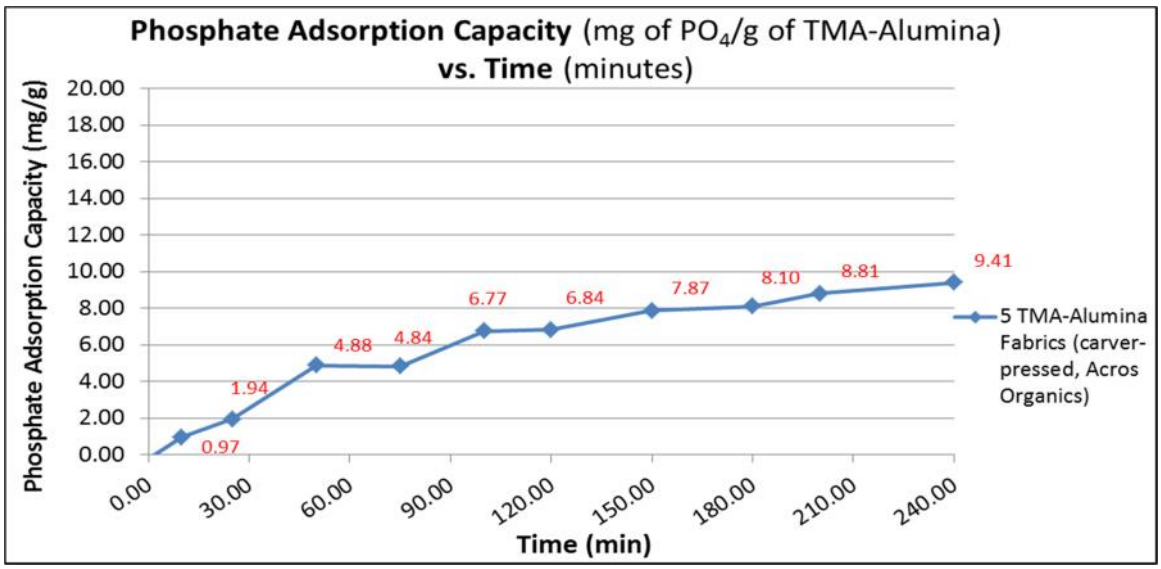

Figure 52. Phosphate adsorption capacity of 5 TMA-Alumina grafted fabric samples (Carver® pressed, Acros Organics) in 1L of ~30 mg/L phosphate solution. PET blood filtration fabrics grafted with a total of 1.400g TMA-Alumina hemoadsorbent, loaded into test cell and exposed to circulating phosphate solution for 4 hours.

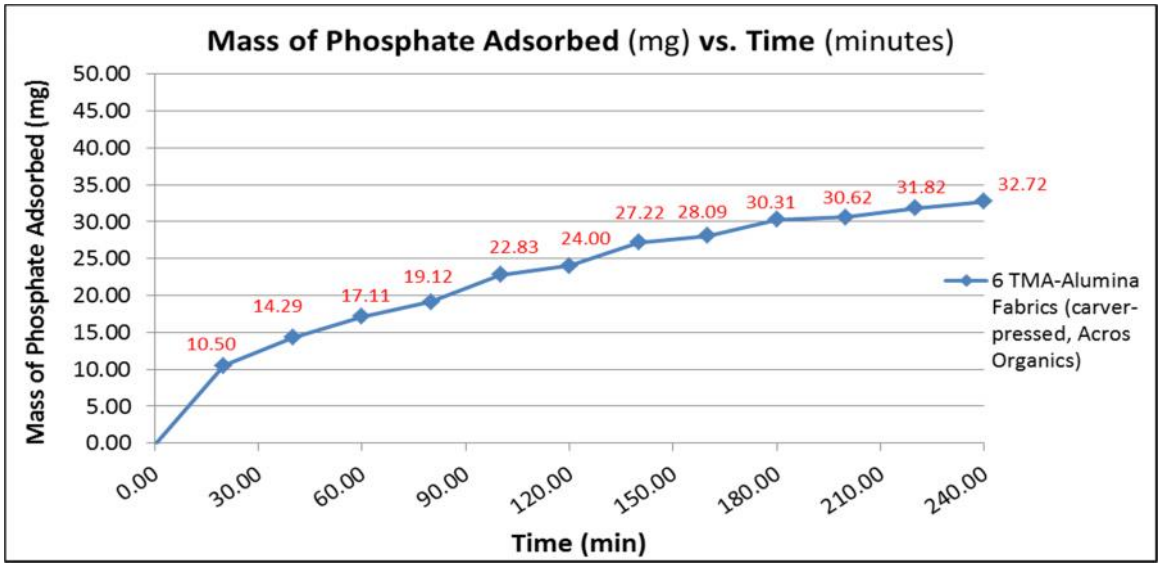

Figure 53. Mass of phosphate adsorbed from 1L of ~50 mg/L phosphate solution by 6 TMA-Alumina grafted fabric samples (Carver® pressed, Acros Organics). PET blood filtration fabrics grafted with a total of 1.926g of TMA-Alumina hemoadsorbent, loaded into test cell and exposed to circulating phosphate solution for 4 hours.

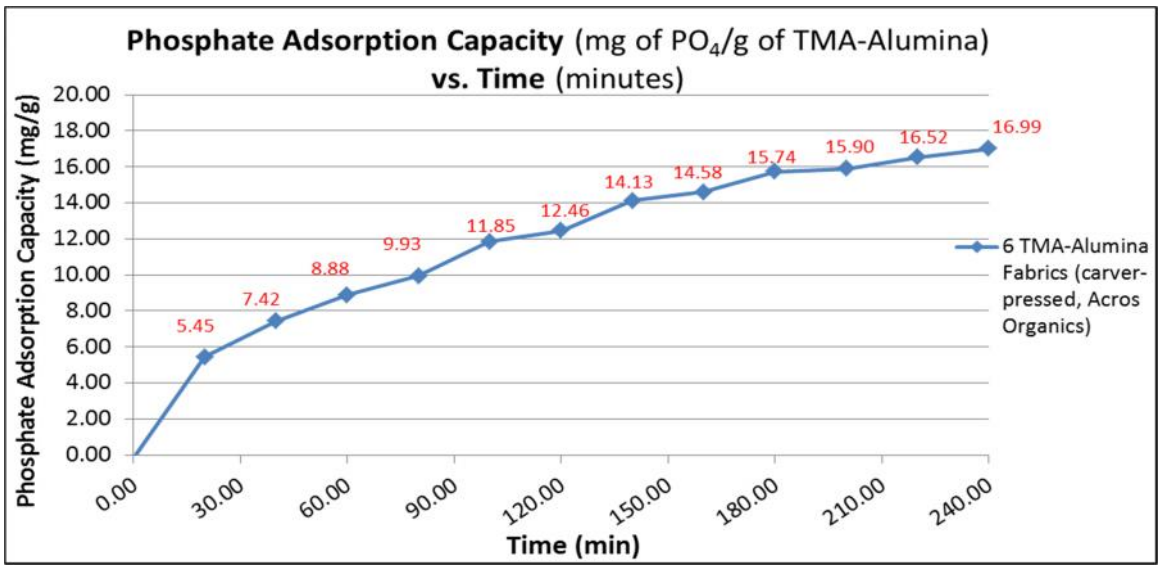

Figure 54. Phosphate adsorption capacity of 6 TMA-Alumina grafted fabric samples (Carver® pressed, Acros Organics) in 1L of ~50 mg/L phosphate solution. PET blood filtration fabrics grafted with a total of 1.926g TMA-Alumina hemoadsorbent, loaded into test cell and exposed to circulating phosphate solution for 4 hours.

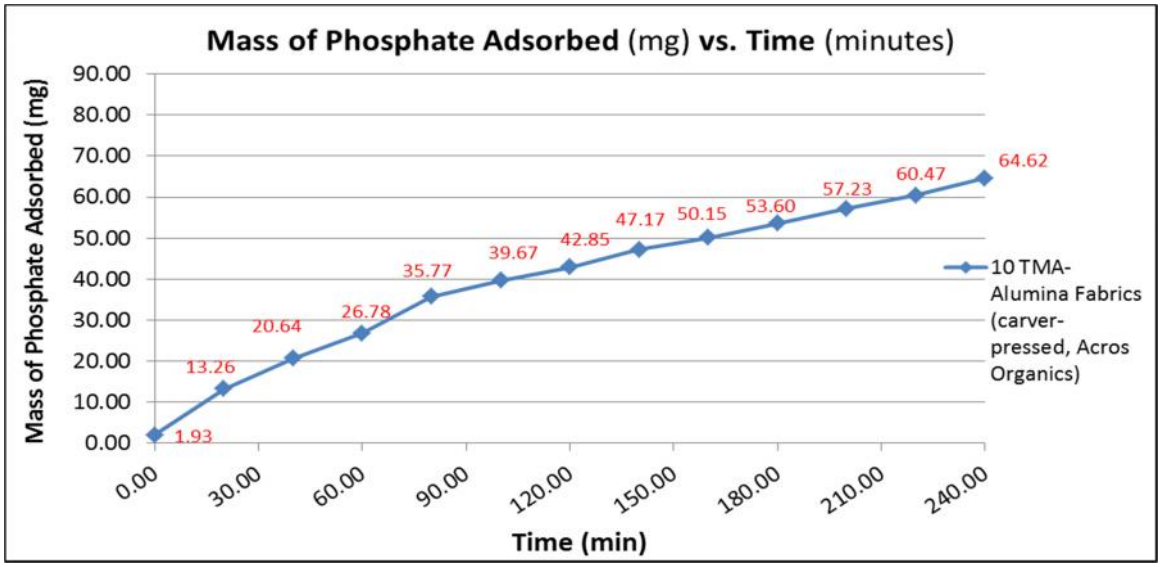

Figure 55. Mass of phosphate adsorbed from 1L of ~90 mg/L phosphate solution by 10 TMA-Alumina grafted fabric samples (Carver® pressed, Acros Organics). PET blood filtration fabrics grafted with a total of 3.299g of TMA-Alumina hemoadsorbent, loaded into test cell and exposed to circulating phosphate solution for 4 hours.

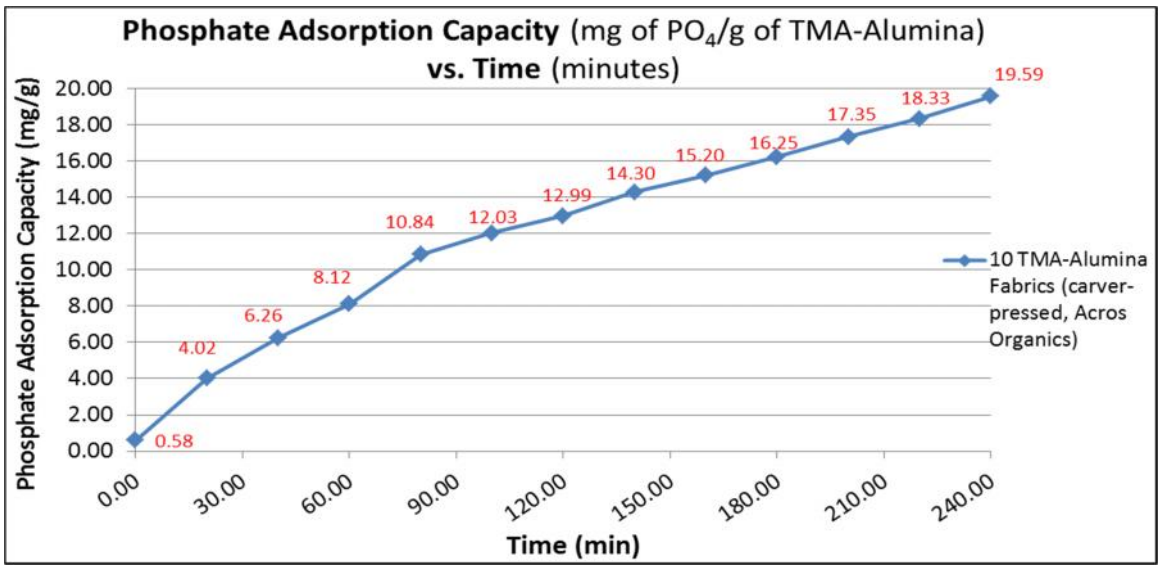

Figure 56. Phosphate adsorption capacity of 10 TMA-Alumina grafted fabric samples (Carver® pressed, Acros Organics) in 1L of ~90 mg/L phosphate solution. PET blood filtration fabrics grafted with a total of 3.299g TMA-Alumina hemoadsorbent, loaded into test cell and exposed to circulating phosphate solution for 4 hours.

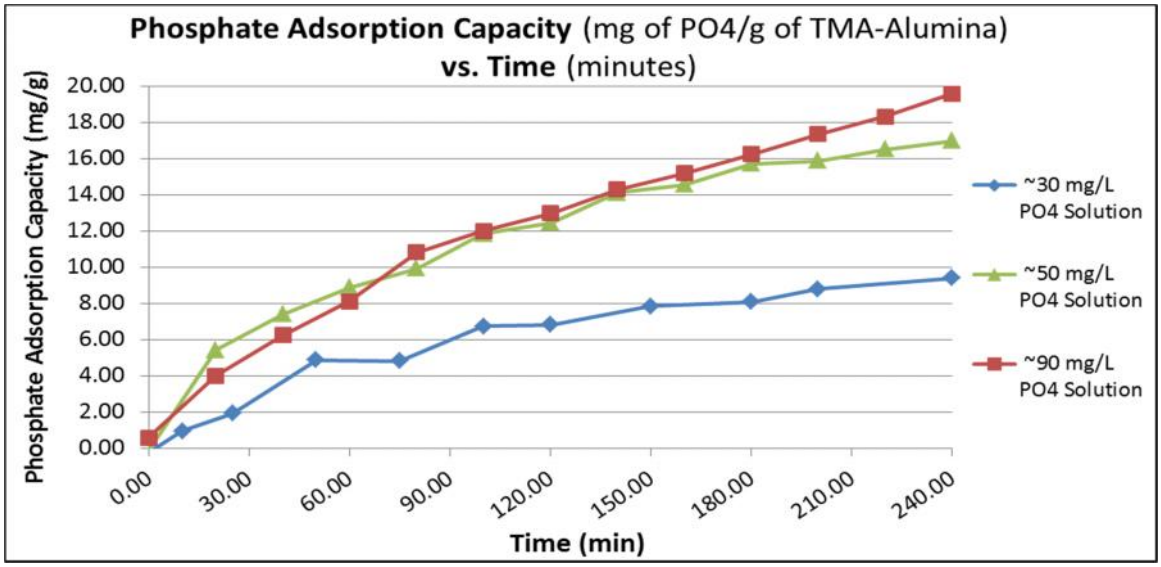

Figure 57. Phosphate adsorption capacities of TMA-Alumina grafted fabric samples (Carver® pressed, Acros Organics) in 1L of ~30, ~50, and ~90 mg/L phosphate solutions. PET blood filtration fabrics grafted with TMA-Alumina hemoadsorbents, loaded into test cell and exposed to circulating phosphate solutions for 4 hours.

6.7.2 Bovine Whole Blood

Figure 58 displays the mass of phosphate adsorbed by 10 Carver® pressed TMA-alumina fabrics (Acros Organics) from 1 liter of circulating bovine whole blood at an initial plasma concentration of 89 mg/L, over the 4-hour duration. From figure 58, it can be seen that 38 mg of phosphate, out of a total of 89 mg of phosphate initially present, was adsorbed by the 10 TMA-alumina fabrics during the 4-hour span. 3.846g of the TMA-alumina hemoadsorbent was grafted to the 10 PET filtration fabrics used in the hemoperfusion experiment, reflecting a calculated adsorption capacity of 9.88 mg/g, as shown in Figure 59.

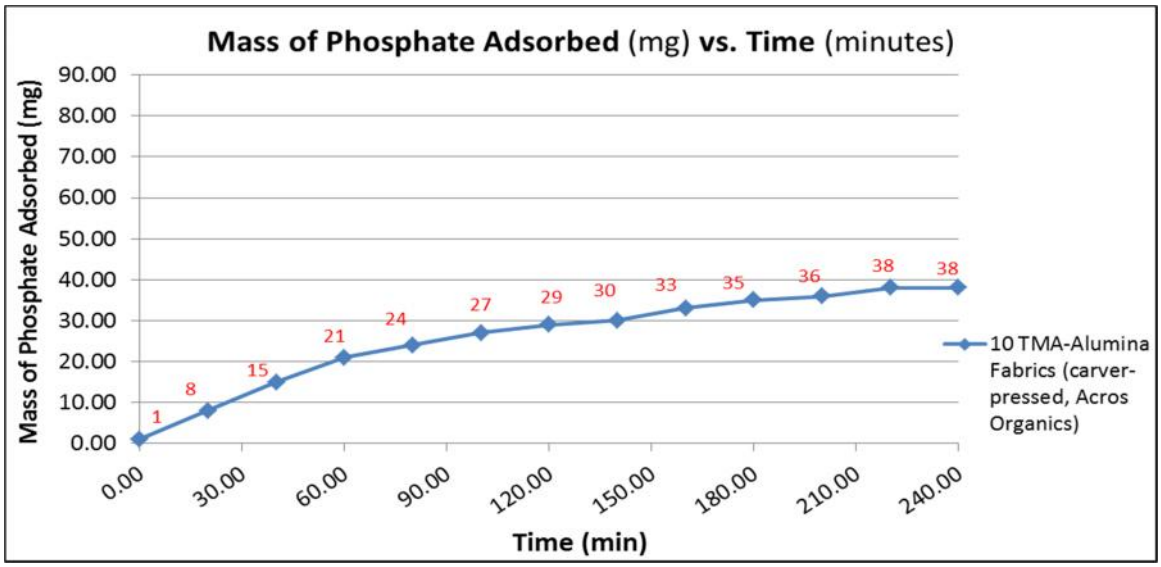

Figure 58. Mass of phosphate adsorbed from 1L of heparinized bovine whole blood by 10 TMA-Alumina grafted fabric samples (Carver® pressed, Acros Organics). PET blood filtration fabrics grafted with a total of 3.846g of TMA-Alumina hemoadsorbent, loaded into test cell and exposed to circulating whole blood, with an initial measured phosphate concentration of 89 mg/L, for 4 hours.

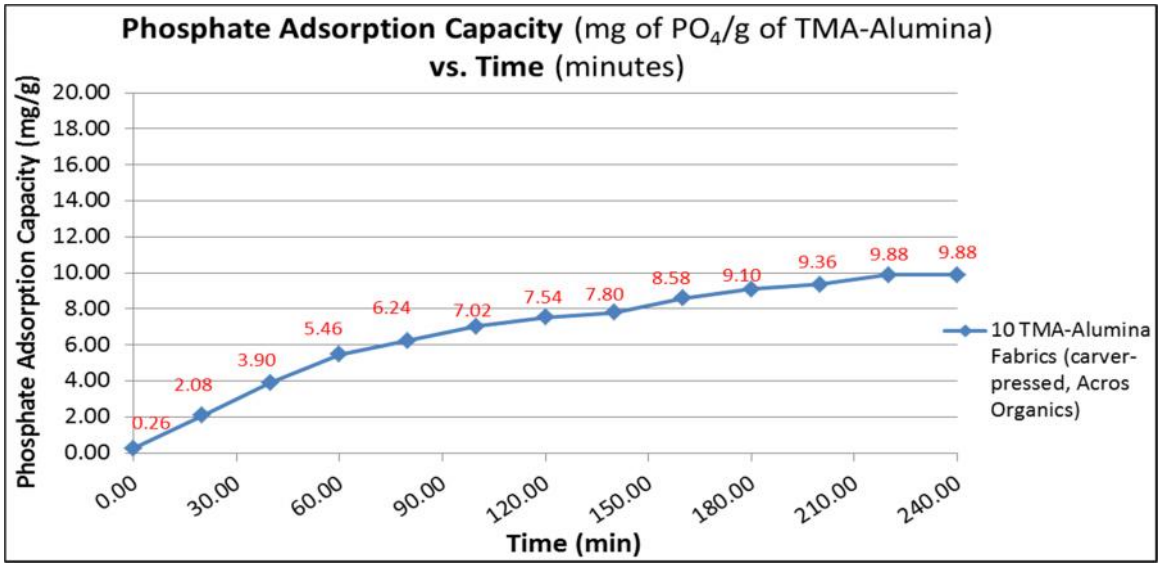

Figure 59. Phosphate adsorption capacity of 10 TMA-Alumina grafted fabric samples (carver® pressed, Acros Organics) in 1L of heparinized bovine whole blood. PET blood filtration fabrics grafted with a total of 3.846g TMA-Alumina hemoadsorbent, loaded into test cell and exposed to circulating whole blood for 4 hours.

6.8 Alumina Particulate Shedding/Dissolution Studies (ICP-MS)

Table 10 and Table 11 display the results from the ICP-Mass Spectrometry analyses of bovine blood and human blood samples exposed to PET filtration fabrics that were first Carver® pressed with TMA-treated Acros Organics alumina powders. The results indicate substantial increases in the measured aluminum ion concentrations of the collected blood samples versus the control samples, following the 60-minute exposure of the blood to the hemoadsorbent-loaded substrate and the execution of the trace metal testing protocol.

Table 10. Results from ICP-Mass Spectroscopy analyses of plasma samples derived from heparinized bovine blood, with and without exposure to TMA-Alumina Fabrics (Carver® pressed, Acros Organics). 0.158g of TMA-Alumina grafted to fabric sample used in experiment.

Blood Type	**Sample Collection Time** (min.)	**Experimental Condition**	**Measured Aluminum Concentration** (ng/mL)	**Mass of Aluminum in Sample** (ng)
Bovine	**0.00**	**Whole Blood Only** (initial)	**7**	**7**
	60.00	**Whole Blood Only** (control)	**7**	**7**
	Aluminum mass increase during 60-minute exposure to TMA-Alumina fabric (ng)**:**			**0**
Bovine	**0.00**	**Whole Blood Only** (initial)	**7**	**7**
	60.00	**Whole Blood + TMA-Alumina Fabric**	**418**	**418**
	Aluminum mass increase during 60-minute exposure to TMA-Alumina fabric (ng)**:**			**411**

Table 11. Results from ICP-Mass Spectroscopy analyses of plasma samples derived from heparinized human blood, with and without exposure to TMA-Alumina Fabrics (Carver® pressed, Acros Organics). 0.150g of TMA-Alumina grafted to fabric sample used in experiment.

Blood Type	**Sample Collection Time** (min.)	**Experimental Condition**	**Measured Aluminum Concentration** (ng/mL)	**Mass of Aluminum in Sample** (ng)
Human	**0.00**	**Whole Blood Only** (initial)	**5**	**5**
	60.00	**Whole Blood Only** (control)	**6**	**6**
	Aluminum mass increase during 60-minute exposure to TMA-Alumina fabric (ng)**:**			**1**
Human	**0.00**	**Whole Blood Only** (initial)	**5**	**5**
	60.00	**Whole Blood + TMA-Alumina Fabric**	**490**	**490**
	Aluminum mass increase during 60-minute exposure to TMA-Alumina fabric (ng)**:**			**485**

7. Discussion

The purpose of the TMA-treatment was to impart surface functionalities to the alumina powders that have been proven by previous research to be both efficient at phosphate adsorption and phosphate selective.[65] Contrary to previously published works,[86] comparisons of the SEM images that display the 1000x magnified surface of the untreated alumina powders and the 1000x magnified surface of TMA-treated alumina powders (Figure 20) revealed that the TMA-treatment produced no significant alterations in surface morphology. Although, it should be noted that the magnifications used in the previously

published work is slightly greater than the magnification used in the current research. However, the results of the X-ray photoelectron spectroscopy analysis (Table 8) indicated that significant chemical alterations on the surface of the Acros Organics alumina powders were caused by the application of the TMA-treatment. The percentage elemental composition of carbon was observed, by XPS, to increase following the TMA-treatment, a phenomenon consistent with the increases in carbon that are afforded by the addition of the benzene rings and carboxyl groups to the alumina surface. While the overall surface oxygen content decreased following the TMA-treatment, this was likely a result of the increased carbon content added by the TMA-treatment and was not indicative that the overall quantity of oxygen atoms decreased. The oxygen to aluminum ratio also increased following TMA-treatment, lending further credence to this concept.

The mechanistic scheme of TMA-alumina based phosphate adsorption shown below (Figure 60), which was adapted from mechanistic insights provided by Saha et al.[65] indicated that the magnitude of phosphate adsorption should be dependent upon the number of TMA molecules present in the system. Moreover, the scheme suggests that the number of TMA molecules that are imparted to the alumina surface is directly determined by the quantity of accessible –OH and O^- sites that are present on the alumina surface. The results of the current study reinforce these concepts. Despite the use of the same mass of TMA-alumina, all TMA-treated alumina powder formulations except for the TMA-treated thermal spray powders showed significant phosphate adsorption at a bench-top scale (Figure 45). Moreover, the SEM images obtained for the alumina powders revealed the Acros Organics

alumina powders and the Selecto Scientific alumina powders to be fused agglomerates of smaller particles (Figure 17 and Figure 18), a morphology indicative of high surface area. In contrast, the thermal spray powders appear to be smooth, spherical particles with minimal surface area (Figure 23). A comparison of the manufacturers' specifications also shows that the measured surface area of the alumina particles was the greatest for the Acros Organics powders. When taken together, these findings suggest the importance of the provision of a highly porous alumina surface to present a significant amount of reactive surface functionalities for a high degree of TMA attachment. The Acros Organics powders, with the highest reported surface areas and a surface morphology indicative of high porosity, also showed the greatest phosphate adsorption capacities of all of the powders in the bench-top phosphate adsorption experiments (Figure 45). Consequently, the Acros Organics alumina powders were determined to be the best performing of the alumina powders and were chosen for use in all Carver® pressing experiments that followed.

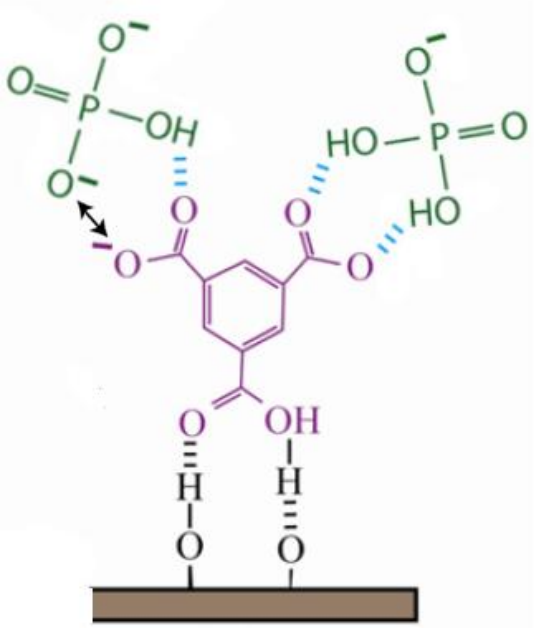

Figure 60. Mechanistic view of phosphate adsorption exhibited by TMA-alumina at the physiologic pH of 7.4.[65]

Various grafting methods were explored throughout the course of this research in an effort to optimize the amount of alumina powders added to the material substrate and to provide a strong and robust degree of adhesion. Initially the deposition characteristics of Carver® pressing and flame-spraying methods were evaluated. Although the SEM images obtained of fabrics flame-sprayed with thermal sprayed powders displayed uniform coverage of a large fraction of the fabric surface (Figure 22 and Figure 23), subsequent evaluations of phosphate removal provided by the TMA-treated thermal spray powders (Figure 38) and the TMA-treated flame-sprayed fabrics (with thermal sprayed powders) (Figure 49) showed that both sample types were unable to provide a significant amount of phosphate adsorption. In an effort to provide a powder sample for flame-spraying that was proven to

be phosphate adsorptive, the Selecto Scientific alumina powders were ball-milled and the resulting powder was flame-sprayed to PET filtration fabrics. However, SEM images (Figure 24) and the calculated grafting yield (Table 7) of the resulting fabric surface showed that the alumina deposition was sparse. Though the milled powders were appropriately sized for the flame-spraying operation, their irregular morphology and tendency to self-agglomerate caused caking of the powder sample in the hopper and flow-paths of the flame-spray apparatus, resulting in very little alumina mass transference to the PET substrate. On the other hand, the Carver® press grafting method, using the Acros Organics alumina, was shown to provide significant grafting yields (Table 7) and substantial phosphate adsorption (Figure 48). Moreover, the Carver® press method was versatile in that substrates of varying sizes could be quickly manufactured using a variety of readily adjustable process parameters. In an effort to provide chemical attachment of alumina to the fabric substrates, the use of atomic layer deposition (ALD) and sequential vapor infiltration (SVI) techniques were later explored. However, both of these methods failed to add alumina in quantities that were sufficient for the hemoperfusion application (Table 7). Furthermore, examination of SEM images showed that the surfaces of fabrics treated with ALD were devoid of surface modifications (Figure 25) and SVI treated fabrics showed fiber surface degradation but no indications of alumina addition (Figure 26). With these results in mind, the Carver® pressed fabrics, using Acros Organics alumina, were selected for further evaluation.

Evaluations of the phosphate adsorption characteristics of the TMA-treated Carver® pressed fabrics were first carried out in a bench-top scenario. Measured phosphate adsorption results in experiments with fabrics exposed to solutions with a range of initial phosphate concentrations (Figure 48) indicated phosphate adsorption capacities ranging from 4.2 mg/g – 19.6 mg/g. This follows similar reaction kinetics as studies involving only TMA-treated powders, which are reported in this research (Figure 28) and in previously published studies.[65] The magnitude of adsorption capacities of the TMA-alumina fabrics (Figure 48) were lower than that measured for the powders (Figure 45) – a phenomenon that can be attributed to the partial sequestering of the alumina surface area following the Carver® press grafting procedures. The kinetics observed are indicative of a Langmuir process,[65,83,84] where all adsorption occurs through the same process and maximum adsorption results in monolayer coverage of the adsorbent. Bench-top selectivity studies indicated that TMA-alumina selectively adsorbed phosphate from complex physiologic solutions with minimal off-target binding. Preliminary phosphate adsorption studies assessing the phosphate adsorption capacity of TMA-alumina in a physiologically relevant lactated Ringer's solution (Figure 50) indicated that phosphate adsorption capacities of the TMA-Alumina fabrics were not reduced by the presence of other electrolytes. In fact, phosphate adsorption capacities appeared to be greater in lactated Ringer's solution than in solutions containing phosphate alone (Figure 45). Full-chemistry analyses of bovine blood exposed to TMA-alumina fabrics in the bench-top experiment (Table 9) showed that the TMA-alumina hemoadsorbents were far more selective towards phosphate than other

anions present in blood and that calcium was the only cation that was significantly reduced. Glucose, total protein and albumin showed minor increases due to unknown causes. Studies in the hemoperfusion circuit indicated that by combining TMA-alumina fabrics together to provide an increased adsorbent mass, large amounts of phosphate that are more consistent with levels of reduction necessary for physiologically effective phosphate hemoperfusion can be achieved. Moreover, the graphical results depicting phosphate adsorption capacities in circulating phosphate solution of varying concentrations (Figure 57) did not show obvious tapering of phosphate removal over the 4-hour span, suggesting that saturation of the adsorbent system has not yet occurred. Experiments that exposed 1 liter of continuously circulating bovine whole blood to 10 hemoperfusion fabrics, Carver® pressed with a total of 3.846g of TMA-alumina showed that a total of 38 mg of phosphate were removed from bovine whole blood (Figure 58), representing a 42.7% mass reduction of phosphate after 4-hours of hemoperfusion with the TMA-alumina modified fabrics. Interestingly, the 38 mg mass of phosphate reduced from the 1 liter of circulating bovine whole blood (Figure 58), with an initial phosphate mass of 89 mg was much lower than the 64.62 mg of phosphate adsorbed from 1 liter of phosphate solution with an initial phosphate mass of 90 mg (Figure 55). This is perhaps due to the fact that 40% of circulating blood is composed of red blood cells and phosphate is primarily found in the extracellular space;[1,5,21] therefore it can be reasoned that less than 60% of the circulating blood volume contains phosphate that is available for adsorption.

Results of the ICP-MS analyses of heparinized human whole blood samples (Table 10) and heparinized bovine whole blood samples (Table 11) showed additions of 485ng and 411ng of aluminum, respectively, following 60 minutes of exposure to a TMA-Alumina Carver® pressed fabrics. As this concentration should be equivalent throughout the entire 50mL test volume, these measurements are indicative of total TMA-alumina percentage mass reductions of 0.016% and 0.013% from the hemoperfusion fabrics after exposure to the heparinized human whole blood and heparinized bovine whole blood, respectively. As previously mentioned, the ICP-MS protocol used to evaluate aluminum concentrations present in the blood requires the application of an aqueous acid diluent to the samples, prior to analysis. Alumina is practically insoluble at the physiologic pH of blood, but displays increasing solubility profiles as pH values shift towards more acidic or alkaline values.[97] Therefore, the pre-analysis application of the aqueous acid diluent to the blood sample would cause the dissociation of aluminum ions from alumina particulate matter that was present in the blood samples derived from the experiment. Consequently, it is unclear whether the aluminum concentration measured by ICP-MS was a result of alumina particulate matter that was shed from the hemoperfusion fabric during the experiment or of aluminum ions that were dissociatively expelled into the blood during the experiment. Although aluminum ion dissociation from the hemoperfusion system would be considered a more deleterious health hazard than the deposition of alumina particles, both are undesirable results and would almost certainly inhibit adoption of the technology in a clinical setting. There are no known uses of aluminum by the cells of the human body and

its accumulation is instead associated with various negative health consequences. Aluminum toxicity can cause developmental issues in children, alterations in bone metabolism and neurological impairments – including marked declines in motor and cognitive performance.[98] Normal exposure to aluminum occurs by ingestion (typically from trace amounts found in water) and is of negligible consequence, as the bioavailability of aluminum in humans is poor due to poor gastrointestinal adsorption.[98] Only 1% of ingested aluminum is adsorbed through the gastrointestinal tract and 95% of that portion is excreted in urine.[98] However, due to the inability of individuals with renal complications to effectively filter such toxins, this subset of the population is particularly at risk to the accumulation of aluminum and its intoxicating effects. For these reasons, the deposition of aluminum or aluminum containing products, such as alumina, to patients with renal impairments is an unacceptable outcome of the application of this hemoperfusion system. Moreover, the nature of the hemoperfusion system as a direct-blood contacting device means that the bioavailability of aluminum in this setting is much greater than the bioavailability observed through ingestion, as deposited aluminum has effectively bypassed gastrointestinal screening in the hemoperfusion scenario and is immediately available for blood circulation.

8. Future Research and Recommendations

While the phosphate adsorption capacities exhibited by the fabricated TMA-alumina hemoperfusion fabrics are substantial, considerable increases in phosphate reduction can be provided by improving the grafting yields of the TMA-alumina hemoadsorbent material. The current research demonstrated the efficacy of TMA-alumina in selectively removing

phosphate from whole blood in both static bench-top and dynamic flow settings, suggesting that similar results could also be realized in a clinical setting. However, a critical factor that also influences the viability of the overall concept in a clinical setting is safety and the preliminary alumina shedding/aluminum dissociation results reported in the current research indicate that significant amounts of alumina/aluminum are able to be removed from the TMA-Alumina hemoperfusion fabrics by blood exposure. To address this issue, further studies should first evaluate the root cause of the increased aluminum concentrations detected in this research after blood exposure to the hemoperfusion fabrics. If the measured aluminum concentrations are found to result from the shedding of particulate matter from the hemoperfusion fabrics, it is suggested that particle shedding be mitigated by the application of a polymer microencapsulation process to sheathe the hemoadsorbent particles and prevent their release into the blood stream.

9. References

1. Podd, D. Hyperphosphatemia : Understanding the role of phosphate metabolism. *Journal of the American Academy of Physicians Assistants* **23**, 32–37 (2010).

2. Lovekar, S. & Chen, J. L. T. A 90-Year-Old Man With Hyperphosphatemia. *American Journal of Kidney Diseases* **57**, 342–346 (2011).

3. Chertow, G. M. *et al.* Poly[allylamine Hydrochloride] (RenaGel): A Noncalcemic Phosphate Binder for the Treatment of Hyperphosphatemia in Chronic Renal Failure. *American Journal of Kidney Diseases* **29**, 66–71 (1997).

4. Noori, N., Sims, J., Kopple, J. & Shah, A. Organic and inorganic dietary phosphorus and its management in chronic kidney disease. *Iranian Journal of Kidney Diseases* **4**, 89–100 (2010).

5. Kuhlmann, M. K. Management of hyperphosphatemia. *Hemodialysis international. International Symposium on Home Hemodialysis* **10**, 338–45 (2006).

6. Tentori, F. *et al.* Mortality risk for dialysis patients with different levels of serum calcium, phosphorus, and PTH: the Dialysis Outcomes and Practice Patterns Study (DOPPS). *American journal of kidney diseases : the official journal of the National Kidney Foundation* **52**, 519–30 (2008).

7. Kimata, N. *et al.* Association of mineral metabolism factors with all-cause and cardiovascular mortality in hemodialysis patients: the Japan dialysis outcomes and practice patterns study. *Hemodialysis international. International Symposium on Home Hemodialysis* **11**, 340–8 (2007).

8. Finn, W. & Malluche, H. Regulation of Phosphate in Health and Disease. *John's Hopkins Advanced Studies in Medicine* **7**, 133–139 (2007).

9. Albaaj, F. & Hutchison, A. Hyperphosphataemia in renal failure: causes, consequences and current management. *Drugs* **63**, 577–96 (2003).

10. Tonelli, M., Pannu, N. & Manns, B. Oral phosphate binders in patients with kidney failure. *The New England journal of medicine* **362**, 1312–24 (2010).

11. Kooienga, L. Phosphorus Metabolism and Management in Chronic Kidney Disease: Phosphorus Balance with Daily Dialysis. *Seminars in Dialysis* **20**, 342–345 (2007).

12. Kestenbaum, B. PHOSPHORUS METABOLISM AND MANAGEMENT IN CHRONIC KIDNEY DISEASE: Phosphate Metabolism in the Setting of Chronic Kidney Disease: Significance and Recommendations for Treatment. *Seminars in Dialysis* **20**, 286–294 (2007).

13. Levey, A. S. & Coresh, J. Chronic kidney disease. *Lancet* **379**, 165–80 (2012).

14. Tomasello, S. Secondary Hyperparathyroidism and Chronic Kidney Disease. *Diabetes Spectrum* **21**, 19–25 (2008).

15. Baek, S. *et al.* Does Stage III Chronic Kidney Disease Always Progress to End-Stage Renal Disease? A Ten-Year Follow-up Study. *Scandinavian Journal of Urology and Nephrology* **46**, 232–238 (2012).

16. Giachelli, C. M. The emerging role of phosphate in vascular calcification. *Kidney international* **75**, 890–7 (2009).

17. Hollander, M. *et al.* Comparison between measures of atherosclerosis and risk of stroke: the Rotterdam Study. *Stroke; a journal of cerebral circulation* **34**, 2367–72 (2003).

18. Marchais, S. J., Metivier, F., Guerin, A. P. & London, M. Association of hyperphosphataemia with haemodynamic disturbances in end-stage renal disease. *Nephrology Dialysis Transplantation* **14**, 2178–2183 (1999).

19. Mucsi, I. *et al.* Control of serum phosphate without any phosphate binders in patients treated with nocturnal hemodialysis. *Kidney international* **53**, 1399–404 (1998).

20. Pohlmeier, R. & Vienken, J. Phosphate removal and hemodialysis conditions. *Kidney international. Supplement* **78**, S190–4 (2001).

21. Kjellstrand, C. M., Ing, T. S., Kjellstrand, P. T., Odar-Cederlof, I. & Lagg, C. R. B. Phosphorus dynamics during hemodialysis. *Hemodialysis international. International Symposium on Home Hemodialysis* **15**, 226–33 (2011).

22. Tonelli, M., Wang, W., Hemmelgarn, B., Lloyd, A. & Manns, B. Phosphate Removal With Several Thrice-weekly Dialysis Methods in Overweight Hemodialysis Patients. *American Journal of Kidney Diseases* **54**, 1108–1115 (2009).

23. Mikhalovsky, S. V Emerging technologies in extracorporeal treatment: focus on adsorption. *Perfusion* **18**, 47–54 (2003).

24. Block, G. *et al.* How should hyperphosphatemia be managed in dialysis patients? *Seminars in dialysis* **15**, 315–28 (2002).

25. Gutzwiller, J.-P. *et al.* Estimating phosphate removal in haemodialysis: an additional tool to quantify dialysis dose. *Nephrology, dialysis, transplantation : official publication of the European Dialysis and Transplant Association - European Renal Association* **17**, 1037–44 (2002).

26. Foundation, N. K. K/DOQI Clinical Practice Guidelines for Cardiovascular Disease in Dialysis Patients. *American Journal of Kidney Diseases* **45**, S1–153 (2005).

27. Foundation, N. K. K/DOQI Clinical Practice Guidelines for Bone Metabolism and Disease in Chronic Kidney Disease. *American Journal of Kidney Diseases* **42**, S1 – S102 (2003).

28. Achinger, S. G. & Ayus, J. C. The role of daily dialysis in the control of hyperphosphatemia. *Kidney international. Supplement* **67**, S28–32 (2005).

29. Lee, C. J., Hsu, H. W. & Chang, Y. L. Performance characteristics of combined haemodialysis/haemoperfusion system for removal of blood toxins. *Medical engineering & physics* **19**, 658–67 (1997).

30. Winchester, J. F. Sorbent hemoperfusion in end-stage renal disease: an in-depth review. *Advances in renal replacement therapy* **9**, 19–25 (2002).

31. Schefold, J. & Jorres, A. Extracorporeal Therapies and Immunodialation During Sepsis. *Management of Acute Kidney Problems* 629–636 (2010).doi:10.1007/978-3-540-69441-0

32. Spengler, K., Follmann, H., Boos, K. S., Seidel, D. & Maywald, F. Characterization and extracorporeal application of a new phosphate-binding agent. *European journal of clinical chemistry and clinical biochemistry : journal of the Forum of European Clinical Chemistry Societies* **32**, 733–9 (1994).

33. Hootkins, R., Lerman, J. & Thompson, R. Sequential and Simultaneous “In Series” Hemodialysis and Hemoperfusion in the Management of Theophylline Intoxication. *Journal of the American Society of Nephrology* **1**, 923–926 (1990).

34. Sasamura, H. *et al.* Effects of hemoperfusion plus high-flux hemodialysis in a patient with methotrexate toxicity. *Clinical and Experimental Nephrology* **2**, 75–79 (1998).

35. Schiavi, S. C. & Kumar, R. The phosphatonin pathway: new insights in phosphate homeostasis. *Kidney international* **65**, 1–14 (2004).

36. Muirhead, E. & A, R. Resin Artificial Kidney. *Journal of Laboratory and Clinical Medicine* **33**, 841–849 (1948).

37. Yatzidis, H. A Convenient Haemoperfusion Micro-Apparatus Over Charcoal for the Treatment of Endogenous and Exogenous Intoxications. *European Dialysis and Transplant Association* 83–89 (1964).

38. Winchester, J. F. & Harbord, N. B. Extracorporeal Removal of Drugs and Toxins. *Management of Acute Kidney Problems* 647–659 (2010).doi:10.1007/978-3-540-69441-0

39. Gutch, C. F. Artificial Kidneys: Problems and Approaches. *Annual Review of Biophysics and Bioengineering* **4**, 405–429 (1975).

40. Chang, T. M. S. Semipermeable Microcapsules. **146**, 524–525 (1964).

41. Chang, T. M. S., Gonda, A. & Dirks, J. Clinical Evaluation of Chronic Intermittent and Short-term Hemoperfusion in Patients with Chronic Renal Failure Using Semi-permeable microcapsules (artificial cells) formed from membrane coated activated charcoal. *Transactions - American Society for Artificial Internal Organs* **17**, 246 (1971).

42. Chang, T. M. S. *et al.* Microcapsule artificial kidney : treatment of patients with acute drug intoxication. *Canadian Medical Association Journal* **108**, 429–433 (1973).

43. Chavers, B. M., Kjellstrand, C. M., Wiegand, C., Ebben, J. & Mauer, S. M. Techniques for use of Charcoal Hemoperfusion in Infants : Experience in Two Patients. *Kidney International* **18**, 386–389 (1980).

44. Denti, E., Tessore, V. & Luboz, M. Adsorption Characteristics of Cellulose Acetate Coated Charcoals. *Journal of Biomedical Materials Research* **9**, 143–150 (1975).

45. Sideman, S. *et al.* Tailor-made agarose-based reactive beads for hemoperfusion and plasma perfusion. *Applied biochemistry and biotechnology* **10**, 167–82 (1984).

46. Holubek, W. J., Hoffman, R. S., Goldfarb, D. S. & Nelson, L. S. Use of hemodialysis and hemoperfusion in poisoned patients. *Kidney international* **74**, 1327–34 (2008).

47. Wang, Y.-J. & Yu, Y.-T. Development of resin adsorbents for blood purification at Nankai University in China. *Artificial cells, blood substitutes, and immobilization biotechnology* **39**, 92–7 (2011).

48. Briglia, A. E. The current state of nonuremic applications for extracorporeal blood purification. *Seminars in dialysis* **18**, 380–90

49. Pilapil, M. & Petersen, J. Efficacy of hemodialysis and charcoal hemoperfusion in carbamazepine overdose. *Clinical toxicology (Philadelphia, Pa.)* **46**, 342–3 (2008).

50. Gambro Lundia AB *Polyvalence and Simplicity for Safe Treatment - The PrismafleX eXeed™ Hemoperfusion System*. 1–8 (2009).

51. Andrade, J. D. *et al.* Coated adsorbents for direct blood perfusion II. *Transactions - American Society for Artificial Internal Organs* **17**, 222–228 (1971).

52. Siemsen, A., Dunea, G., Bashir, M. & Guruprakash, G. Charcoal Hemoperfusion for Chronic Renal Failure. *Nephron* **22**, 386–390 (1978).

53. Margel, S. & Marcus, L. Specific hemoperfusion through agarose acrobeads. *Applied biochemistry and biotechnology* **12**, 37–66 (1986).

54. Denizli, A. Extracorporeal Affinity Therapy. *Hacettepe Journal of Biology and Chemistry* **39**, 93–110 (2011).

55. Shoji, H., Tani, T., Hanasawa, K. & Kodama, M. Extracorporeal endotoxin removal by polymyxin B immobilized fiber cartridge: designing and antiendotoxin efficacy in the clinical application. *Therapeutic apheresis : official journal of the International Society for Apheresis and the Japanese Society for Apheresis* **2**, 3–12 (1998).

56. Novelli, G. *et al.* Clinical results of treatment of postsurgical endotoxin-mediated sepsis with polymyxin-B direct hemoperfusion. *Transplantation proceedings* **42**, 1021–1024 (2010).

57. Hou, G. *et al.* Preparation of Adsorbents for the Removal of Endotoxin. *Artificial Cells, Blood Substitutes and Biotechnology* **33**, 227–237 (2005).

58. Fang, H., Wei, J. & Yu, Y. T. In-vivo Studies of Endotoxin Removal by Lysine-Cellulose Adsorbents. *Biomaterials* **25**, 5433–5440 (2004).

59. Toraymyxin. *Spectral Diagnostics, Inc.* (2011).at <http://www.spectraldx.com/toraymyxin.html>

60. Duarte, G. R. M. *et al.* Characterization of dynamic solid phase DNA extraction from blood with magnetically controlled silica beads. *Analyst* **135**, 531–537 (2010).

61. Zhang, M., Cheng, D., He, X., Chen, L. & Zhang, Y. Magnetic silica-coated sub-microspheres with immobilized metal ions for the selective removal of bovine hemoglobin from bovine blood. *Chemistry, an Asian journal* **5**, 1332–1340 (2010).

62. Hong, J., Azens, A., Ekdahl, K. N., Granqvist, C. G. & Nilsson, B. Material-specific thrombin generation following contact between metal surfaces and whole blood. *Biomaterials* **26**, 1397–1403 (2005).

63. Denti, E., Walker, J., Brancaccio, D. & Tessore, V. Evaluation of novel sorbent systems for joint hemodialysis and hemoperfusion. *Medical Instrumentation* **11**, 212–216 (1977).

64. Kabalka, G. W. & Pagni, R. M. Organic Reactions on Alumina. *Tetrahedron* **53**, 7999–8065 (1997).

65. Saha, B., Chakraborty, S. & Das, G. A mechanistic insight into enhanced and selective phosphate adsorption on a coated carboxylated surface. *Journal of colloid and interface science* **331**, 21–6 (2009).

66. Kloprogge, J. T., Duong, L. V, Wood, B. J. & Frost, R. L. XPS Study of the Major Minerals in Bauxite, Gibbsite, Bayerite and (Pseudo-) Boehmite. *Journal of colloid and interface science* **296**, 572–576 (2006).

67. D'Angelo, A. *Adsorbed Organic Species on Inhalable γ-Alumina Particles*. 1–45 (2008).

68. Misra, C. ALUMINUM OXIDE (ALUMINA), HYDRATED. *Kirk-Othmer Encyclopedia of Chemical Technology* **2**, 421–433 (2003).

69. Pearson, A. ALUMINUM OXIDE (ALUMINA), ACTIVATED. *Kirk-Othmer Encyclopedia of Chemical Technology* **2**, 391–403 (2003).

70. Li, H., Addai-Mensah, J., Thomas, J. C. & Gerson, A. R. The crystallization mechanism of Al(OH)3 from sodium aluminate solutions. *Journal of Crystal Growth* **279**, 508–520 (2005).

71. Panias, D. & Krestou, A. Effect of synthesis parameters on precipitation of nanocrystalline boehmite from aluminate solutions. *Powder Technology* **175**, 163–173 (2007).

72. Hind, A. R., Bhargava, S. K. & Grocott, S. C. The surface chemistry of Bayer process solids: a review. *Colloids and Surfaces A: Physicochemical and Engineering Aspects* **146**, 359–374 (1999).

73. Krewski, D. *et al.* Human Health Risk Assessment for Aluminium, Aluminium Oxide, and Aluminium Hydroxide. *Journal of Toxicology and Environmental Health , Part B : Critical Reviews* **10**, 1–269 (2007).

74. Santos, P. S., Santos, H. S. & Toledo, S. P. Standard transition aluminas. Electron microscopy studies. *Materials Research* **3**, 104–114 (2000).

75. Ivanova, A. S. Aluminum oxide and systems based on it: Properties and applications. *Kinetics and Catalysis* **53**, 425–439 (2012).

76. Franks, G. V. & Gan, Y. Charging Behavior at the Alumina–Water Interface and Implications for Ceramic Processing. *Journal of the American Ceramic Society* **90**, 3373–3388 (2007).

77. Kasprzyk-Hordern, B. Chemistry of alumina, reactions in aqueous solution and its application in water treatment. *Advances in colloid and interface science* **110**, 19–48 (2004).

78. Wang, Y. G., Bronsveld, P. M., Dehosson, J. T. M., Mcgarry, D. & Pickering, S. Ordering of Octahedral Vacancies in Transition Aluminas. *Journal of American Ceramic Society* **81**, 1655–1660 (1998).

79. Boumaza, a. *et al.* Transition alumina phases induced by heat treatment of boehmite: An X-ray diffraction and infrared spectroscopy study. *Journal of Solid State Chemistry* **182**, 1171–1176 (2009).

80. Cai, S.-H., Rashkeev, S., Pantelides, S. & Sohlberg, K. Phase transformation mechanism between γ- and θ-alumina. *The American Physical Society - Physical Review B* **67**, 224104 (2003).

81. Łodziana, Z. & Parliński, K. Dynamical stability of the α and θ phases of alumina. *Physical Review B* **67**, 174106 (2003).

82. Kosmulski, M. Evaluation of Points of Zero Charge of Aluminum Oxide Reported in the Literature. 6–14 (2001).

83. Borah, J. M. & Mahiuddin, S. Adsorption and surface complexation of trimesic acid at the alpha-alumina-electrolyte interface. *Journal of colloid and interface science* **322**, 6–12 (2008).

84. Borah, J. M., Sarma, J. & Mahiuddin, S. Influence of functional groups on the adsorption behaviour of substituted benzoic acids at the α-alumina/water interface. *Colloids and Surfaces A: Physicochemical and Engineering Aspects* **375**, 42–49 (2011).

85. Mao, Y. & Fung, B. A Study of the Adsorption of Acrylic Acid and Maleic Acid from Aqueous Solutions onto Alumina. *Journal of colloid and interface science* **191**, 216–21 (1997).

86. Saha, B., Chakraborty, S. & Das, G. Trimesic acid coated alumina: an efficient multi-cyclic adsorbent for toxic Cu(II). *Journal of colloid and interface science* **320**, 30–9 (2008).

87. Saha, B., Chakraborty, S. & Das, G. A comparative metal ion adsorption study by trimesic acid coated alumina: a potent adsorbent. *Journal of colloid and interface science* **323**, 26–32 (2008).

88. Borah, B. M., Saha, B., Dey, S. K. & Das, G. Surface-modification-directed controlled adsorption of serum albumin onto magnetite nanocuboids synthesized in a gel-diffusion technique. *Journal of colloid and interface science* **349**, 114–21 (2010).

89. SaatiTech *SaatiCare - Precision Fabrics for Healthcare Applications*. 1–13at <http://www.s-tek.com.tw/SaatiCare.pdf>

90. Pacific Biolabs USP Class Plastics. (2009).at <http://www.pacificbiolabs.com/testing_usp_plastics.asp>

91. Porcayo-Calderon, J., Brito-Figueroa, E. & Gonzalez-Rodriguez, J. G. Oxidation behaviour of Fe – Si thermal spray coatings. *Materials Letters* **38**, 45–53 (1999).

92. Akyildiz, H. I., Padbury, R. P., Parsons, G. N. & Jur, J. S. Temperature and exposure dependence of hybrid organic-inorganic layer formation by sequential vapor infiltration into polymer fibers. *Langmuir : the ACS journal of surfaces and colloids* **28**, 15697–704 (2012).

93. Biovison *Phosphate Colorimetric Assay Kit*. 1–2 (2013).

94. Churchwell, M. D., Pasko, D. a & Mueller, B. a Daptomycin clearance during modeled continuous renal replacement therapy. *Blood purification* **24**, 548–54 (2006).

95. Medical Education Indistitution, I., Curtis, J. & Baxter Dialysis Museum. *Home Dialysis Central* (2004).at <http://homedialysis.org/types/museum/P10>

96. Herget, M., Hassli, S., Schatell, D., Smith, L. & Wong, F. Today's Dialysis Environment: an Overview. *Module 11-18* (2004).

97. Carrier, X., Marceau, E., Lambert, J.-F. & Che, M. Transformations of gamma-alumina in aqueous suspensions 1. Alumina chemical weathering studied as a function of pH. *Journal of colloid and interface science* **308**, 429–37 (2007).

98. Schafer, U. & Jahreis, G. Exposure, bioavailability, distribution and excretion of aluminum and its toxicological relevance to humans. *Trace Elements and Electrolytes* **23**, 162–172 (2006).

APPENDICES

Appendix A: TMA-Treatment and Alumina Grafting Protocols

TMA Treatment Protocol:

1. Mix 500mL methanol with 2.5g Trimesic Acid (1,3,5-benzene tricarboxylic acid) in a boiling flask and stir on medium-low speed until all of the trimesic acid is dissolved (~2 hours).
2. After all Trimesic Acid has dissolved, add 5g of Alumina particles to the boiling flask and continue to stir on med-low speed.
    a. Maintain the pH of the solution at 2.4 by adding HCl when appropriate
3. Once the pH is stable, allow the treatment to continue for 6+ hours (typically performed overnight) - continuously stirring.
4. After the duration of the treatment has elapsed (at least 6 hours), pour off the excess methanol solvent and filter the alumina particles through filter paper using vacuum filtration.
5. Rinse the particles in methanol to remove any residual Trimesic acid impurities
6. Rinse the particles in deionized water to remove any residual methanol or TMA.
7. Place the alumina particles in a glass petri dish and place the petri dish in a vacuum oven for 2 hours @ room temperature to ensure that all of the remaining methanol is safely evaporated.

Fabrics + Powders - Carver® Press Protocol:

Alumina Grafting Protocol:

1. Cut PET filtration fabric into rectangular shapes with desired dimensions
    a. Mass each fabric sample, record this as initial fabric mass
2. Pre-heat Carver press to desired temperature (300, 400 or 500°F)
3. Obtain 10 grams of alumina powders
4. Thoroughly coat one surface of PET fabric sample with alumina by simply sprinkling the powder over the surface of the fabric, until the fabric surface is no longer visible
5. Place alumina coated fabric sample between the two steel Carver-press plates
6. Place the steel plates (with alumina coated fabric between them) into the Carver-press and jack up the carver press platform until the pressure gauge reads 4500psi

(31026.41 kPa), which correlates to a pressure of 411.75 psi (2838.92 kPa) applied to the sample.

7. Leave the sample in the heated Carver-press at this pressure for 90 seconds.
8. Immediately release platform and remove sample
    a. Allow sample to cool for ~1 minute
9. Mass sample, record this measurement as the amount of alumina added after each press
10. Starting at step 4, repeat steps 4-9 two more times

Fabric Washing Protocol:

1. Submerge each alumina coated fabric in deionized water and agitate for 10 seconds.
    a. Repeat step 1 of the washing protocol two more times.
2. Allow the alumina-coated fabric to dry for 45 minutes in a vacuum oven at room temperature.
3. Mass the alumina-coated fabric and record as final mass.
4. Subtract the initial measured mass of the untreated fabric from the mass obtained from step 3 of the washing protocol to yield the final amount of alumina grafted to the fabric sample.
5. Proceed with TMA-methanol treatment to obtain the final TMA-alumina treated fabric.

Appendix B: Experimental Protocols

Bench-top Phosphate Adsorption Testing Protocol:

(For phosphate test solutions and Lactated Ringer's solutions):

1. Fill a 250mL plastic container with 50-80ml of desired test solution.
2. Place the filled plastic container within a shaking water bath, pre-set at 37 degrees Celsius and 154 rpm (circular motion shaker).
3. Take a 500 microliter initial sample of the test solution from the plastic container, prior to inserting any adsorbents.
4. Place the 500 microliter sample of the test solution in a new, 1.5mL microcentrifuge tube for analysis via the Biovision Phosphate Colorimetric Assay kit.
5. Place the adsorbent that is to be evaluated (powder, fabric, etc.) in the 250mL plastic container, ensuring that the adsorbent is completely submerged in the test solution.
6. Take another 500 microliter sample of the test solution, immediately after inserting the adsorbent into the plastic container, this will serve as the "t = 0" sample.
7. Place the "t = 0" sample in a new, microcentrifuge tube for later analysis via the Biovision Phosphate Colorimetric Assay kit.
8. At each designated time period (t = 10, 25, 50, 75, 100, 120, 150, 180, 200, 240 minutes), collect another 500 microliter sample and place each sample into a 1.5 milliliter microcentrifuge tube for analysis via the Biovision Phosphate Colorimetric Assay.
9. Between time intervals return the plastic container to the water bath until the next time step is reached.

Phosphate Colorimetric Assay:

1. Always make the working standard for use in the calibration curve first. To do this, combine 990 microliters of De-ionized H_2O with 10 microliters of the manufacturer's phosphate standard (small cylindrical tube in the assay kit) in a new 1.5mL microcentrifuge tube and vortex the closed tube for 20 seconds.
2. Obtain a fresh 96-well ELISA plate for analyzing the collected samples.
3. The first two rows of the ELISA plate should be reserved for the graduating concentrations of standard, used for the calibration curve. The two rows will look identical; one will simply be a replicate of the first. These wells will consist of a set amount of DI-H_2O and a set amount of the working standard which was mentioned in the previous step. The combinations of DI-H2O and working phosphate standard needed

to make the respective concentrations of the phosphate standards used for the assays calibration curve are listed below.

- 0 nM = 200 microliters of DIH2O
- 1 nM = 190 microliters of DIH2O + 10 microliters of working standard
- 2 nM = 180 microliters of DIH2O + 20 microliters of working standard
- 3 nM = 170 microliters of DIH2O + 30 microliters of working standard
- 4 nM = 160 microliters of DIH2O + 40 microliters of working standard.

4. The remainder of the 96-well plate is designated for plating the samples collected during the experimental protocol. Again, these should be plated in duplicate. Each of these wells will consist of a pre-set volume of de-ionized water and a pre-set volume of sample. The phosphate concentration of the test solution will determine the volume of sample that I to be allocated to each well of the 96-well plate. The total volume in each well will be 200 microliters (prior to the addition of the colorimetric reagent), meaning the total volume of de-ionized water in each well will be dependent upon the volume of sample used in each well. Below is a guide for the volume of sample to insert into each well based on the initial concentration of the test solution. Place the required volume of DI-H_2O in each well, prior to adding the required volume of each sample of test solution.
    - 100 mg/L initial PO_4 = (2 microliters of sample + 198 microliters of DIH2O)
    - 90 mg/L initial PO_4 = (2 microliters of sample + 198 microliters of DIH2O)
    - 80 mg/L initial PO_4 = (3 microliters of sample + 197 microliters of DIH2O)
    - 70 mg/L initial PO_4 = (4 microliters of sample + 196 microliters of DIH2O)
    - 60 mg/L initial PO_4 = (5 microliters of sample + 195 microliters of DIH2O)
    - 50 mg/L initial PO_4 = (6 microliters of sample + 194 microliters of DIH2O)
    - 40 mg/L initial PO_4 = (7 microliters of sample + 193 microliters of DIH2O)
    - 30 mg/L initial PO_4 = (8 microliters of sample + 192 microliters of DIH2O)
    - 20 mg/L initial PO_4 = (9 microliters of sample + 192 microliters of DIH2O)
    - 10 mg/L initial PO_4 = (10 microliters of sample + 190 microliters of DIH2O)

5. Once each sample is plated in the 96-well plate, add 30 microliters of colorimetric reagent to each well.
6. Following the addition of the colorimetric reagent to the last well, wait a period of 30 minutes before inserting the plate into the plate reader for analysis.
7. Read the plate in the spectrophotometer in absorbance mode, at a wavelength of 650nm.
8. Record and save the absorbance data (OD 650) that is yielded from the spectrophotometer reading for the successive calculations and evaluation of phosphate mass adsorbed (mg) and phosphate adsorption capacity (mg/g).

Flow Circuit Phosphate Adsorption Protocol (with phosphate test solutions):

Materials:

- 1L Polypropylene Blood Reservoir (Thermo Scientific)
- 1L Phosphate Test Solution
- 3/16" Silicone Tubing (Thermo Scientific)
- Peristaltic Pump (Thermo Scientific)
- Hose-barbs for connecting tube segments together
- 3-way Leur-lock stopcock
- Polycarbonate Phos-filter Test Device
    - Loaded with TMA-Al treated fabrics
- 3 Quick-grip clamps
- Plastic Leur-lock syringes

Experimental Method:

1. Load the Phos-filter test device with the desired number of TMA-Al treated fabrics and firmly close the chamber. Securely seal the device by placing and tightening the three clamps at the appropriate positions. Place the device in the vertical position for use in the study.
2. Fill the Polypropylene reservoir with 1L of phosphate test solution, formulated to the desired phosphate concentration.
3. Connect all of the circuit components, being sure that any junctions are tightly fastened with zip-ties as a secondary precaution.
4. Set the peristaltic pump at a speed of 45 rpm (~150 ml/min), ensuring that the pump is set to generate flow in the proper direction.
5. Collect one initial 3.0mL sample from the solution reservoir, immediately prior to the first circulation of the solution through the circuit. This will serve as the "no fabric sample." *Collect this sample according to the "sample collection protocol" below.*
6. After collecting the first sample and re-closing the stopcock, start the pump and allow the test solution to circulate through the system until the next sample collection time point is reached. *Collect all successive samples according to the "sample collection protocol" below.*
7. Using a 3mL leur-lock syringe, collect samples from the stopcock, positioned immediately downstream from the device, at the following time points: t = 0, 10, 25, 50, 75, 100, 120, 150, 180, 200, 240 minutes.

Sample Collection Protocol:

1. When collecting samples of phosphate test solution, ensure that the pump is first paused and that the stopcock is open in the appropriate orientation.
2. All collected samples should be immediately transferred from the 3mL leur-lock syringe to a new, 1.5mL plastic microcentrifuge tube.
3. Each collected sample should be 500 microliters in volume and 1 mL should be drawn from the stopcock and discarded immediately prior to the collection of each sample to prevent cross-contamination of samples.
4. Cap the microcentrifuge tube and store at room temperature for analysis after the experiment concludes.
5. After collecting each sample, return the stopcock to its closed orientation and re-start the circuit until the next time point is reached.
6. Analyze the samples of the test solution using the Biovision Colorimetric Assay kit, using the same protocol detailed in the section above.

Flow Circuit Phosphate Adsorption Protocol (with blood):

Materials:

- 1L Polypropylene Blood Reservoir (Thermo Scientific)
- 1L Heparinized Bovine Blood (Supplied by Quad Five)
- 3/16" Silicone Tubing (Thermo Scientific)
- Peristaltic Pump (Thermo Scientific)
- Hose-barbs for connecting tube segments together
- 3-way Leur-lock stopcock
- Polycarbonate Phos-filter Test Device
    - Loaded with TMA-Al treated fabrics
- 3 Quick-grip clamps
- Plastic Leur-lock Syringes

Experimental Method:

1. Load the Phos-filter test device with 10 TMA-Al treated fabrics and firmly close the chamber. Securely seal the device by placing and tightening the three clamps at the appropriate positions. Place the device in the vertical position for use in the study.
2. Fill the Polypropylene blood reservoir with 1L of heparinized bovine blood.
3. Connect all of the circuit components, being sure that any junctions are tightly fastened with zip-ties as a secondary precaution.

4. Set the peristaltic pump at a speed of 45 rpm (~150 ml/min), ensuring that the pump is set to generate blood-flow in the proper direction.
5. Collect one initial 3.0mL sample from the blood reservoir, immediately prior to the first circulation of the blood through the circuit. This will serve as the "no fabric sample." *Collect this sample according to the "sample collection protocol" below.*
6. After collecting the first sample and re-closing the stopcock, start the pump and allow the blood to circulate through the system until the next sample collection time point is reached. *Collect all successive samples according to the "sample collection protocol" below.*
7. Using a 3mL leur-lock syringe, collect samples from the stopcock, positioned immediately downstream from the device, at the following time points: t = 0, 10, 25, 50, 75, 100, 120, 150, 180, 200, 240 minutes.

Sample Collection Protocol:

1. When collecting blood samples, ensure that the pump is first paused and that the stopcock is open in the appropriate orientation.
2. All collected samples should be immediately transferred from the 3mL leur-lock syringe to a 6mL orange-capped BD Vacutainer Tube (thrombin tube).
3. Each collected sample should be 3.0mL in volume and 1 mL should be drawn from the stopcock and discarded immediately prior to the collection of each sample.
4. Invert the 6mL orange-capped BD Vacutainer Tube (thrombin tube) 5-6 times and allow to sit at room temperature prior to analysis.
5. After collecting each sample, return the stopcock to its closed orientation and re-start the circuit until the next time point is reached.
6. Send all collected samples to the UNC Hospital Core Lab (McClendon Lab) for the analysis of phosphate concentration.

Bench-top Aluminum Trace Metal Testing Protocol:

1. Make 2 Lexan frames to hold aluminum-coated fabric and 2 Lexan frames for control studies.
2. Attach one TMA-Alumina coated fabric to each Lexan frame.
3. Fill 2, 50-mL BD Falcon conical tubes with 40 mL of heparinized *human* blood
4. Take 2, 3-mL "no-fabric" samples from each 50-mL tube prior to the insertion of fabric into tube (one for analysis of whole blood, one for analysis of serum). Place each 3-mL sample into a 6-mL blue-capped trace metal testing tube
5. Fill 2, 50-mL BD Falcon conical tubes with 40 mL of heparinized *bovine* blood

6. Take 2, 3-mL “no-fabric” samples from each 50-mL tube prior to the insertion of fabric into tube (one for analysis of whole blood, one for analysis of serum). Place each 3-mL sample into a 6-mL blue-capped trace metal testing tube
7. Insert one Lexan frame and TMA-Alumina coated fabric into one of the 50-mL conical tubes containing heparinized human blood.
8. Insert one Lexan frame (no fabric) into the other 50-mL conical tube containing heparinized human blood.
9. Insert one Lexan frame and TMA-Alumina coated fabric into one of the 50-mL conical tubes containing heparinized bovine blood.
10. Insert one Lexan frame (no fabric) into the other 50-mL conical tube containing heparinized bovine blood.
11. Seal all of the tubes and attach them securely to the rotating mixer. Set the mixer on 15 rpm and allow the tubes to continuously rotate/mix for a duration of 60 minutes.
12. After the 60 minute duration, remove all tubes from the rotating mixer and collect two more, 3-mL samples from each tube. Place each 3-mL sample into a 6-mL blue-capped trace metal testing tube. Label these samples with their respective tube type and “t = 60 minutes”.
13. Submit all samples to the appropriate testing site for analysis of Aluminum content via Ion Coupled Plasma Mass Spectrometry.

Appendix C: Experimental Data

Table 12. Masses of alumina (g) added to fabric samples of varying sizes by various grafting methods. The table also shows which fabric samples were used in each experiment.

Experiment	Fabric Number	Grafting Method	Alumina Type Used	Surface Area of Fabric Sample (cm^2)	Hemoadsorbent Grafting Yield (g)	Hemoadsorbent Mass Grafted per Surface Area (mg/cm^2)
Circuit - Bovine Blood	1	Carver-Press	Acros Organics	200.0	0.346	1.73
Circuit - Bovine Blood	2	Carver-Press	Acros Organics	200.0	0.328	1.64
Circuit - Bovine Blood	3	Carver-Press	Acros Organics	200.0	0.350	1.75
Circuit - Bovine Blood	4	Carver-Press	Acros Organics	200.0	0.595	2.97
Circuit - Bovine Blood	5	Carver-Press	Acros Organics	200.0	0.326	1.63
Circuit - Bovine Blood	6	Carver-Press	Acros Organics	200.0	0.333	1.66
Circuit - Bovine Blood	7	Carver-Press	Acros Organics	200.0	0.486	2.43
Circuit - Bovine Blood	8	Carver-Press	Acros Organics	200.0	0.180	0.90
Circuit - Bovine Blood	9	Carver-Press	Acros Organics	200.0	0.656	3.28
Circuit - Bovine Blood	10	Carver-Press	Acros Organics	200.0	0.248	1.24
Circuit - Phosphate Solution - 30 mg_L	11	Carver-Press	Acros Organics	200.0	0.308	1.54
Circuit - Phosphate Solution - 30 mg_L	12	Carver-Press	Acros Organics	200.0	0.262	1.31
Circuit - Phosphate Solution - 30 mg_L	13	Carver-Press	Acros Organics	200.0	0.261	1.31
Circuit - Phosphate Solution - 30 mg_L	14	Carver-Press	Acros Organics	200.0	0.277	1.39
Circuit - Phosphate Solution - 30 mg_L	15	Carver-Press	Acros Organics	200.0	0.292	1.46
Circuit - Phosphate Solution - 50 mg_L	16	Carver-Press	Acros Organics	200.0	0.274	1.37
Circuit - Phosphate Solution - 50 mg_L	17	Carver-Press	Acros Organics	200.0	0.090	0.45
Circuit - Phosphate Solution - 50 mg_L	18	Carver-Press	Acros Organics	200.0	0.362	1.81
Circuit - Phosphate Solution - 50 mg_L	19	Carver-Press	Acros Organics	200.0	0.263	1.32
Circuit - Phosphate Solution - 50 mg_L	20	Carver-Press	Acros Organics	200.0	0.602	3.01
Circuit - Phosphate Solution - 50 mg_L	21	Carver-Press	Acros Organics	200.0	0.336	1.68
Circuit - Phosphate Solution - 90 mg_L	22	Carver-Press	Acros Organics	200.0	0.228	1.14
Circuit - Phosphate Solution - 90 mg_L	23	Carver-Press	Acros Organics	200.0	0.417	2.09
Circuit - Phosphate Solution - 90 mg_L	24	Carver-Press	Acros Organics	200.0	0.305	1.52
Circuit - Phosphate Solution - 90 mg_L	25	Carver-Press	Acros Organics	200.0	0.173	0.86
Circuit - Phosphate Solution - 90 mg_L	26	Carver-Press	Acros Organics	200.0	0.243	1.22
Circuit - Phosphate Solution - 90 mg_L	27	Carver-Press	Acros Organics	200.0	0.373	1.87
Circuit - Phosphate Solution - 90 mg_L	28	Carver-Press	Acros Organics	200.0	0.261	1.31
Circuit - Phosphate Solution - 90 mg_L	29	Carver-Press	Acros Organics	200.0	0.443	2.22
Circuit - Phosphate Solution - 90 mg_L	30	Carver-Press	Acros Organics	200.0	0.659	3.30
Circuit - Phosphate Solution - 90 mg_L	31	Carver-Press	Acros Organics	200.0	0.196	0.98
Circuit - Saturation Study - Phosphate Solution - 30 mg_L	32	Carver-Press	Acros Organics	200.0	0.322	1.61
Circuit - Saturation Study - Phosphate Solution - 30 mg_L	33	Carver-Press	Acros Organics	200.0	0.354	1.77
Circuit - Saturation Study - Phosphate Solution - 30 mg_L	34	Carver-Press	Acros Organics	200.0	0.339	1.70
Circuit - Saturation Study - Phosphate Solution - 30 mg_L	35	Carver-Press	Acros Organics	200.0	0.345	1.73
Circuit - Saturation Study - Phosphate Solution - 30 mg_L	36	Carver-Press	Acros Organics	200.0	0.352	1.76

Table 12. Continued

Adsorption Capacity Comparison- 10 mg/L	37	Carver-Press	Acros Organics	108.0	0.220	2.04
Adsorption Capacity Comparison- 20 mg/L	38	Carver-Press	Acros Organics	108.0	0.243	2.25
Adsorption Capacity Comparison- 40 mg/L	39	Carver-Press	Acros Organics	108.0	0.314	2.91
Adsorption Capacity Comparison- 60 mg/L	40	Carver-Press	Acros Organics	108.0	0.308	2.85
Adsorption Capacity Comparison- 80 mg/L	41	Carver-Press	Acros Organics	108.0	0.326	3.02
Adsorption Capacity Comparison- 100 mg/L	42	Carver-Press	Acros Organics	108.0	0.399	3.69
Lactated Ringer's - 10 mg/L PO4	43	Carver-Press	Acros Organics	54.0	0.0251	0.46
Lactated Ringer's - 10 mg/L PO4	44	Carver-Press	Acros Organics	54.0	0.021	0.39
Lactated Ringer's - 20 mg/L PO4	45	Carver-Press	Acros Organics	54.0	0.0341	0.63
Lactated Ringer's - 30 mg/L PO4	46	Carver-Press	Acros Organics	54.0	0.0241	0.45
Lactated Ringer's - 30 mg/L PO4	47	Carver-Press	Acros Organics	54.0	0.0256	0.47
Porcine Plasma Benchtop	48	Carver-Press	Acros Organics	54.0	0.139	2.57
Bovine Blood Whole Chemistry Benchtop	49	Carver-Press	Acros Organics	54.0	0.158	2.93
Bovine Blood Whole Chemistry Benchtop	50	Carver-Press	Acros Organics	54.0	0.150	2.78
				AVERAGES	0.291	1.77
Thermal Spray PO4 Solution	51	Thermal Spray	Thermal Spray Formulation	54.0	0.041	0.76
SEM - milled Thermal Spray	52	Thermal Spray	milled, Selecto Scientific	54.0	0.007	0.13
Atomic Layer Deposition	53	Atomic Layer Deposition	ALD Al_2O_3	108.0	NONE DETECTED	0.00
Sequential Vapor Infiltration	54	Sequential Vapor Infiltration	SVI Al_2O_3	108.0	NONE DETECTED	0.00

Table 13. Sample plating sequence for phosphate colorimetric assay (top) and the corresponding spectrophotometer absorbance data (bottom). The absorbance data shown was ultimately used to generate the graphs depicted in Figure 27 and Figure 28.

	1	2	3	4	5	6	7	8	9	10	11	12
Standards	Standard 0Nm	Standard 1Nm	Standard 2Nm	Standard 3Nm	Standard 4Nm							
Standards	Standard 0Nm	Standard 1Nm	Standard 2Nm	Standard 3Nm	Standard 4Nm							
30 mg/L - 0.1g TMA-Alumina (Acros Organics) - 50 mL	No Powder	t = 0	t = 10	t = 25	t = 50	t = 75	t = 100	t = 120	t = 150	t = 180	t = 200	t = 240
30 mg/L - 0.1g TMA-Alumina (Acros Organics) - 50 mL	No Powder	t = 0	t = 10	t = 25	t = 50	t = 75	t = 100	t = 120	t = 150	t = 180	t = 200	t = 240

	1	2	3	4	5	6	7	8	9	10	11	12
Standards	0.031	0.279	0.535	0.784	1.017							
Standards	0.029	0.278	0.537	0.776	1.021							
30 mg/L - 0.1g TMA-Alumina (Acros Organics) - 50 mL	0.733	0.729	0.604	0.440	0.318	0.212	0.161	0.121	0.094	0.07	0.063	0.053
30 mg/L - 0.1g TMA-Alumina (Acros Organics) - 50 mL	0.725	0.743	0.600	0.469	0.315	0.228	0.164	0.123	0.093	0.078	0.064	0.064

Table 14. Calculations used to determine masses of phosphate adsorbed (mg) and phosphate adsorption capacities (mg/g) from the experimentally derived spectrophotometer absorbance data. The calculations and values displayed in the table were used to generate the graphs depicted in Figure 27 and Figure 28.

Adsorbent Type:	Time Elapsed at Sample Collection (min)	OD 650	OD 650	Average OD 650	Phosphate Concentration (Nm)	Phosphate Concentration (ng/well)	Phosphate Concentration (mg/well)	Phosphate Concentration (mg/µl)	Phosphate Concentration (mg/L)	Concentration Decrease (mg/L)	Mass of PO_4 Adsorbed (mg)	PO_4 Fraction Adsorbed	Percentage Phosphate Adsorbed (%)	Mass of Adsorbent Present (g)	Phosphate Adsorption Capacity (mg/g)
No Adsorbent	0.00	0.733	0.725	0.729	2.80782	266.659	0.000267	0.000033	33.332	0.000	0.0000	0.00000	0.000		
0.1g TMA-Alumina (Acros Organics)	0.00	0.729	0.743	0.736	2.83606	269.340	0.000269	0.000034	33.668	-0.335	-0.0168	-0.01005	-1.005	0.100	-0.168
0.1g TMA-Alumina (Acros Organics)	10.00	0.604	0.600	0.602	2.29562	218.015	0.000218	0.000027	27.252	6.080	0.3040	0.18242	18.242	0.100	3.040
0.1g TMA-Alumina (Acros Organics)	25.00	0.440	0.469	0.455	1.70075	161.520	0.000162	0.000020	20.190	13.142	0.6571	0.39428	39.428	0.100	6.571
0.1g TMA-Alumina (Acros Organics)	50.00	0.318	0.315	0.317	1.14418	108.663	0.000109	0.000014	13.583	19.750	0.9875	0.59250	59.250	0.100	9.875
0.1g TMA-Alumina (Acros Organics)	75.00	0.212	0.228	0.220	0.75499	71.701	0.000072	0.000009	8.963	24.370	1.2185	0.73111	73.111	0.100	12.185
0.1g TMA-Alumina (Acros Organics)	100.00	0.161	0.164	0.163	0.52309	49.678	0.000050	0.000006	6.210	27.123	1.3561	0.81370	81.370	0.100	13.561
0.1g TMA-Alumina (Acros Organics)	120.00	0.121	0.123	0.122	0.35975	34.165	0.000034	0.000004	4.271	29.062	1.4531	0.87188	87.188	0.100	14.531
0.1g TMA-Alumina (Acros Organics)	150.00	0.094	0.093	0.094	0.24481	23.249	0.000023	0.000003	2.906	30.426	1.5213	0.91281	91.281	0.100	15.213
0.1g TMA-Alumina (Acros Organics)	180.00	0.070	0.078	0.074	0.16616	15.780	0.000016	0.000002	1.973	31.360	1.5680	0.94082	94.082	0.100	15.680
0.1g TMA-Alumina (Acros Organics)	200.00	0.063	0.064	0.064	0.12382	11.759	0.000012	0.000001	1.470	31.863	1.5931	0.95590	95.590	0.100	15.931
0.1g TMA-Alumina (Acros Organics)	240.00	0.053	0.064	0.059	0.10365	9.844	0.000010	0.000001	1.230	32.102	1.6051	0.96309	96.309	0.100	16.051

Table 15. Sample plating sequence for phosphate colorimetric assay (top) and the corresponding spectrophotometer absorbance data (bottom). The absorbance data shown was ultimately used to generate the graphs depicted in Figure 29 and Figure 30.

	1	2	3	4	5	6	7	8	9	10	11	12
Standards	Standard 0Nm	Standard 1Nm	Standard 2Nm	Standard 3Nm	Standard 4Nm							
Standards	Standard 0Nm	Standard 1Nm	Standard 2Nm	Standard 3Nm	Standard 4Nm							
30 mg/L - 0.1g Alumina (no TMA) (Acros Organics) - 50 mL	No Powder	t = 0	t = 10	t = 25	t = 50	t = 75	t = 100	t = 120	t = 150	t = 180	t = 200	t = 240
30 mg/L - 0.1g Alumina (no TMA) (Acros Organics) - 50 mL	No Powder	t = 0	t = 10	t = 25	t = 50	t = 75	t = 100	t = 120	t = 150	t = 180	t = 200	t = 240

	1	2	3	4	5	6	7	8	9	10	11	12
Standards	0.031	0.279	0.535	0.784	1.017							
Standards	0.029	0.278	0.537	0.776	1.021							
30 mg/L - 0.1g Alumina (no TMA) (Acros Organics) - 50 mL	0.762	0.707	0.661	0.622	0.523	0.484	0.467	0.408	0.388	0.347	0.322	0.283
30 mg/L - 0.1g Alumina (no TMA) (Acros Organics) - 50 mL	0.718	0.722	0.622	0.58	0.545	0.512	0.438	0.432	0.391	0.365	0.313	0.298

Table 16. Calculations used to determine masses of phosphate adsorbed (mg) and phosphate adsorption capacities (mg/g) from the experimentally derived spectrophotometer absorbance data. The calculations and values displayed in the table were used to generate the graphs depicted in Figure 29 and Figure 30.

Adsorbent Type:	Time Elapsed at Sample Collection (min)	OD 650	OD 650	Average OD 650	Phosphate Concentration (Nm)	Phosphate Concentration (ng/well)	Phosphate Concentration (mg/well)	Phosphate Concentration (mg/µl)	Phosphate Concentration (mg/L)	Concentration Decrease (mg/L)	Mass of PO_4 Adsorbed (mg)	PO_4 Fraction Adsorbed	Percentage Phosphate Adsorbed (%)	Mass of Adsorbent Present (g)	Phosphate Adsorption Capacity (mg/g)
No Powder	0.00	0.762	0.718	0.740	2.85219	270.872	0.000271	0.000034	33.859	0.000	0.0000	0.00000	0.000		
0.1g Untreated Alumina (Acros Organics)	0.00	0.707	0.722	0.715	2.74934	261.105	0.000261	0.000033	32.638	1.221	0.0610	0.03606	3.606	0.100	0.610
0.1g Untreated Alumina (Acros Organics)	10.00	0.661	0.622	0.642	2.45493	233.145	0.000233	0.000029	29.143	4.716	0.2358	0.13928	13.928	0.100	2.358
0.1g Untreated Alumina (Acros Organics)	25.00	0.622	0.580	0.601	2.29159	217.632	0.000218	0.000027	27.204	6.655	0.3327	0.19655	19.655	0.100	3.327
0.1g Untreated Alumina (Acros Organics)	50.00	0.523	0.545	0.534	2.02138	191.970	0.000192	0.000024	23.996	9.863	0.4931	0.29129	29.129	0.100	4.931
0.1g Untreated Alumina (Acros Organics)	75.00	0.484	0.512	0.498	1.87618	178.181	0.000178	0.000022	22.273	11.586	0.5793	0.34219	34.219	0.100	5.793
0.1g Untreated Alumina (Acros Organics)	100.00	0.467	0.438	0.453	1.69268	160.754	0.000161	0.000020	20.094	13.765	0.6882	0.40653	40.653	0.100	6.882
0.1g Untreated Alumina (Acros Organics)	120.00	0.408	0.432	0.420	1.56161	148.306	0.000148	0.000019	18.538	15.321	0.7660	0.45249	45.249	0.100	7.660
0.1g Untreated Alumina (Acros Organics)	150.00	0.388	0.391	0.390	1.43860	136.624	0.000137	0.000017	17.078	16.781	0.8391	0.49562	49.562	0.100	8.391
0.1g Untreated Alumina (Acros Organics)	180.00	0.347	0.365	0.356	1.30349	123.792	0.000124	0.000015	15.474	18.385	0.9192	0.54299	54.299	0.100	9.192
0.1g Untreated Alumina (Acros Organics)	200.00	0.322	0.313	0.318	1.14822	109.046	0.000109	0.000014	13.631	20.228	1.0114	0.59743	59.743	0.100	10.114
0.1g Untreated Alumina (Acros Organics)	240.00	0.283	0.298	0.291	1.03932	98.704	0.000099	0.000012	12.338	21.521	1.0760	0.63561	63.561	0.100	10.760

Table 17. Sample plating sequence for phosphate colorimetric assay (top) and the corresponding spectrophotometer absorbance data (bottom). The absorbance data shown was ultimately used to generate the graphs depicted in Figure 32 and Figure 33.

	1	2	3	4	5	6	7	8	9	10	11	12
Standards	Standard 0Nm	Standard 1Nm	Standard 2Nm	Standard 3Nm	Standard 4Nm							
Standards	Standard 0Nm	Standard 1Nm	Standard 2Nm	Standard 3Nm	Standard 4Nm							
30 mg/L - 0.1g TMA-Alumina (Superbasic) - 50 mL	No Powder	t = 0	t = 10	t = 25	t = 50	t = 75	t = 100	t = 120	t = 150	t = 180	t = 200	t = 240
30 mg/L - 0.1g TMA-Alumina (Superbasic) - 50 mL	No Powder	t = 0	t = 10	t = 25	t = 50	t = 75	t = 100	t = 120	t = 150	t = 180	t = 200	t = 240

	1	2	3	4	5	6	7	8	9	10	11	12
Standards	0.089	0.363	0.634	0.875	1.124							
Standards	0.092	0.366	0.633	0.829	1.107							
30 mg/L - 0.1g TMA-Alumina (Superbasic) - 50 mL	0.816	0.535	0.399	0.348	0.316	0.289	0.232	0.228	0.214	0.204	0.195	0.187
30 mg/L - 0.1g TMA-Alumina (Superbasic) - 50 mL	0.767	0.537	0.398	0.342	0.289	0.310	0.240	0.229	0.219	0.187	0.196	0.177

Table 18. Calculations used to determine masses of phosphate adsorbed (mg) and phosphate adsorption capacities (mg/g) from the experimentally derived spectrophotometer absorbance data. The calculations and values displayed in the table were used to generate the graphs depicted in Figure 32 and Figure 33.

Adsorbent Type:	Time Elapsed at Sample Collection (min)	OD 650	OD 650	Average OD 650	Phosphate Concentration (Nm)	Phosphate Concentration (ng/well)	Phosphate Concentration (mg/well)	Phosphate Concentration (mg/µl)	Phosphate Concentration (mg/L)	Concentration Decrease (mg/L)	Mass of PO_4 Adsorbed (mg)	PO_4 Fraction Adsorbed	Percentage Phosphate Adsorbed (%)	Mass of Adsorbent Present (g)	Phosphate Adsorption Capacity (mg/g)
No Powder	0.00	0.816	0.767	0.792	2.70058	256.555	0.000257	0.000032	32.069						
0.1g TMA-Alumina (Superbasic)	0.00	0.535	0.537	0.536	1.70028	161.527	0.000162	0.000020	20.191	11.878	0.5939	0.37040	37.040	0.100	5.939
0.1g TMA-Alumina (Superbasic)	10.00	0.399	0.398	0.399	1.16136	110.329	0.000110	0.000014	13.791	18.278	0.9139	0.56996	56.996	0.100	9.139
0.1g TMA-Alumina (Superbasic)	25.00	0.348	0.342	0.345	0.95085	90.330	0.000090	0.000011	11.291	20.778	1.0389	0.64791	64.791	0.100	10.389
0.1g TMA-Alumina (Superbasic)	50.00	0.316	0.289	0.303	0.78537	74.610	0.000075	0.000009	9.326	22.743	1.1372	0.70918	70.918	0.100	11.372
0.1g TMA-Alumina (Superbasic)	75.00	0.289	0.310	0.299	0.77323	73.457	0.000073	0.000009	9.182	22.887	1.1444	0.71368	71.368	0.100	11.444
0.1g TMA-Alumina (Superbasic)	100.00	0.232	0.240	0.236	0.52394	49.774	0.000050	0.000006	6.222	25.848	1.2924	0.80599	80.599	0.100	12.924
0.1g TMA-Alumina (Superbasic)	120.00	0.228	0.229	0.229	0.49652	47.170	0.000047	0.000006	5.896	26.173	1.3087	0.81614	81.614	0.100	13.087
0.1g TMA-Alumina (Superbasic)	150.00	0.214	0.219	0.216	0.44737	42.500	0.000043	0.000005	5.313	26.757	1.3378	0.83434	83.434	0.100	13.378
0.1g TMA-Alumina (Superbasic)	180.00	0.204	0.187	0.196	0.36649	34.817	0.000035	0.000004	4.352	27.717	1.3859	0.86429	86.429	0.100	13.859
0.1g TMA-Alumina (Superbasic)	200.00	0.195	0.196	0.195	0.36591	34.761	0.000035	0.000004	4.345	27.724	1.3862	0.86451	86.451	0.100	13.862
0.1g TMA-Alumina (Superbasic)	240.00	0.187	0.177	0.182	0.31303	29.738	0.000030	0.000004	3.717	28.352	1.4176	0.88409	88.409	0.100	14.176

Table 19. Sample plating sequence for phosphate colorimetric assay (top) and the corresponding spectrophotometer absorbance data (bottom). The absorbance data shown was ultimately used to generate the graphs depicted in Figure 34 and Figure 35.

	1	2	3	4	5	6	7	8	9	10	11	12
Standards	Standard 0Nm	Standard 1Nm	Standard 2Nm	Standard 3Nm	Standard 4Nm							
Standards	Standard 0Nm	Standard 1Nm	Standard 2Nm	Standard 3Nm	Standard 4Nm							
30 mg/L - 0.1g Untreated Alumina (Selecto Scientific) - 50 mL	No Powder	t = 0	t = 10	t = 25	t = 50	t = 75	t = 100	t = 120	t = 150	t = 180	t = 200	t = 240
30 mg/L - 0.1g Untreated Alumina (Selecto Scientific) - 50 mL	No Powder	t = 0	t = 10	t = 25	t = 50	t = 75	t = 100	t = 120	t = 150	t = 180	t = 200	t = 240

	1	2	3	4	5	6	7	8	9	10	11	12
Standards	0.031	0.279	0.535	0.784	1.017							
Standards	0.029	0.278	0.537	0.776	1.021							
30 mg/L - 0.1g Untreated Alumina (Selecto Scientific) - 50 mL	0.742	0.736	0.680	0.606	0.565	0.509	0.527	0.496	0.485	0.434	0.416	0.409
30 mg/L - 0.1g Untreated Alumina (Selecto Scientific) - 50 mL	0.748	0.781	0.706	0.635	0.593	0.559	0.527	0.503	0.486	0.452	0.440	0.421

Table 20. Calculations used to determine masses of phosphate adsorbed (mg) and phosphate adsorption capacities (mg/g) from the experimentally derived spectrophotometer absorbance data. The calculations and values displayed in the table were used to generate the graphs depicted in Figure 34 and Figure 35.

Adsorbent Type:	Time Elapsed at Sample Collection (min)	OD 650	OD 650	Average OD 650	Phosphate Concentration (Nm)	Phosphate Concentration (ng/well)	Phosphate Concentration (mg/well)	Phosphate Concentration (mg/µl)	Phosphate Concentration (mg/L)	Concentration Decrease (mg/L)	Mass of PO_4 Adsorbed (mg)	PO_4 Fraction Adsorbed	Percentage Phosphate Adsorbed (%)	Mass of Adsorbent Present (g)	Phosphate Adsorption Capacity (mg/g)
No Powder	0.00	0.742	0.748	0.745	2.87235	272.787	0.000273	0.000034	34.098	0.000	0.0000	0.00000	0.000		
0.1g Untreated Alumina (Selecto Scientific)	0.00	0.736	0.781	0.759	2.92680	277.958	0.000278	0.000035	34.745	-0.646	-0.0323	-0.01896	-1.896	0.100	-0.323
0.1g Untreated Alumina (Selecto Scientific)	10.00	0.680	0.706	0.693	2.66263	252.870	0.000253	0.000032	31.609	2.490	0.1245	0.07301	7.301	0.100	1.245
0.1g Untreated Alumina (Selecto Scientific)	25.00	0.606	0.635	0.621	2.37024	225.101	0.000225	0.000028	28.138	5.961	0.2980	0.17481	17.481	0.100	2.980
0.1g Untreated Alumina (Selecto Scientific)	50.00	0.565	0.593	0.579	2.20286	209.206	0.000209	0.000026	26.151	7.948	0.3974	0.23308	23.308	0.100	3.974
0.1g Untreated Alumina (Selecto Scientific)	75.00	0.509	0.559	0.534	2.02138	191.970	0.000192	0.000024	23.996	10.102	0.5051	0.29627	29.627	0.100	5.051
0.1g Untreated Alumina (Selecto Scientific)	100.00	0.527	0.527	0.527	1.99314	189.289	0.000189	0.000024	23.661	10.437	0.5219	0.30609	30.609	0.100	5.219
0.1g Untreated Alumina (Selecto Scientific)	120.00	0.496	0.503	0.500	1.88223	178.756	0.000179	0.000022	22.344	11.754	0.5877	0.34471	34.471	0.100	5.877
0.1g Untreated Alumina (Selecto Scientific)	150.00	0.485	0.486	0.486	1.82577	173.394	0.000173	0.000022	21.674	12.424	0.6212	0.36436	36.436	0.100	6.212
0.1g Untreated Alumina (Selecto Scientific)	180.00	0.434	0.452	0.443	1.65437	157.115	0.000157	0.000020	19.639	14.459	0.7230	0.42404	42.404	0.100	7.230
0.1g Untreated Alumina (Selecto Scientific)	200.00	0.416	0.440	0.428	1.59387	151.370	0.000151	0.000019	18.921	15.177	0.7589	0.44510	44.510	0.100	7.589
0.1g Untreated Alumina (Selecto Scientific)	240.00	0.409	0.421	0.415	1.54144	146.391	0.000146	0.000018	18.299	15.800	0.7900	0.46335	46.335	0.100	7.900

Table 21. Sample plating sequence for phosphate colorimetric assay (top) and the corresponding spectrophotometer absorbance data (bottom). The absorbance data shown was ultimately used to generate the graphs depicted in Figure 37 and Figure 38.

	1	2	3	4	5	6	7	8	9	10	11	12
Standards	Standard 0Nm	Standard 1Nm	Standard 2Nm	Standard 3Nm	Standard 4Nm							
Standards	Standard 0Nm	Standard 1Nm	Standard 2Nm	Standard 3Nm	Standard 4Nm							
30 mg/L - 0.1g TMA-Alumina (Thermal Spray) - 50 mL	No Powder	t = 0	t = 10	t = 25	t = 50	t = 75	t = 100	t = 120	t = 150	t = 180	t = 200	t = 240
30 mg/L - 0.1g TMA-Alumina (Thermal Spray) - 50 mL	No Powder	t = 0	t = 10	t = 25	t = 50	t = 75	t = 100	t = 120	t = 150	t = 180	t = 200	t = 240

	1	2	3	4	5	6	7	8	9	10	11	12
Standards	0.089	0.385	0.629	0.887	1.144							
Standards	0.088	0.375	0.643	0.897	1.124							
30 mg/L - 0.1g TMA-Alumina (Thermal Spray) - 50 mL	0.790	0.760	0.755	0.768	0.794	0.681	0.712	0.763	0.754	0.784	0.773	0.756
30 mg/L - 0.1g TMA-Alumina (Thermal Spray) - 50 mL	0.774	0.746	0.786	0.785	0.783	0.824	0.762	0.787	0.774	0.808	0.823	0.744

Table 22. Calculations used to determine masses of phosphate adsorbed (mg) and phosphate adsorption capacities (mg/g) from the experimentally derived spectrophotometer absorbance data. The calculations and values displayed in the table were used to generate the graphs depicted in Figure 37 and Figure 38.

Adsorbent Type:	Time Elapsed at Sample Collection (min)	OD 650	OD 650	Average OD 650	Phosphate Concentration (Nm)	Phosphate Concentration (ng/well)	Phosphate Concentration (mg/well)	Phosphate Concentration (mg/µl)	Phosphate Concentration (mg/L)	Concentration Decrease (mg/L)	Mass of PO_4 Adsorbed (mg)	PO_4 Fraction Adsorbed	Percentage Phosphate Adsorbed (%)	Mass of Adsorbent Present (g)	Phosphate Adsorption Capacity (mg/g)
No Powder	0.00	0.790	0.774	0.782	2.56015	243.215	0.000243	0.000030	30.402						
0.1g TMA-Alumina (Thermal Spray)	0.00	0.760	0.746	0.753	2.45104	232.849	0.000233	0.000029	29.106	1.296	0.0648	0.04262	4.262	0.100	0.648
0.1g TMA-Alumina (Thermal Spray)	10.00	0.755	0.786	0.770	2.51647	239.065	0.000239	0.000030	29.883	0.519	0.0259	0.01706	1.706	0.100	0.259
0.1g TMA-Alumina (Thermal Spray)	25.00	0.768	0.785	0.776	2.53953	241.255	0.000241	0.000030	30.157	0.245	0.0122	0.00806	0.806	0.100	0.122
0.1g TMA-Alumina (Thermal Spray)	50.00	0.794	0.783	0.788	2.58378	245.459	0.000245	0.000031	30.682	-0.281	-0.0140	-0.00923	-0.923	0.100	-0.140
0.1g TMA-Alumina (Thermal Spray)	75.00	0.681	0.824	0.752	2.45010	232.760	0.000233	0.000029	29.095	1.307	0.0653	0.04299	4.299	0.100	0.653
0.1g TMA-Alumina (Thermal Spray)	100.00	0.712	0.762	0.737	2.39236	227.274	0.000227	0.000028	28.409	1.993	0.0996	0.06554	6.554	0.100	0.996
0.1g TMA-Alumina (Thermal Spray)	120.00	0.763	0.787	0.775	2.53484	240.810	0.000241	0.000030	30.101	0.301	0.0150	0.00989	0.989	0.100	0.150
0.1g TMA-Alumina (Thermal Spray)	150.00	0.754	0.774	0.764	2.49341	236.874	0.000237	0.000030	29.609	0.793	0.0396	0.02607	2.607	0.100	0.396
0.1g TMA-Alumina (Thermal Spray)	180.00	0.784	0.808	0.796	2.61415	248.344	0.000248	0.000031	31.043	-0.641	-0.0321	-0.02109	-2.109	0.100	-0.321
0.1g TMA-Alumina (Thermal Spray)	200.00	0.773	0.823	0.798	2.62071	248.967	0.000249	0.000031	31.121	-0.719	-0.0360	-0.02365	-2.365	0.100	-0.360
0.1g TMA-Alumina (Thermal Spray)	240.00	0.756	0.744	0.750	2.44035	231.834	0.000232	0.000029	28.979	1.423	0.0711	0.04679	4.679	0.100	0.711

Table 23. Sample plating sequence for phosphate colorimetric assay (top) and the corresponding spectrophotometer absorbance data (bottom). The absorbance data shown was ultimately used to generate the graphs depicted in Figure 39 and Figure 40.

	1	2	3	4	5	6	7	8	9	10	11	12
Standards	Standard 0Nm	Standard 1Nm	Standard 2Nm	Standard 3Nm	Standard 4Nm							
Standards	Standard 0Nm	Standard 1Nm	Standard 2Nm	Standard 3Nm	Standard 4Nm							
30 mg/L - 0.1g Untreated Alumina (Thermal Spray) - 50 mL	No Powder	t = 0	t = 10	t = 25	t = 50	t = 75	t = 100	t = 120	t = 150	t = 180	t = 200	t = 240
30 mg/L - 0.1g Untreated Alumina (Thermal Spray) - 50 mL	No Powder	t = 0	t = 10	t = 25	t = 50	t = 75	t = 100	t = 120	t = 150	t = 180	t = 200	t = 240

	1	2	3	4	5	6	7	8	9	10	11	12
Standards	0.089	0.385	0.629	0.887	1.144							
Standards	0.088	0.375	0.643	0.897	1.124							
30 mg/L - 0.1g Untreated Alumina (Thermal Spray) - 50 mL	0.772	0.794	0.787	0.769	0.785	0.777	0.800	0.803	0.773	0.787	0.780	0.773
30 mg/L - 0.1g Untreated Alumina (Thermal Spray) - 50 mL	0.795	0.782	0.783	0.779	0.782	0.778	0.785	0.785	0.782	0.779	0.801	0.781

Table 24. Calculations used to determine masses of phosphate adsorbed (mg) and phosphate adsorption capacities (mg/g) from the experimentally derived spectrophotometer absorbance data. The calculations and values displayed in the table were used to generate the graphs depicted in Figure 39 and Figure 40.

Adsorbent Type:	Time Elapsed at Sample Collection (min)	OD 650	OD 650	Average OD 650	Phosphate Concentration (Nm)	Phosphate Concentration (ng/well)	Phosphate Concentration (mg/well)	Phosphate Concentration (mg/µl)	Phosphate Concentration (mg/L)	Concentration Decrease (mg/L)	Mass of PO_4 Adsorbed (mg)	PO_4 Fraction Adsorbed	Percentage Phosphate Adsorbed (%)	Mass of Adsorbent Present (g)	Phosphate Adsorption Capacity (mg/g)
No Powder	0.00	0.772	0.795	0.783	2.56559	243.731	0.000244	0.000030	30.466						
0.1g Untreated Alumina (Thermal Spray)	0.00	0.794	0.782	0.788	2.58303	245.387	0.000245	0.000031	30.673	-0.218	-0.0109	-0.00716	-0.716	0.100	-0.104
0.1g Untreated Alumina (Thermal Spray)	10.00	0.787	0.783	0.785	2.57365	244.497	0.000244	0.000031	30.562	-0.107	-0.0053	-0.00351	-0.351	0.100	-0.048
0.1g Untreated Alumina (Thermal Spray)	25.00	0.769	0.779	0.774	2.53091	240.436	0.000240	0.000030	30.055	0.401	0.0200	0.01316	1.316	0.100	0.206
0.1g Untreated Alumina (Thermal Spray)	50.00	0.785	0.782	0.784	2.56653	243.820	0.000244	0.000030	30.478	-0.022	-0.0011	-0.00073	-0.073	0.100	-0.006
0.1g Untreated Alumina (Thermal Spray)	75.00	0.777	0.778	0.777	2.54365	241.647	0.000242	0.000030	30.206	0.249	0.0125	0.00819	0.819	0.100	0.130
0.1g Untreated Alumina (Thermal Spray)	100.00	0.800	0.785	0.792	2.59990	246.990	0.000247	0.000031	30.874	-0.419	-0.0209	-0.01374	-1.374	0.100	-0.204
0.1g Untreated Alumina (Thermal Spray)	120.00	0.803	0.785	0.794	2.60552	247.525	0.000248	0.000031	30.941	-0.485	-0.0243	-0.01594	-1.594	0.100	-0.237
0.1g Untreated Alumina (Thermal Spray)	150.00	0.782	0.773	0.777	2.54365	241.647	0.000242	0.000030	30.206	0.249	0.0125	0.00819	0.819	0.100	0.130
0.1g Untreated Alumina (Thermal Spray)	180.00	0.787	0.779	0.783	2.56428	243.606	0.000244	0.000030	30.451	0.004	0.0002	0.00015	0.015	0.100	0.008
0.1g Untreated Alumina (Thermal Spray)	200.00	0.780	0.801	0.790	2.59240	246.278	0.000246	0.000031	30.785	-0.329	-0.0165	-0.01082	-1.082	0.100	-0.159
0.1g Untreated Alumina (Thermal Spray)	240.00	0.773	0.785	0.779	2.54815	242.075	0.000242	0.000030	30.259	0.207	0.0104	0.00680	0.680	0.100	0.104

Table 25. Sample plating sequence for phosphate colorimetric assay (top) and the corresponding spectrophotometer absorbance data (bottom). The absorbance data shown was ultimately used to generate the graphs depicted in Figure 42 and Figure 43.

	1	2	3	4	5	6	7	8	9	10	11	12
Standards	Standard 0Nm	Standard 1Nm	Standard 2Nm	Standard 3Nm	Standard 4Nm							
Standards	Standard 0Nm	Standard 1Nm	Standard 2Nm	Standard 3Nm	Standard 4Nm							
30 mg/L - 0.1g TMA-Alumina (milled, Selecto Scientific)	No Powder	t = 0	t = 10	t = 25	t = 50	t = 75	t = 100	t = 120	t = 150	t = 180	t = 200	t = 240
30 mg/L - 0.1g TMA-Alumina (milled, Selecto Scientific)	No Powder	t = 0	t = 10	t = 25	t = 50	t = 75	t = 100	t = 120	t = 150	t = 180	t = 200	t = 240

	1	2	3	4	5	6	7	8	9	10	11	12
Standards	0.107	0.394	0.693	0.975	1.186							
Standards	0.105	0.397	0.667	0.903	1.159							
30 mg/L - 0.1g TMA-Alumina (milled, Selecto Scientific)	0.934	0.792	0.597	0.452	0.373	0.326	0.298	0.281	0.263	0.253	0.254	0.231
30 mg/L - 0.1g TMA-Alumina (milled, Selecto Scientific)	0.915	0.789	0.591	0.464	0.371	0.324	0.305	0.288	0.269	0.257	0.253	0.242

Table 26. Calculations used to determine masses of phosphate adsorbed (mg) and phosphate adsorption capacities (mg/g) from the experimentally derived spectrophotometer absorbance data. The calculations and values displayed in the table were used to generate the graphs depicted in Figure 42 and Figure 43.

Adsorbent Type:	Time Elapsed at Sample Collection (min)	OD 650	OD 650	Average OD 650	Phosphate Concentration (Nm)	Phosphate Concentration (ng/well)	Phosphate Concentration (mg/well)	Phosphate Concentration (mg/µl)	Phosphate Concentration (mg/L)	Concentration Decrease (mg/L)	Mass of PO_4 Adsorbed (mg)	PO_4 Fraction Adsorbed	Percentage Phosphate Adsorbed (%)	Mass of Adsorbent Present (g)	Phosphate Adsorption Capacity (mg/g)
No Adsorbant	0.00	0.934	0.915	0.924	2.91607	277.027	0.000277	0.000035	34.628						
0.1g TMA-Alumina (milled, Selecto Scientific)	0.00	0.792	0.789	0.791	2.43508	231.333	0.000231	0.000029	28.917	5.712	0.2856	0.16494	16.494	0.100	2.856
0.1g TMA-Alumina (milled, Selecto Scientific)	10.00	0.597	0.591	0.594	1.72886	164.242	0.000164	0.000021	20.530	14.098	0.7049	0.40712	40.712	0.100	7.049
0.1g TMA-Alumina (milled, Selecto Scientific)	25.00	0.452	0.464	0.458	1.23943	117.746	0.000118	0.000015	14.718	19.910	0.9955	0.57496	57.496	0.100	9.955
0.1g TMA-Alumina (milled, Selecto Scientific)	50.00	0.373	0.371	0.372	0.93177	88.518	0.000089	0.000011	11.065	23.564	1.1782	0.68047	68.047	0.100	11.782
0.1g TMA-Alumina (milled, Selecto Scientific)	75.00	0.326	0.324	0.325	0.76294	72.479	0.000072	0.000009	9.060	25.568	1.2784	0.73837	73.837	0.100	12.784
0.1g TMA-Alumina (milled, Selecto Scientific)	100.00	0.298	0.305	0.301	0.67798	64.408	0.000064	0.000008	8.051	26.577	1.3289	0.76750	76.750	0.100	13.289
0.1g TMA-Alumina (milled, Selecto Scientific)	120.00	0.281	0.288	0.284	0.61602	58.522	0.000059	0.000007	7.315	27.313	1.3657	0.78875	78.875	0.100	13.657
0.1g TMA-Alumina (milled, Selecto Scientific)	150.00	0.263	0.269	0.266	0.55154	52.396	0.000052	0.000007	6.550	28.079	1.4039	0.81086	81.086	0.100	14.039
0.1g TMA-Alumina (milled, Selecto Scientific)	180.00	0.253	0.257	0.255	0.51238	48.676	0.000049	0.000006	6.085	28.544	1.4272	0.82429	82.429	0.100	14.272
0.1g TMA-Alumina (milled, Selecto Scientific)	200.00	0.254	0.253	0.253	0.50502	47.977	0.000048	0.000006	5.997	28.631	1.4316	0.82681	82.681	0.100	14.316
0.1g TMA-Alumina (milled, Selecto Scientific)	240.00	0.231	0.242	0.237	0.44629	42.397	0.000042	0.000005	5.300	29.329	1.4664	0.84696	84.696	0.100	14.664

Table 27. Sample plating sequence for phosphate colorimetric assay (top) and the corresponding spectrophotometer absorbance data (bottom). The absorbance data shown was ultimately used to generate the graph depicted in Figure 48.

	1	2	3	4	5	6	7	8	9	10	11	12	13
Standards	Standard 0Nm	Standard 1Nm	Standard 2Nm	Standard 3Nm	Standard 4Nm								
Standards	Standard 0Nm	Standard 1Nm	Standard 2Nm	Standard 3Nm	Standard 4Nm								
10 mg/L - Carver-Pressed TMA-Alumina Fabric (Fabric #37)	No Adsorbent	t = 0	t = 10	t = 20	t = 30	t = 45	t = 60	t = 90	t = 120	t = 150	t = 180	t = 210	t = 240
10 mg/L - Carver-Pressed TMA-Alumina Fabric (Fabric #37)	No Adsorbent	t = 0	t = 10	t = 20	t = 30	t = 45	t = 60	t = 90	t = 120	t = 150	t = 180	t = 210	t = 240
20 mg/L - Carver-Pressed TMA-Alumina Fabric (Fabric #38)	No Adsorbent	t = 0	t = 10	t = 20	t = 30	t = 45	t = 60	t = 90	t = 120	t = 150	t = 180	t = 210	t = 240
20 mg/L - Carver-Pressed TMA-Alumina Fabric (Fabric #38)	No Adsorbent	t = 0	t = 10	t = 20	t = 30	t = 45	t = 60	t = 90	t = 120	t = 150	t = 180	t = 210	t = 240
40 mg/L - Carver-Pressed TMA-Alumina Fabric (Fabric #39)	No Adsorbent	t = 0	t = 10	t = 20	t = 30	t = 45	t = 60	t = 90	t = 120	t = 150	t = 180	t = 210	t = 240
40 mg/L - Carver-Pressed TMA-Alumina Fabric (Fabric #39)	No Adsorbent	t = 0	t = 10	t = 20	t = 30	t = 45	t = 60	t = 90	t = 120	t = 150	t = 180	t = 210	t = 240
60 mg/L - Carver-Pressed TMA-Alumina Fabric (Fabric #40)	No Adsorbent	t = 0	t = 10	t = 20	t = 30	t = 45	t = 60	t = 90	t = 120	t = 150	t = 180	t = 210	t = 240
60 mg/L - Carver-Pressed TMA-Alumina Fabric (Fabric #40)	No Adsorbent	t = 0	t = 10	t = 20	t = 30	t = 45	t = 60	t = 90	t = 120	t = 150	t = 180	t = 210	t = 240
80 mg/L - Carver-Pressed TMA-Alumina Fabric (Fabric #41)	No Adsorbent	t = 0	t = 10	t = 20	t = 30	t = 45	t = 60	t = 90	t = 120	t = 150	t = 180	t = 210	t = 240
80 mg/L - Carver-Pressed TMA-Alumina Fabric (Fabric #41)	No Adsorbent	t = 0	t = 10	t = 20	t = 30	t = 45	t = 60	t = 90	t = 120	t = 150	t = 180	t = 210	t = 240
100 mg/L - Carver-Pressed TMA-Alumina Fabric (Fabric #42)	No Adsorbent	t = 0	t = 10	t = 20	t = 30	t = 45	t = 60	t = 90	t = 120	t = 150	t = 180	t = 210	t = 240
100 mg/L - Carver-Pressed TMA-Alumina Fabric (Fabric #42)	No Adsorbent	t = 0	t = 10	t = 20	t = 30	t = 45	t = 60	t = 90	t = 120	t = 150	t = 180	t = 210	t = 240

	1	2	3	4	5	6	7	8	9	10	11	12	13
Standards	0.079	0.285	0.514	0.752	0.927								
Standards	0.081	0.293	0.524	0.756	0.890								
10 mg/L - Carver-Pressed TMA-Alumina Fabric (Fabric #37)	0.344	0.320	0.210	0.145	0.121	0.110	0.096	0.097	0.093	0.089	0.088	0.083	0.085
10 mg/L - Carver-Pressed TMA-Alumina Fabric (Fabric #37)	0.338	0.333	0.208	0.152	0.130	0.106	0.100	0.088	0.095	0.091	0.091	0.086	0.088
20 mg/L - Carver-Pressed TMA-Alumina Fabric (Fabric #38)	0.552	0.518	0.286	0.201	0.173	0.160	0.126	0.107	0.103	0.096	0.093	0.092	0.089
20 mg/L - Carver-Pressed TMA-Alumina Fabric (Fabric #38)	0.531	0.521	0.298	0.209	0.163	0.144	0.125	0.110	0.100	0.094	0.091	0.092	0.087
40 mg/L - Carver-Pressed TMA-Alumina Fabric (Fabric #39)	0.719	0.791	0.411	0.268	0.207	0.171	0.147	0.129	0.118	0.108	0.104	0.101	0.102
40 mg/L - Carver-Pressed TMA-Alumina Fabric (Fabric #39)	0.759	0.733	0.379	0.268	0.213	0.170	0.150	0.131	0.130	0.111	0.104	0.103	0.095
60 mg/L - Carver-Pressed TMA-Alumina Fabric (Fabric #40)	0.876	0.773	0.518	0.431	0.437	0.330	0.355	0.284	0.275	0.262	0.234	0.242	0.229
60 mg/L - Carver-Pressed TMA-Alumina Fabric (Fabric #40)	0.718	0.797	0.571	0.478	0.453	0.393	0.35	0.308	0.29	0.258	0.239	0.232	0.217
80 mg/L - Carver-Pressed TMA-Alumina Fabric (Fabric #41)	0.653	0.596	0.455	0.404	0.334	0.352	0.303	0.265	0.247	0.237	0.211	0.201	0.212
80 mg/L - Carver-Pressed TMA-Alumina Fabric (Fabric #41)	0.637	0.581	0.471	0.446	0.395	0.330	0.312	0.276	0.249	0.223	0.229	0.208	0.200
100 mg/L - Carver-Pressed TMA-Alumina Fabric (Fabric #42)	0.503	0.491	0.322	0.267	0.241	0.239	0.191	0.200	0.162	0.180	0.169	0.161	0.139
100 mg/L - Carver-Pressed TMA-Alumina Fabric (Fabric #42)	0.566	0.525	0.374	0.268	0.260	0.243	0.209	0.184	0.181	0.159	0.159	0.153	0.137

Table 28. Calculations used to determine masses of phosphate adsorbed (mg) and phosphate adsorption capacities (mg/g) from the experimentally derived spectrophotometer absorbance data. The calculations and values displayed in the table were used to generate the graph depicted in Figure 48.

Adsorbent Type:	Time Elapsed at Sample Collection (min)	OD 650	OD 650	Average OD 650	Phosphate Concentration (Nm)	Phosphate Concentration (ng/well)	Phosphate Concentration (mg/well)	Phosphate Concentration (mg/µl)	Phosphate Concentration (mg/L)	Concentration Decrease (mg/L)	Mass of PO_4 Adsorbed (mg)	PO_4 Fraction Adsorbed	Percentage Phosphate Adsorbed (%)	Mass of Adsorbent Present (g)	Phosphate Adsorption Capacity (mg/g)
No Adsorbent	0.00	0.344	0.338	0.341	1.20311	114.295	0.000114	0.000011	11.430						
Carver-Pressed TMA-Alumina Fabric (Fabric #37)	0.00	0.320	0.333	0.327	1.13478	107.804	0.000108	0.000011	10.780	0.649	0.0519	0.05680	5.680	0.220	0.236
Carver-Pressed TMA-Alumina Fabric (Fabric #37)	10.00	0.210	0.208	0.209	0.58106	55.200	0.000055	0.000006	5.520	5.910	0.4728	0.51704	51.704	0.220	2.149
Carver-Pressed TMA-Alumina Fabric (Fabric #37)	20.00	0.145	0.152	0.149	0.29595	28.115	0.000028	0.000003	2.811	8.618	0.6894	0.75401	75.401	0.220	3.134
Carver-Pressed TMA-Alumina Fabric (Fabric #37)	30.00	0.121	0.130	0.126	0.18756	17.818	0.000018	0.000002	1.782	9.648	0.7718	0.84410	84.410	0.220	3.508
Carver-Pressed TMA-Alumina Fabric (Fabric #37)	45.00	0.110	0.106	0.108	0.10509	9.984	0.000010	0.000001	0.998	10.431	0.8345	0.91265	91.265	0.220	3.793
Carver-Pressed TMA-Alumina Fabric (Fabric #37)	60.00	0.096	0.100	0.098	0.05796	5.507	0.000006	0.000001	0.551	10.879	0.8703	0.95182	95.182	0.220	3.956
Carver-Pressed TMA-Alumina Fabric (Fabric #37)	90.00	0.097	0.088	0.093	0.03205	3.044	0.000003	0.000000	0.304	11.125	0.8900	0.97336	97.336	0.220	4.045
Carver-Pressed TMA-Alumina Fabric (Fabric #37)	120.00	0.093	0.095	0.094	0.03911	3.716	0.000004	0.000000	0.372	11.058	0.8846	0.96749	96.749	0.220	4.021
Carver-Pressed TMA-Alumina Fabric (Fabric #37)	150.00	0.089	0.091	0.090	0.02026	1.925	0.000002	0.000000	0.193	11.237	0.8990	0.98316	98.316	0.220	4.086
Carver-Pressed TMA-Alumina Fabric (Fabric #37)	180.00	0.088	0.091	0.090	0.01791	1.701	0.000002	0.000000	0.170	11.259	0.9008	0.98512	98.512	0.220	4.094
Carver-Pressed TMA-Alumina Fabric (Fabric #37)	210.00	0.083	0.086	0.085	-0.00566	-0.537	-0.000001	0.000000	-0.054	11.483	0.9187	1.00470	100.470	0.220	4.176
Carver-Pressed TMA-Alumina Fabric (Fabric #37)	240.00	0.085	0.088	0.087	0.00377	0.358	0.000000	0.000000	0.036	11.394	0.9115	0.99687	99.687	0.220	4.143
No Adsorbent	0.00	0.552	0.531	0.542	2.14797	204.057	0.000204	0.000023	22.673						
Carver-Pressed TMA-Alumina Fabric (Fabric #38)	0.00	0.518	0.521	0.520	2.04430	194.208	0.000194	0.000022	21.579	1.094	0.0875	0.04827	4.827	0.243	0.360
Carver-Pressed TMA-Alumina Fabric (Fabric #38)	10.00	0.286	0.298	0.292	0.97220	92.359	0.000092	0.000010	10.262	12.411	0.9929	0.54739	54.739	0.243	4.086
Carver-Pressed TMA-Alumina Fabric (Fabric #38)	20.00	0.201	0.209	0.205	0.56221	53.410	0.000053	0.000006	5.934	16.739	1.3391	0.73826	73.826	0.243	5.511
Carver-Pressed TMA-Alumina Fabric (Fabric #38)	30.00	0.173	0.163	0.168	0.38784	36.845	0.000037	0.000004	4.094	18.579	1.4863	0.81944	81.944	0.243	6.117
Carver-Pressed TMA-Alumina Fabric (Fabric #38)	45.00	0.160	0.144	0.152	0.31244	29.682	0.000030	0.000003	3.298	19.375	1.5500	0.85454	85.454	0.243	6.379
Carver-Pressed TMA-Alumina Fabric (Fabric #38)	60.00	0.126	0.125	0.126	0.18756	17.818	0.000018	0.000002	1.980	20.693	1.6555	0.91268	91.268	0.243	6.813
Carver-Pressed TMA-Alumina Fabric (Fabric #38)	90.00	0.107	0.110	0.109	0.10745	10.207	0.000010	0.000001	1.134	21.539	1.7231	0.94998	94.998	0.243	7.091
Carver-Pressed TMA-Alumina Fabric (Fabric #38)	120.00	0.103	0.100	0.102	0.07446	7.074	0.000007	0.000001	0.786	21.887	1.7510	0.96534	96.534	0.243	7.206
Carver-Pressed TMA-Alumina Fabric (Fabric #38)	150.00	0.096	0.094	0.095	0.04383	4.164	0.000004	0.000000	0.463	22.210	1.7768	0.97960	97.960	0.243	7.312
Carver-Pressed TMA-Alumina Fabric (Fabric #38)	180.00	0.093	0.091	0.092	0.02969	2.820	0.000003	0.000000	0.313	22.360	1.7888	0.98618	98.618	0.243	7.361
Carver-Pressed TMA-Alumina Fabric (Fabric #38)	210.00	0.092	0.092	0.092	0.02969	2.820	0.000003	0.000000	0.313	22.360	1.7888	0.98618	98.618	0.243	7.361
Carver-Pressed TMA-Alumina Fabric (Fabric #38)	240.00	0.089	0.087	0.088	0.01084	1.030	0.000001	0.000000	0.114	22.559	1.8047	0.99495	99.495	0.243	7.427
No Adsorbent	0.00	0.719	0.759	0.739	3.07870	292.476	0.000292	0.000042	41.782						
Carver-Pressed TMA-Alumina Fabric (Fabric #39)	0.00	0.791	0.733	0.762	3.18709	302.773	0.000303	0.000043	43.253	-1.471	-0.1177	-0.03521	-3.521	0.314	-0.375
Carver-Pressed TMA-Alumina Fabric (Fabric #39)	10.00	0.411	0.379	0.395	1.45759	138.471	0.000138	0.000020	19.782	22.001	1.7601	0.52656	52.656	0.314	5.605
Carver-Pressed TMA-Alumina Fabric (Fabric #39)	20.00	0.268	0.268	0.268	0.85910	81.614	0.000082	0.000012	11.659	30.123	2.4099	0.72096	72.096	0.314	7.675
Carver-Pressed TMA-Alumina Fabric (Fabric #39)	30.00	0.207	0.213	0.210	0.58577	55.648	0.000056	0.000008	7.950	33.833	2.7066	0.80974	80.974	0.314	8.620
Carver-Pressed TMA-Alumina Fabric (Fabric #39)	45.00	0.171	0.170	0.171	0.39962	37.964	0.000038	0.000005	5.423	36.359	2.9087	0.87020	87.020	0.314	9.263
Carver-Pressed TMA-Alumina Fabric (Fabric #39)	60.00	0.147	0.150	0.149	0.29595	28.115	0.000028	0.000004	4.016	37.766	3.0213	0.90387	90.387	0.314	9.622
Carver-Pressed TMA-Alumina Fabric (Fabric #39)	90.00	0.129	0.131	0.130	0.20877	19.833	0.000020	0.000003	2.833	38.949	3.1159	0.93219	93.219	0.314	9.923
Carver-Pressed TMA-Alumina Fabric (Fabric #39)	120.00	0.118	0.130	0.124	0.18049	17.147	0.000017	0.000002	2.450	39.333	3.1466	0.94137	94.137	0.314	10.021
Carver-Pressed TMA-Alumina Fabric (Fabric #39)	150.00	0.108	0.111	0.110	0.11216	10.655	0.000011	0.000002	1.522	40.260	3.2208	0.96357	96.357	0.314	10.257
Carver-Pressed TMA-Alumina Fabric (Fabric #39)	180.00	0.104	0.104	0.104	0.08624	8.193	0.000008	0.000001	1.170	40.612	3.2490	0.97199	97.199	0.314	10.347
Carver-Pressed TMA-Alumina Fabric (Fabric #39)	210.00	0.101	0.103	0.102	0.07681	7.297	0.000007	0.000001	1.042	40.740	3.2592	0.97505	97.505	0.314	10.380
Carver-Pressed TMA-Alumina Fabric (Fabric #39)	240.00	0.102	0.095	0.099	0.06032	5.730	0.000006	0.000001	0.819	40.964	3.2771	0.98041	98.041	0.314	10.437

Table 28. Continued

Adsorbent Type:	Time Elapsed at Sample Collection (min)	OD 650	OD 650	Average OD 650	Phosphate Concentration (Nm)	Phosphate Concentration (ng/well)	Phosphate Concentration (mg/well)	Phosphate Concentration (mg/µl)	Phosphate Concentration (mg/L)	Concentration Decrease (mg/L)	Mass of PO_4 Adsorbed (mg)	PO_4 Fraction Adsorbed	Percentage Phosphate Adsorbed (%)	Mass of Adsorbent Present (g)	Phosphate Adsorption Capacity (mg/g)
Carver-Pressed TMA-Alumina Fabric (Fabric #40)	10.00	0.518	0.571	0.545	2.16211	205.401	0.000205	0.000041	41.080	22.608	1.8087	0.35498	35.498	0.308	5.872
Carver-Pressed TMA-Alumina Fabric (Fabric #40)	20.00	0.431	0.478	0.455	1.73798	165.108	0.000165	0.000033	33.022	30.667	2.4533	0.48151	48.151	0.308	7.965
Carver-Pressed TMA-Alumina Fabric (Fabric #40)	30.00	0.437	0.453	0.445	1.69321	160.855	0.000161	0.000032	32.171	31.517	2.5214	0.49487	49.487	0.308	8.186
Carver-Pressed TMA-Alumina Fabric (Fabric #40)	45.00	0.330	0.393	0.362	1.29972	123.473	0.000123	0.000025	24.695	38.994	3.1195	0.61226	61.226	0.308	10.128
Carver-Pressed TMA-Alumina Fabric (Fabric #40)	60.00	0.355	0.350	0.353	1.25730	119.444	0.000119	0.000024	23.889	39.800	3.1840	0.62491	62.491	0.308	10.338
Carver-Pressed TMA-Alumina Fabric (Fabric #40)	90.00	0.284	0.308	0.296	0.99105	94.149	0.000094	0.000019	18.830	44.859	3.5887	0.70434	70.434	0.308	11.652
Carver-Pressed TMA-Alumina Fabric (Fabric #40)	120.00	0.275	0.290	0.283	0.92743	88.106	0.000088	0.000018	17.621	46.067	3.6854	0.72332	72.332	0.308	11.966
Carver-Pressed TMA-Alumina Fabric (Fabric #40)	150.00	0.262	0.258	0.260	0.82139	78.033	0.000078	0.000016	15.607	48.082	3.8466	0.75496	75.496	0.308	12.489
Carver-Pressed TMA-Alumina Fabric (Fabric #40)	180.00	0.234	0.239	0.237	0.71065	67.512	0.000068	0.000014	13.502	50.186	4.0149	0.78799	78.799	0.308	13.035
Carver-Pressed TMA-Alumina Fabric (Fabric #40)	210.00	0.242	0.232	0.237	0.71301	67.736	0.000068	0.000014	13.547	50.141	4.0113	0.78729	78.729	0.308	13.024
Carver-Pressed TMA-Alumina Fabric (Fabric #40)	240.00	0.229	0.217	0.223	0.64703	61.468	0.000061	0.000012	12.294	51.395	4.1116	0.80697	80.697	0.308	13.349
No Adsorbent	0.00	0.653	0.637	0.645	2.63572	250.393	0.000250	0.000083	83.464						
Carver-Pressed TMA-Alumina Fabric (Fabric #41)	0.00	0.596	0.581	0.589	2.36946	225.099	0.000225	0.000075	75.033	8.432	0.6745	0.10102	10.102	0.326	2.069
Carver-Pressed TMA-Alumina Fabric (Fabric #41)	10.00	0.455	0.471	0.463	1.77804	168.914	0.000169	0.000056	56.305	27.160	2.1728	0.32541	32.541	0.326	6.665
Carver-Pressed TMA-Alumina Fabric (Fabric #41)	20.00	0.404	0.446	0.425	1.59896	151.902	0.000152	0.000051	50.634	32.831	2.6265	0.39335	39.335	0.326	8.057
Carver-Pressed TMA-Alumina Fabric (Fabric #41)	30.00	0.334	0.395	0.365	1.31385	124.816	0.000125	0.000042	41.605	41.859	3.3487	0.50152	50.152	0.326	10.272
Carver-Pressed TMA-Alumina Fabric (Fabric #41)	45.00	0.352	0.330	0.341	1.20311	114.295	0.000114	0.000038	38.098	45.366	3.6293	0.54354	54.354	0.326	11.133
Carver-Pressed TMA-Alumina Fabric (Fabric #41)	60.00	0.303	0.312	0.308	1.04524	99.298	0.000099	0.000033	33.099	50.365	4.0292	0.60343	60.343	0.326	12.360
Carver-Pressed TMA-Alumina Fabric (Fabric #41)	90.00	0.265	0.276	0.271	0.87088	82.733	0.000083	0.000028	27.578	55.887	4.4709	0.66959	66.959	0.326	13.715
Carver-Pressed TMA-Alumina Fabric (Fabric #41)	120.00	0.247	0.249	0.248	0.76484	72.660	0.000073	0.000024	24.220	59.244	4.7396	0.70982	70.982	0.326	14.539
Carver-Pressed TMA-Alumina Fabric (Fabric #41)	150.00	0.237	0.223	0.230	0.68002	64.602	0.000065	0.000022	21.534	61.931	4.9544	0.74200	74.200	0.326	15.198
Carver-Pressed TMA-Alumina Fabric (Fabric #41)	180.00	0.211	0.229	0.220	0.63289	60.125	0.000060	0.000020	20.042	63.423	5.0738	0.75988	75.988	0.326	15.564
Carver-Pressed TMA-Alumina Fabric (Fabric #41)	210.00	0.201	0.208	0.205	0.55985	53.186	0.000053	0.000018	17.729	65.736	5.2589	0.78759	78.759	0.326	16.132
Carver-Pressed TMA-Alumina Fabric (Fabric #41)	240.00	0.212	0.200	0.206	0.56692	53.857	0.000054	0.000018	17.952	65.512	5.2410	0.78491	78.491	0.326	16.077
No Adsorbent	0.00	0.503	0.566	0.535	2.11499	200.924	0.000201	0.000100	100.462						
Carver-Pressed TMA-Alumina Fabric (Fabric #42)	0.00	0.491	0.525	0.508	1.99010	189.060	0.000189	0.000095	94.530	5.932	0.4746	0.05905	5.905	0.399	1.189
Carver-Pressed TMA-Alumina Fabric (Fabric #42)	10.00	0.322	0.374	0.348	1.23610	117.429	0.000117	0.000059	58.715	41.747	3.3398	0.41555	41.555	0.399	8.370
Carver-Pressed TMA-Alumina Fabric (Fabric #42)	20.00	0.267	0.268	0.268	0.85674	81.390	0.000081	0.000041	40.695	59.767	4.7813	0.59492	59.492	0.399	11.983
Carver-Pressed TMA-Alumina Fabric (Fabric #42)	30.00	0.241	0.260	0.251	0.77663	73.779	0.000074	0.000037	36.890	63.572	5.0858	0.63280	63.280	0.399	12.746
Carver-Pressed TMA-Alumina Fabric (Fabric #42)	45.00	0.239	0.243	0.241	0.73186	69.526	0.000070	0.000035	34.763	65.699	5.2559	0.65397	65.397	0.399	13.173
Carver-Pressed TMA-Alumina Fabric (Fabric #42)	60.00	0.191	0.209	0.200	0.53864	51.171	0.000051	0.000026	25.586	74.876	5.9901	0.74532	74.532	0.399	15.013
Carver-Pressed TMA-Alumina Fabric (Fabric #42)	90.00	0.200	0.184	0.192	0.50094	47.590	0.000048	0.000024	23.795	76.667	6.1334	0.76315	76.315	0.399	15.372
Carver-Pressed TMA-Alumina Fabric (Fabric #42)	120.00	0.162	0.181	0.172	0.40434	38.412	0.000038	0.000019	19.206	81.256	6.5005	0.80882	80.882	0.399	16.292
Carver-Pressed TMA-Alumina Fabric (Fabric #42)	150.00	0.180	0.159	0.170	0.39491	37.516	0.000038	0.000019	18.758	81.704	6.5363	0.81328	81.328	0.399	16.382
Carver-Pressed TMA-Alumina Fabric (Fabric #42)	180.00	0.169	0.159	0.164	0.36899	35.054	0.000035	0.000018	17.527	82.935	6.6348	0.82553	82.553	0.399	16.629
Carver-Pressed TMA-Alumina Fabric (Fabric #42)	210.00	0.161	0.153	0.157	0.33600	31.920	0.000032	0.000016	15.960	84.502	6.7601	0.84113	84.113	0.399	16.943
Carver-Pressed TMA-Alumina Fabric (Fabric #42)	240.00	0.139	0.137	0.138	0.24647	23.414	0.000023	0.000012	11.707	88.755	7.1004	0.88347	88.347	0.399	17.795

Table 29. Sample plating sequence for phosphate colorimetric assay (top) and the corresponding spectrophotometer absorbance data (bottom). The absorbance data shown was ultimately used to generate the graphs depicted in Figure 50.

	1	2	3	4	5	6	7	8	9	10	11	12
Standards	Standard 0Nm	Standard 1Nm	Standard 2Nm	Standard 3Nm	Standard 4Nm							
Standards	Standard 0Nm	Standard 1Nm	Standard 2Nm	Standard 3Nm	Standard 4Nm							
10 mg/L Lact. Ringer's, Carver-Pressed TMA-Alumina Fabric (#43 & 44)	No Adsorbent	t = 0	t = 10	t = 25	t = 50	t = 75	t = 100	t = 120	t = 150	t = 180	t = 200	t = 240
10 mg/L Lact. Ringer's, Carver-Pressed TMA-Alumina Fabric (#43 & 44)	No Adsorbent	t = 0	t = 10	t = 25	t = 50	t = 75	t = 100	t = 120	t = 150	t = 180	t = 200	t = 240
20 mg/L Lact. Ringer's, Carver-Pressed TMA-Alumina Fabric (#45)	No Adsorbent	t = 0	t = 10	t = 25	t = 50	t = 75	t = 100	t = 120	t = 150	t = 180	t = 200	t = 240
20 mg/L Lact. Ringer's, Carver-Pressed TMA-Alumina Fabric (#45)	No Adsorbent	t = 0	t = 10	t = 25	t = 50	t = 75	t = 100	t = 120	t = 150	t = 180	t = 200	t = 240
30 mg/L Lact. Ringer's, Carver-Pressed TMA-Alumina Fabric (#46 & 47)	No Adsorbent	t = 0	t = 10	t = 25	t = 50	t = 75	t = 100	t = 120	t = 150	t = 180	t = 200	t = 240
30 mg/L Lact. Ringer's, Carver-Pressed TMA-Alumina Fabric (#46 & 47)	No Adsorbent	t = 0	t = 10	t = 25	t = 50	t = 75	t = 100	t = 120	t = 150	t = 180	t = 200	t = 240

	1	2	3	4	5	6	7	8	9	10	11	12
Standards	0.091	0.418	0.651	0.882	1.146							
Standards	0.090	0.382	0.638	0.898	1.157							
10 mg/L Lact. Ringer's, Carver-Pressed TMA-Alumina Fabric (#43 & 44)	0.382	0.376	0.353	0.298	0.258	0.243	0.227	0.218	0.204	0.207	0.216	0.198
10 mg/L Lact. Ringer's, Carver-Pressed TMA-Alumina Fabric (#43 & 44)	0.375	0.345	0.344	0.314	0.269	0.240	0.225	0.209	0.201	0.212	0.197	0.212
20 mg/L Lact. Ringer's, Carver-Pressed TMA-Alumina Fabric (#45)	0.560	0.553	0.555	0.532	0.509	0.482	0.468	0.464	0.459	0.451	0.447	0.447
20 mg/L Lact. Ringer's, Carver-Pressed TMA-Alumina Fabric (#45)	0.576	0.563	0.531	0.535	0.487	0.486	0.465	0.454	0.455	0.461	0.448	0.441
30 mg/L Lact. Ringer's, Carver-Pressed TMA-Alumina Fabric (#46 & 47)	0.780	0.783	0.744	0.689	0.666	0.632	0.616	0.601	0.587	0.581	0.574	0.526
30 mg/L Lact. Ringer's, Carver-Pressed TMA-Alumina Fabric (#46 & 47)	0.791	0.785	0.739	0.681	0.641	0.631	0.613	0.608	0.600	0.573	0.562	0.595

Table 30. Calculations used to determine masses of phosphate adsorbed (mg) and phosphate adsorption capacities (mg/g) from the experimentally derived spectrophotometer absorbance data. The calculations and values displayed in the table were used to generate the graph depicted in Figure 50.

Adsorbent Type:	Time Elapsed at Sample Collection (min)	OD 650	OD 650	Average OD 650	Phosphate Concentration (Nm)	Phosphate Concentration (ng/well)	Phosphate Concentration (mg/well)	Phosphate Concentration (mg/µl)	Phosphate Concentration (mg/L)	Concentration Decrease (mg/L)	Mass of PO_4 Adsorbed (mg)	PO_4 Fraction Adsorbed	Percentage Phosphate Adsorbed (%)	Mass of Adsorbent Present (g)	Phosphate Adsorption Capacity (mg/g)
No Adsorbent	0.00	0.382	0.375	0.379	1.01685	96.601	0.0000966	0.0000097	9.660						
Carver-Pressed TMA-Alumina Fabric (#43 & 44)	0.00	0.376	0.345	0.361	0.94829	90.088	0.0000901	0.0000090	9.009	0.651	0.0326	0.0674	6.743	0.046	0.706
Carver-Pressed TMA-Alumina Fabric (#43 & 44)	10.00	0.353	0.344	0.348	0.90156	85.648	0.0000856	0.0000086	8.565	1.095	0.0548	0.1134	11.338	0.046	1.188
Carver-Pressed TMA-Alumina Fabric (#43 & 44)	25.00	0.298	0.314	0.306	0.74011	70.310	0.0000703	0.0000070	7.031	2.629	0.1315	0.2722	27.216	0.046	2.852
Carver-Pressed TMA-Alumina Fabric (#43 & 44)	50.00	0.258	0.269	0.263	0.57559	54.681	0.0000547	0.0000055	5.468	4.192	0.2096	0.4339	43.395	0.046	4.547
Carver-Pressed TMA-Alumina Fabric (#43 & 44)	75.00	0.243	0.240	0.241	0.49190	46.730	0.0000467	0.0000047	4.673	4.987	0.2494	0.5163	51.625	0.046	5.409
Carver-Pressed TMA-Alumina Fabric (#43 & 44)	100.00	0.227	0.225	0.226	0.43195	41.036	0.0000410	0.0000041	4.104	5.557	0.2778	0.5752	57.521	0.046	6.027
Carver-Pressed TMA-Alumina Fabric (#43 & 44)	120.00	0.218	0.209	0.213	0.38446	36.523	0.0000365	0.0000037	3.652	6.008	0.3004	0.6219	62.192	0.046	6.516
Carver-Pressed TMA-Alumina Fabric (#43 & 44)	150.00	0.204	0.201	0.203	0.34290	32.575	0.0000326	0.0000033	3.258	6.403	0.3201	0.6628	66.279	0.046	6.944
Carver-Pressed TMA-Alumina Fabric (#43 & 44)	180.00	0.207	0.212	0.209	0.36856	35.013	0.0000350	0.0000035	3.501	6.159	0.3079	0.6375	63.755	0.046	6.680
Carver-Pressed TMA-Alumina Fabric (#43 & 44)	200.00	0.216	0.197	0.206	0.35688	33.903	0.0000339	0.0000034	3.390	6.270	0.3135	0.6490	64.904	0.046	6.800
Carver-Pressed TMA-Alumina Fabric (#43 & 44)	240.00	0.198	0.212	0.205	0.35132	33.376	0.0000334	0.0000033	3.338	6.323	0.3161	0.6545	65.450	0.046	6.857
No Adsorbent	0.00	0.560	0.576	0.568	1.74195	165.485	0.0001655	0.0000207	20.686						
Carver-Pressed TMA-Alumina Fabric (#45)	0.00	0.553	0.563	0.558	1.70460	161.937	0.0001619	0.0000202	20.242	0.443	0.0222	0.0214	2.144	0.034	0.650
Carver-Pressed TMA-Alumina Fabric (#45)	10.00	0.555	0.531	0.543	1.64676	156.442	0.0001564	0.0000196	19.555	1.130	0.0565	0.0546	5.464	0.034	1.657
Carver-Pressed TMA-Alumina Fabric (#45)	25.00	0.532	0.535	0.534	1.61095	153.040	0.0001530	0.0000191	19.130	1.556	0.0778	0.0752	7.520	0.034	2.281
Carver-Pressed TMA-Alumina Fabric (#45)	50.00	0.509	0.487	0.498	1.47305	139.940	0.0001399	0.0000175	17.493	3.193	0.1597	0.1544	15.436	0.034	4.682
Carver-Pressed TMA-Alumina Fabric (#45)	75.00	0.482	0.486	0.484	1.41924	134.827	0.0001348	0.0000169	16.853	3.832	0.1916	0.1853	18.526	0.034	5.619
Carver-Pressed TMA-Alumina Fabric (#45)	100.00	0.468	0.465	0.467	1.35431	128.660	0.0001287	0.0000161	16.082	4.603	0.2302	0.2225	22.253	0.034	6.750
Carver-Pressed TMA-Alumina Fabric (#45)	120.00	0.464	0.454	0.459	1.32463	125.839	0.0001258	0.0000157	15.730	4.956	0.2478	0.2396	23.957	0.034	7.266
Carver-Pressed TMA-Alumina Fabric (#45)	150.00	0.459	0.455	0.457	1.31811	125.221	0.0001252	0.0000157	15.653	5.033	0.2517	0.2433	24.331	0.034	7.380
Carver-Pressed TMA-Alumina Fabric (#45)	180.00	0.451	0.461	0.456	1.31467	124.893	0.0001249	0.0000156	15.612	5.074	0.2537	0.2453	24.529	0.034	7.440
Carver-Pressed TMA-Alumina Fabric (#45)	200.00	0.447	0.448	0.448	1.28211	121.800	0.0001218	0.0000152	15.225	5.461	0.2730	0.2640	26.398	0.034	8.007
Carver-Pressed TMA-Alumina Fabric (#45)	240.00	0.447	0.441	0.444	1.26679	120.345	0.0001203	0.0000150	15.043	5.643	0.2821	0.2728	27.278	0.034	8.273
No Adsorbent	0.00	0.780	0.791	0.786	2.57621	244.740	0.0002447	0.0000306	30.592						
Carver-Pressed TMA-Alumina Fabric (#46 & 47)	0.00	0.783	0.785	0.784	2.57046	244.194	0.0002442	0.0000305	30.524	0.068	0.0034	0.0022	0.223	0.050	0.069
Carver-Pressed TMA-Alumina Fabric (#46 & 47)	10.00	0.744	0.739	0.742	2.40767	228.729	0.0002287	0.0000286	28.591	2.001	0.1001	0.0654	6.542	0.050	2.013
Carver-Pressed TMA-Alumina Fabric (#46 & 47)	25.00	0.689	0.681	0.685	2.19144	208.187	0.0002082	0.0000260	26.023	4.569	0.2285	0.1494	14.935	0.050	4.597
Carver-Pressed TMA-Alumina Fabric (#46 & 47)	50.00	0.666	0.641	0.654	2.07098	196.743	0.0001967	0.0000246	24.593	6.000	0.3000	0.1961	19.611	0.050	6.036
Carver-Pressed TMA-Alumina Fabric (#46 & 47)	75.00	0.632	0.631	0.632	1.98709	188.774	0.0001888	0.0000236	23.597	6.996	0.3498	0.2287	22.868	0.050	7.038
Carver-Pressed TMA-Alumina Fabric (#46 & 47)	100.00	0.616	0.613	0.614	1.91949	182.351	0.0001824	0.0000228	22.794	7.799	0.3899	0.2549	25.492	0.050	7.846
Carver-Pressed TMA-Alumina Fabric (#46 & 47)	120.00	0.601	0.608	0.605	1.88290	178.876	0.0001789	0.0000224	22.359	8.233	0.4116	0.2691	26.912	0.050	8.283
Carver-Pressed TMA-Alumina Fabric (#46 & 47)	150.00	0.587	0.600	0.594	1.84058	174.855	0.0001749	0.0000219	21.857	8.736	0.4368	0.2855	28.555	0.050	8.788
Carver-Pressed TMA-Alumina Fabric (#46 & 47)	180.00	0.581	0.573	0.577	1.77680	168.796	0.0001688	0.0000211	21.100	9.493	0.4746	0.3103	31.030	0.050	9.550
Carver-Pressed TMA-Alumina Fabric (#46 & 47)	200.00	0.574	0.562	0.568	1.74348	165.630	0.0001656	0.0000207	20.704	9.889	0.4944	0.3232	32.324	0.050	9.948
Carver-Pressed TMA-Alumina Fabric (#46 & 47)	240.00	0.526	0.595	0.560	1.71322	162.756	0.0001628	0.0000203	20.344	10.248	0.5124	0.3350	33.498	0.050	10.310

Table 31. Sample plating sequence for phosphate colorimetric assay (top) and the corresponding spectrophotometer absorbance data (bottom). The absorbance data shown was ultimately used to generate the graphs depicted in Figure 51 and Figure 52.

	1	2	3	4	5	6	7	8	9	10	11	12
Standards	Standard 0Nm	Standard 1Nm	Standard 2Nm	Standard 3Nm	Standard 4Nm							
Standards	Standard 0Nm	Standard 1Nm	Standard 2Nm	Standard 3Nm	Standard 4Nm							
30 mg/L PO_4 Solution - 1 Liter - 5 Carver Pressed TMA-Alumina Fabrics (#11-15)	No Adsorbent	t = 0	t = 10	t = 25	t = 50	t = 75	t = 100	t = 120	t = 150	t = 180	t = 200	t = 240
30 mg/L PO_4 Solution - 1 Liter - 5 Carver Pressed TMA-Alumina Fabrics (#11-15)	No Adsorbent	t = 0	t = 10	t = 25	t = 50	t = 75	t = 100	t = 120	t = 150	t = 180	t = 200	t = 240

	1	2	3	4	5	6	7	8	9	10	11	12
Standards	0.077	0.431	0.691	0.944	1.243							
Standards	0.078	0.383	0.670	0.951	1.210							
30 mg/L PO_4 Solution - 1 Liter - 5 Carver Pressed TMA-Alumina Fabrics (#11-15)	0.849	0.806	0.763	0.641	0.657	0.612	0.596	0.558	0.555	0.522	0.518	0.835
30 mg/L PO_4 Solution - 1 Liter - 5 Carver Pressed TMA-Alumina Fabrics (#11-15)	0.835	0.796	0.773	0.695	0.682	0.596	0.607	0.575	0.562	0.547	0.510	0.833

Table 32. Calculations used to determine masses of phosphate adsorbed (mg) and phosphate adsorption capacities (mg/g) from the experimentally derived spectrophotometer absorbance data. The calculations and values displayed in the table were used to generate the graphs depicted in Figure 51 and 52.

Adsorbent Type:	Time Elapsed at Sample Collection (min)	OD 650	OD 650	Average OD 650	Phosphate Concentration (Nm)	Phosphate Concentration (ng/well)	Phosphate Concentration (mg/well)	Phosphate Concentration (mg/µl)	Phosphate Concentration (mg/L)	Concentration Decrease (mg/L)	Mass of PO_4 Adsorbed (mg)	PO_4 Fraction Adsorbed	Percentage Phosphate Adsorbed (%)	Mass of Adsorbent Present (g)	Phosphate Adsorption Capacity (mg/g)
No Adsorbent	0.00	0.835	0.833	0.834	2.56078	243.274	0.000243	0.000030	30.409						
5 Carver-Pressed TMA-Alumina Fabrics (Fabrics #11-15)	0.00	0.849	0.835	0.842	2.58852	245.909	0.000246	0.000031	30.739	-0.329	-0.3295	-0.01083	-1.083	1.400	-0.235
5 Carver-Pressed TMA-Alumina Fabrics (Fabrics #11-15)	10.00	0.806	0.796	0.801	2.44633	232.402	0.000232	0.000029	29.050	1.359	1.3590	0.04469	4.469	1.400	0.971
5 Carver-Pressed TMA-Alumina Fabrics (Fabrics #11-15)	25.00	0.763	0.773	0.768	2.33189	221.529	0.000222	0.000028	27.691	2.718	2.7181	0.08938	8.938	1.400	1.941
5 Carver-Pressed TMA-Alumina Fabrics (Fabrics #11-15)	50.00	0.641	0.695	0.668	1.98509	188.583	0.000189	0.000024	23.573	6.836	6.8363	0.22481	22.481	1.400	4.883
5 Carver-Pressed TMA-Alumina Fabrics (Fabrics #11-15)	75.00	0.657	0.682	0.670	1.99029	189.078	0.000189	0.000024	23.635	6.775	6.7745	0.22278	22.278	1.400	4.839
5 Carver-Pressed TMA-Alumina Fabrics (Fabrics #11-15)	100.00	0.612	0.596	0.604	1.76314	167.498	0.000167	0.000021	20.937	9.472	9.4720	0.31148	31.148	1.400	6.766
5 Carver-Pressed TMA-Alumina Fabrics (Fabrics #11-15)	120.00	0.596	0.607	0.602	1.75447	166.674	0.000167	0.000021	20.834	9.575	9.5750	0.31487	31.487	1.400	6.839
5 Carver-Pressed TMA-Alumina Fabrics (Fabrics #11-15)	150.00	0.558	0.575	0.567	1.63308	155.143	0.000155	0.000019	19.393	11.016	11.0163	0.36227	36.227	1.400	7.869
5 Carver-Pressed TMA-Alumina Fabrics (Fabrics #11-15)	180.00	0.555	0.562	0.559	1.60534	152.507	0.000153	0.000019	19.063	11.346	11.3458	0.37310	37.310	1.400	8.104
5 Carver-Pressed TMA-Alumina Fabrics (Fabrics #11-15)	200.00	0.522	0.547	0.535	1.52211	144.600	0.000145	0.000018	18.075	12.334	12.3342	0.40561	40.561	1.400	8.810
5 Carver-Pressed TMA-Alumina Fabrics (Fabrics #11-15)	240.00	0.518	0.510	0.514	1.45101	137.846	0.000138	0.000017	17.231	13.178	13.1784	0.43337	43.337	1.400	9.413

Table 33. Sample plating sequence for phosphate colorimetric assay (top) and the corresponding spectrophotometer absorbance data (bottom). The absorbance data shown was ultimately used to generate the graphs depicted in Figure 53 and Figure 54.

	1	2	3	4	5	6	7	8	9	10	11	12
Standards	Standard 0Nm	Standard 1Nm	Standard 2Nm	Standard 3Nm	Standard 4Nm							
Standards	Standard 0Nm	Standard 1Nm	Standard 2Nm	Standard 3Nm	Standard 4Nm							
50 mg/L PO_4 Solution - 1 Liter - 6 Carver Pressed TMA-Alumina Fabrics (#16-21)	No Adsorbent	t = 0	t = 20	t = 40	t = 60	t = 80	t = 100	t = 120	t = 140	t = 160	t = 180	t = 200
50 mg/L PO_4 Solution - 1 Liter - 6 Carver Pressed TMA-Alumina Fabrics (#16-21)	No Adsorbent	t = 0	t = 20	t = 40	t = 60	t = 80	t = 100	t = 120	t = 140	t = 160	t = 180	t = 200
											t = 220	t = 240
											t = 220	t = 240

	1	2	3	4	5	6	7	8	9	10	11	12
Standards	0.076	0.331	0.590	0.832	1.093							
Standards	0.078	0.316	0.575	0.846	1.070							
50 mg/L PO_4 Solution - 1 Liter - 6 Carver Pressed TMA-Alumina Fabrics (#16-21)	0.796	0.819	0.666	0.614	0.578	0.561	0.491	0.489	0.447	0.434	0.415	0.404
50 mg/L PO_4 Solution - 1 Liter - 6 Carver Pressed TMA-Alumina Fabrics (#16-21)	0.816	0.801	0.669	0.620	0.582	0.546	0.517	0.489	0.446	0.435	0.396	0.398
											0.386	0.376
											0.385	0.371

Table 34. Calculations used to determine masses of phosphate adsorbed (mg) and phosphate adsorption capacities (mg/g) from the experimentally derived spectrophotometer absorbance data. The calculations and values displayed in the table were used to generate the graphs depicted in Figure 53 and Figure 54.

Adsorbent Type:	Time Elapsed at Sample Collection (min)	OD 650	OD 650	Average OD 650	Phosphate Concentration (Nm)	Phosphate Concentration (ng/well)	Phosphate Concentration (mg/well)	Phosphate Concentration (mg/µl)	Phosphate Concentration (mg/L)	Concentration Decrease (mg/L)	Mass of PO_4 Adsorbed (mg)	PO_4 Fraction Adsorbed	Percentage Phosphate Adsorbed (%)	Mass of Adsorbent Present (g)	Phosphate Adsorption Capacity (mg/g)
No Adsorbent	0.00	0.796	0.816	0.806	2.90000	275.500	0.000276	0.000055	55.100						
6 Carver-Pressed TMA-Alumina Fabrics (Fabrics #16-21)	0.00	0.819	0.801	0.810	2.91453	276.881	0.000277	0.000055	55.376	-0.276	-0.276	-0.0050	-0.501	1.926	-0.143
6 Carver-Pressed TMA-Alumina Fabrics (Fabrics #16-21)	20.00	0.666	0.669	0.667	2.34752	223.014	0.000223	0.000045	44.603	10.497	10.497	0.1905	19.051	1.926	5.449
6 Carver-Pressed TMA-Alumina Fabrics (Fabrics #16-21)	40.00	0.614	0.620	0.617	2.14789	204.050	0.000204	0.000041	40.810	14.290	14.290	0.2593	25.935	1.926	7.418
6 Carver-Pressed TMA-Alumina Fabrics (Fabrics #16-21)	60.00	0.578	0.582	0.580	1.99962	189.964	0.000190	0.000038	37.993	17.107	17.107	0.3105	31.048	1.926	8.881
6 Carver-Pressed TMA-Alumina Fabrics (Fabrics #16-21)	80.00	0.561	0.546	0.553	1.89354	179.887	0.000180	0.000036	35.977	19.123	19.123	0.3471	34.705	1.926	9.927
6 Carver-Pressed TMA-Alumina Fabrics (Fabrics #16-21)	100.00	0.491	0.517	0.504	1.69830	161.339	0.000161	0.000032	32.268	22.832	22.832	0.4144	41.438	1.926	11.853
6 Carver-Pressed TMA-Alumina Fabrics (Fabrics #16-21)	120.00	0.489	0.489	0.489	1.63680	155.496	0.000155	0.000031	31.099	24.001	24.001	0.4356	43.559	1.926	12.460
6 Carver-Pressed TMA-Alumina Fabrics (Fabrics #16-21)	140.00	0.447	0.446	0.446	1.46763	139.425	0.000139	0.000028	27.885	27.215	27.215	0.4939	49.392	1.926	14.128
6 Carver-Pressed TMA-Alumina Fabrics (Fabrics #16-21)	160.00	0.434	0.435	0.435	1.42166	135.058	0.000135	0.000027	27.012	28.089	28.089	0.5098	50.977	1.926	14.582
6 Carver-Pressed TMA-Alumina Fabrics (Fabrics #16-21)	180.00	0.415	0.396	0.405	1.30463	123.940	0.000124	0.000025	24.788	30.312	30.312	0.5501	55.013	1.926	15.736
6 Carver-Pressed TMA-Alumina Fabrics (Fabrics #16-21)	200.00	0.404	0.398	0.401	1.28831	122.390	0.000122	0.000024	24.478	30.622	30.622	0.5558	55.575	1.926	15.897
6 Carver-Pressed TMA-Alumina Fabrics (Fabrics #16-21)	220.00	0.386	0.385	0.385	1.22542	116.415	0.000116	0.000023	23.283	31.817	31.817	0.5774	57.744	1.926	16.517
6 Carver-Pressed TMA-Alumina Fabrics (Fabrics #16-21)	240.00	0.376	0.371	0.374	1.17786	111.896	0.000112	0.000022	22.379	32.721	32.721	0.5938	59.384	1.926	16.986

Table 35. Sample plating sequence for phosphate colorimetric assay (top) and the corresponding spectrophotometer absorbance data (bottom). The absorbance data shown was ultimately used to generate the graphs depicted in Figure 55 and Figure 56.

	1	2	3	4	5	6	7	8	9	10	11	12
Standards	Standard 0Nm	Standard 1Nm	Standard 2Nm	Standard 3Nm	Standard 4Nm							
Standards	Standard 0Nm	Standard 1Nm	Standard 2Nm	Standard 3Nm	Standard 4Nm							
90 mg/L PO4 Solution - 1 Liter - 10 Carver Pressed TMA-Alumina Fabrics (#22-31)	No Adsorbent	t = 0	t = 20	t = 40	t = 60	t = 80	t = 100	t = 120	t = 140	t = 160	t = 180	t = 200
90 mg/L PO4 Solution - 1 Liter - 10 Carver Pressed TMA-Alumina Fabrics (#22-31)	No Adsorbent	t = 0	t = 20	t = 40	t = 60	t = 80	t = 100	t = 120	t = 140	t = 160	t = 180	t = 200
											t = 220	t = 240
											t = 220	t = 240

	1	2	3	4	5	6	7	8	9	10	11	12
Standards	0.0776	0.3268	0.5377	0.8272	1.0784							
Standards	0.0756	0.335	0.5899	0.8011	1.0734							
90 mg/L PO4 Solution - 1 Liter - 10 Carver Pressed TMA-Alumina Fabrics (#22-31)	0.3148	0.3078	0.2762	0.2603	0.2492	0.2224	0.2071	0.2029	0.1931	0.1822	0.1753	0.1672
90 mg/L PO4 Solution - 1 Liter - 10 Carver Pressed TMA-Alumina Fabrics (#22-31)	0.3122	0.3092	0.2821	0.2597	0.239	0.2192	0.2143	0.202	0.1894	0.1849	0.1739	0.1632
											0.1638	0.1469
											0.1498	0.1452

Table 36. Calculations used to determine masses of phosphate adsorbed (mg) and phosphate adsorption capacities (mg/g) from the experimentally derived spectrophotometer absorbance data. The calculations and values displayed in the table were used to generate the graphs depicted in Figure 55 and Figure 56.

Adsorbent Type:	Time Elapsed at Sample Collection (min)	OD 650	OD 650	Average OD 650	Phosphate Concentration (Nm)	Phosphate Concentration (ng/well)	Phosphate Concentration (mg/well)	Phosphate Concentration (mg/µl)	Phosphate Concentration (mg/L)	Concentration Decrease (mg/L)	Mass of PO_4 Adsorbed (mg)	PO_4 Fraction Adsorbed	Percentage Phosphate Adsorbed (%)	Mass of Adsorbent Present (g)	Phosphate Adsorption Capacity (mg/g)
No Adsorbent	0.00	0.315	0.312	0.314	0.95430	90.659	0.000091	0.000091	90.659						
10 Carver-Pressed TMA-Alumina Fabrics (Fabrics #22-31)	0.00	0.308	0.309	0.309	0.93399	88.729	0.000089	0.000089	88.729	1.929	1.929	0.0213	2.128	3.299	0.585
10 Carver-Pressed TMA-Alumina Fabrics (Fabrics #22-31)	20.00	0.276	0.282	0.279	0.81477	77.404	0.000077	0.000077	77.404	13.255	13.255	0.1462	14.621	3.299	4.018
10 Carver-Pressed TMA-Alumina Fabrics (Fabrics #22-31)	40.00	0.260	0.260	0.260	0.73699	70.014	0.000070	0.000070	70.014	20.645	20.645	0.2277	22.772	3.299	6.259
10 Carver-Pressed TMA-Alumina Fabrics (Fabrics #22-31)	60.00	0.249	0.239	0.244	0.67240	63.878	0.000064	0.000064	63.878	26.780	26.780	0.2954	29.540	3.299	8.119
10 Carver-Pressed TMA-Alumina Fabrics (Fabrics #22-31)	80.00	0.222	0.219	0.221	0.57776	54.887	0.000055	0.000055	54.887	35.771	35.771	0.3946	39.457	3.299	10.844
10 Carver-Pressed TMA-Alumina Fabrics (Fabrics #22-31)	100.00	0.207	0.214	0.211	0.53674	50.990	0.000051	0.000051	50.990	39.669	39.669	0.4376	43.756	3.299	12.026
10 Carver-Pressed TMA-Alumina Fabrics (Fabrics #22-31)	120.00	0.203	0.202	0.202	0.50322	47.806	0.000048	0.000048	47.806	42.852	42.852	0.4727	47.268	3.299	12.991
10 Carver-Pressed TMA-Alumina Fabrics (Fabrics #22-31)	140.00	0.193	0.189	0.191	0.45773	43.484	0.000043	0.000043	43.484	47.174	47.174	0.5203	52.035	3.299	14.301
10 Carver-Pressed TMA-Alumina Fabrics (Fabrics #22-31)	160.00	0.182	0.185	0.184	0.42645	40.513	0.000041	0.000041	40.513	50.146	50.146	0.5531	55.312	3.299	15.202
10 Carver-Pressed TMA-Alumina Fabrics (Fabrics #22-31)	180.00	0.175	0.174	0.175	0.39010	37.059	0.000037	0.000037	37.059	53.599	53.599	0.5912	59.122	3.299	16.249
10 Carver-Pressed TMA-Alumina Fabrics (Fabrics #22-31)	200.00	0.167	0.163	0.165	0.35192	33.432	0.000033	0.000033	33.432	57.226	57.226	0.6312	63.123	3.299	17.349
10 Carver-Pressed TMA-Alumina Fabrics (Fabrics #22-31)	220.00	0.164	0.150	0.157	0.31780	30.191	0.000030	0.000030	30.191	60.468	60.468	0.6670	66.698	3.299	18.331
10 Carver-Pressed TMA-Alumina Fabrics (Fabrics #22-31)	240.00	0.147	0.145	0.146	0.27413	26.043	0.000026	0.000026	26.043	64.616	64.616	0.7127	71.274	3.299	19.589

Table 37. Data yielded from analyzing the phosphate content of bovine blood that was continuously exposed to TMA-Alumina fabrics. The measured phosphate concentration (mg/dL) of each sample was yielded from a Vitros 5600 Integrated Analyzer. The data shown in this table was ultimately used to generate the graphs depicted in Figure 58 and Figure 59.

Adsorbent Type:	Time Elapsed at Sample Collection (min)	Measured Phosphate Concentration (mg/dL)	Phosphate Concentration (mg/L)	Concentration Decrease (mg/L)	Mass of PO_4 Adsorbed (mg)	PO_4 Fraction Adsorbed	Percentage Phosphate Adsorbed (%)	Mass of Adsorbent Present (g)	Phosphate Adsorption Capacity (mg/g)
No Adsorbent	0.00	8.9	89	0	0				
10 Carver-Pressed TMA-Alumina Fabrics (Fabrics #1-10)	0.00	8.8	88	1	1	0.0112	1.124	3.846	0.260
10 Carver-Pressed TMA-Alumina Fabrics (Fabrics #1-10)	20.00	8.1	81	8	8	0.0899	8.989	3.846	2.080
10 Carver-Pressed TMA-Alumina Fabrics (Fabrics #1-10)	40.00	7.4	74	15	15	0.1685	16.854	3.846	3.900
10 Carver-Pressed TMA-Alumina Fabrics (Fabrics #1-10)	60.00	6.8	68	21	21	0.2360	23.596	3.846	5.460
10 Carver-Pressed TMA-Alumina Fabrics (Fabrics #1-10)	80.00	6.5	65	24	24	0.2697	26.966	3.846	6.240
10 Carver-Pressed TMA-Alumina Fabrics (Fabrics #1-10)	100.00	6.2	62	27	27	0.3034	30.337	3.846	7.019
10 Carver-Pressed TMA-Alumina Fabrics (Fabrics #1-10)	120.00	6.0	60	29	29	0.3258	32.584	3.846	7.539
10 Carver-Pressed TMA-Alumina Fabrics (Fabrics #1-10)	140.00	5.9	59	30	30	0.3371	33.708	3.846	7.799
10 Carver-Pressed TMA-Alumina Fabrics (Fabrics #1-10)	160.00	5.6	56	33	33	0.3708	37.079	3.846	8.579
10 Carver-Pressed TMA-Alumina Fabrics (Fabrics #1-10)	180.00	5.4	54	35	35	0.3933	39.326	3.846	9.099
10 Carver-Pressed TMA-Alumina Fabrics (Fabrics #1-10)	200.00	5.3	53	36	36	0.4045	40.449	3.846	9.359
10 Carver-Pressed TMA-Alumina Fabrics (Fabrics #1-10)	220.00	5.1	51	38	38	0.4270	42.697	3.846	9.879
10 Carver-Pressed TMA-Alumina Fabrics (Fabrics #1-10)	240.00	5.1	51	38	38	0.4270	42.697	3.846	9.879